DEVELOPMENT AND EVALUATION OF NEW BLEED BOUNDARY
CONDITION MODELS FOR SUPERSONIC INLET BOUNDARY LAYER
BLEED FLOW

A THESIS SUBMITTED TO
THE GRADUATE SCHOOL OF NATURAL AND APPLIED SCIENCES
OF
MIDDLE EAST TECHNICAL UNIVERSITY

BY

GÖKHAN AKAR

IN PARTIAL FULFILLMENT OF THE REQUIREMENTS
FOR
THE DEGREE OF MASTER OF SCIENCE
IN
AEROSPACE ENGINEERING

SEPTEMBER 2019

Approval of the thesis:

DEVELOPMENT AND EVALUATION OF NEW BLEED BOUNDARY CONDITION MODELS FOR SUPERSONIC INLET BOUNDARY LAYER BLEED FLOW

submitted by **GÖKHAN AKAR** in partial fulfillment of the requirements for the degree of **Master of Science in Aerospace Engineering Department, Middle East Technical University** by,

Prof. Dr. Halil Kalıpçılar
Dean, Graduate School of **Natural and Applied Sciences**   _____

Prof. Dr. İsmail Hakkı Tuncer
Head of Department, **Aerospace Engineering**   _____

Assoc. Prof. Dr. Sinan Eyi
Supervisor, **Aerospace Engineering, METU**   _____

Examining Committee Members:

Prof. Dr. Oğuz Uzol
Aerospace Engineering Dept., METU   _____

Assoc. Prof. Dr. Sinan Eyi
Aerospace Engineering Dept., METU   _____

Assist. Prof. Dr. Sıtkı Uslu
Mechanical Engineering Dept., TOBB ETU   _____

Assist. Prof. Dr. Mustafa Kaya
Aeronautical Engineering Dept., YBU   _____

Assist. Prof. Dr. Ali Türker Kutay
Aerospace Engineering Dept., METU   _____

Date: 13.09.2019

I hereby declare that all information in this document has been obtained and presented in accordance with academic rules and ethical conduct. I also declare that, as required by these rules and conduct, I have fully cited and referenced all material and results that are not original to this work.

Name, Surname: Gökhan Akar

Signature:

ABSTRACT

DEVELOPMENT AND EVALUATION OF NEW BLEED BOUNDARY CONDITION MODELS FOR SUPERSONIC INLET BOUNDARY LAYER BLEED FLOW

Akar, Gökhan
Master of Science, Aerospace Engineering
Supervisor: Assoc. Prof. Dr. Sinan Eyi

September 2019, 113 pages

Shock wave/boundary layer interaction is an important issue that should be considered when studying supersonic inlet design for air vehicles. Porous bleed systems have traditionally been used for increase stability and efficiency of the supersonic inlets by means of removing the lower momentum part of the boundary layer to prevent flow separation caused by adverse pressure gradient. However, evaluating and determining the effect of the boundary layer bleed system on the performance of the supersonic inlet is one of the most challenging problems.

In this thesis, single and porous bleed systems are studied for validation and investigation of bleed boundary condition modeling with concentrating on normal bleed hole configuration in computational fluid dynamics (CFD). Firstly, for validation of the method, three-dimensional CFD simulations are performed on fully resolved models (FRM) with modeling bleed plenum and hole cavity details. Grid converge study is conducted on different levels of grids using Spalart-Allmaras, Realizable k-ε and SST k-ω turbulence models. Optimal grid resolution and turbulence model are determined for bleed simulations. CFD analyses are expanded for different plenum total pressure ratios (P_{pl}/P_t). As a result of validation studies, the CFD results show good agreement with the wind tunnel test data. Furthermore, three new bleed

boundary condition models are introduced to simulate bleed flow without modeling the bleed plenum and cavity details of the holes. Additional CFD analyses on the porous bleed case are performed including blowing effects to examine the correlation between mass flow rate and flow properties at the reference boundaries. Collected data are presented and discussed according to scaled parameters. The best curve fitting models on the scaled parameters are selected for each new bleed boundary condition (BBC) model. In order to evaluate the validity of BBC modeling alternatives, CFD studies are performed on the porous bleed systems with and without shock interaction with the implementation of new BBC models to the solver.

Consequently, the results of the new BBC models are compared with the test data and the results of the FRM simulations. The bleed model based bleed region flow properties predicts bleed flow rates very close to the reference data. Moreover, all three models achieve remarkable success on simulation of flow structure and the models reflect well the impacts of the bleed region on efficiency in terms of total pressure recovery.

Keywords: Computational Fluid Dynamics, CFD, Boundary Layer Control, Shock Wave/Boundary Layer Interaction, Boundary Layer Bleed System, Bleed Boundary Condition Modeling, Supersonic Inlet

ÖZ

SES-ÜSTÜ HAVA ALIĞI SINIR TABAKA TAHLİYE AKIŞI İÇİN YENİ TAHLİYE SINIR KOŞULU MODELLERİNİN GELİŞTİRİLMESİ VE DEĞERLENDİRİLMESİ

Akar, Gökhan
Yüksek Lisans, Havacılık ve Uzay Mühendisliği
Tez Danışmanı: Doç. Dr. Sinan Eyi

Eylül 2019, 113 sayfa

Şok dalgası/sınır tabaka etkileşimi ses-üstü hızlarda hava-alığı tasarımı çalışmalarında dikkate alınması gereken önemli bir konudur. Ses-üstü hava alıklarının kararlık ve verimlerinin arttırılması amacı ile test basınç gradyanı sebebi ile sınır tabaka ayrılmalarının engellenmesi için sınır tabakadaki düşük momentuma sahip akışın tahliye sistemleri ile alınması yaygın olarak kullanılan bir çözümdür. Fakat sınır tabaka tahliye sisteminin ses-üstü hava alığı performansına etkisinin belirlenmesi ve değerlendirilmesi en zorlu problemlerden biridir.

Bu tezde, tek ve çok gözenekli tahliye sistemleri, doğrulama ve tahliye sınır koşulu araştırmaları için normal delik konfigürasyonu üzerinde yoğunlaşılarak hesaplamalı akışkanlar dinamiğinde (HAD) çalışılmıştır. Öncelikle, yöntemin doğrulanması amacı ile tahliye odası ve delik detayları ile modellenen, tümüyle çözümlenmiş tahliye sistemlerinde HAD simülasyonları gerçekleştirilmiştir. Farklı seviyelerdeki cözüm ağı yoğunlukları ile Spalart-Allmaras, Realizable k-ε ve SST k-ω türbülans modelleri kullanılarak çözüm ağı yakınsatma çalışması yapılmıştır. Tahliye akışı için optimum çözüm ağı yoğunluğu ve türbülans modeli belirlenmiştir. Farklı tahliye toplam basınç oranları (P_{pl}/P_t) için HAD analizleri genişletilmiştir. Doğrulama çalışmalarının sonucu olarak HAD sonuçları rüzgar tüneli test verileri ile iyi bir uyum göstermiştir.

Ayrıca, tahliye odası ve delik girintilerini modellemeden tahliye akışını simüle etmek amacı ile üç yeni sınır koşulu modeli ortaya konmuştur. Kütle akış debisi ve referans sınırlardaki akış özellikleri arasında korelasyon incelemek amacı ile gözenekli tahliye sisteminde ters yönde akış etkileri de dahil edilderek ilave CFD analizler yapılmıştır. Toplanan veriler ölçeklendirilmiş parametrelere göre sunulmuş ve tartışılmıştır. Her yeni tahliye sınır koşulu için ölçeklendirilmiş veriler üzerinde en iyi eğri modeli seçilmiştir. Tahliye sınır koşulu modelleme alternatiflerinin doğruluğunu değerlendirmek için yeni delik modelleri çözücüye uygulanarak şok etkisinde olan ve olmayan çok gözenekli tahliye sistemlerinde CFD çalışmaları yapılmıştır.

Sonuç olarak, yeni tahliye sınır modellerinin analiz sonuçları test verileri ve tümüyle çözümlenmiş modeller üzerinde yapılan simülasyonlar ile karşılaştırılmıştır. Tahliye delik etrafındaki yüzeyin akış koşullarına dayanan model ile referans verilere çok yakın tahliye akış debisi tahmini yapılabilmiştir. Ayrıca her üç model de akış yapısının benzetilmesi ve tahliye bölgesinin toplam basınç korunumu açısından verimliliğe etkisinin yansıtılması konusunda dikkate değer bir başarı elde edilmiştir.

Anahtar Kelimeler: Hesaplamalı Akışkanlar Dinamiği, HAD, Sınır Tabaka Kontrolü, Şok Dalgası/Sınır Tabaka Etkileşimi, Sınır Tabaka Tahliye Sistemi, Tahliye Sınır Koşulu Modellemesi, Ses-üstü Hava-alığı

To my family and my friends

ACKNOWLEDGEMENTS

TABLE OF CONTENTS

LIST OF TABLES

TABLES

LIST OF FIGURES

FIGURES

LIST OF ABBREVIATIONS

ABBREVIATIONS

AIP	Aerodynamic Interface Plane
BBC	Bleed boundary condition
BHB	Bleed Hole Boundary
BRB	Bleed Region Boundary
BRDB	Bleed Region Diamond Boundary
CFD	Computational Fluid Dynamics
DC	Distortion Coefficient
FRM	Fully Resolved Model
LSP	Last Stable Point
NASA	National Aeronautics and Space Administration
NRMSD	Normalized root mean square deviation
OP	Operation Point
PR	Total Pressure Recovery
RANS	Reynold averaged Navier-Stokes
RMSD	Root mean square deviation
SM	Stability Margin
SWBLI	Shock wave/boundary layer interaction
UDF	User Defined Functions

LIST OF SYMBOLS

Roman Symbols

a	Speed of sound
A	Area
C	Coefficient
D	Diameter of hole
E	Energy
F	Force
g	Gravity
K	Thousand
L	Length of hole
M	Mach number
P	Static Pressure
Q	Flow coefficient
R	Gas constant
Re	Reynolds number
t	Time
T	Static Temperature
V	Velocity
W	Rate of flow
X	Streamwise coordinate
Y	Vertical coordinate
Z	Lateral coordinate

Greek Symbols

γ	Ratio of specific heats
ε	Turbulence dissipation
ρ	Density
τ	Shear
μ	Dynamic viscosity
ω	Turbulent dissipation
δ	Boundary-layer thickness
δ^*	Displacement thickness
θ	Momentum thickness

Subscripts

∞	Freestream condition

0	Condition at initial profile
2	Condition at AIP
ave	Average
b	Property evaluated at the inlet surface (boundary) condition
bl	Bleed
c	Cowl
corr	Corrected
d	Drag
e	Boundary layer edge
LSP	Last Stable Point
max	Maximum
min	Minimum
OP	Operation Point
pl	Plenum
ref	Reference
sonic	Sonic condition
t	Total condition
w	Wall condition

CHAPTER 1

INTRODUCTION

Boundary layer control is a crucial issue that should be considered when studying supersonic inlet design. Although, many other flow control techniques are investigated to prevent unstable operation of inlet, bleed systems are still the most preferred technique in terms of its advantages and mature technology. Whereas boundary layer bleed system is one of the most challenging problems to find good compromise for providing adequate overall performance work on inlet's whole operation conditions. The development of computer technology and advances in computational fluid dynamics (CFD) have provided the opportunity to simulate and visualize complex bleed flow phenomena. Since the porous surfaces can be composed of hundreds of small holes, the design and optimization of bleed systems require high computer resources. Therefore, extensive studies have been carried out on bleed boundary condition (BBC) modeling to predict bleed flow rate and simulate overall effect on flow field where the bleed holes are located without modeling each bleed hole and bleed plenum. Nevertheless, no perfect method exits that clarifies and covers the problem.

In order to obtain detailed information about boundary layer bleed systems and understand physics on flow control, relevant sources are investigated. Therefore, the following sections are dedicated to literature survey relevant to supersonic inlet design and boundary layer bleed systems. Firstly, general information about supersonic inlets, compression types, operation characteristics, viscous effects and stability problem are discussed to clarify why boundary layer control is so crucial for inlet design. In the subsequent sections, boundary layer bleed control, performance effects on supersonic inlets, types of bleed configuration, effective parameters on typical design process and flow structure around bleed holes are informed in detail. In

addition, bleed system performance evaluation and analyses are discussed with emphasis on how analysis techniques are developed and applied on bleed system.

1.1. Supersonic Inlets and Stability Problem

Inlets have an important role in engine performance and stability in air-breathing systems. The engine inlet (American English) or intake (British English) is responsible to supply required amount of air to the engine at convenient velocity with the best possible efficiency in terms of pressure recovery. Also, an inlet should deliver air with tolerable distortion at pressure and velocity profile at the combustion chamber entrance plane [1]. Inlet's drag, weight and radar cross section area are other important parameters that affect aircraft overall performance and operation capabilities [2].

The inlet design differs according to subsonic and supersonic speed regimes due to the characteristic of the flow. At subsonic speeds, the engine is supplied with the desired speed and amount of flow by means of a subsonic diffuser. For a supersonic inlet, the flow should be slowed down to subsonic speeds before it reaches to aerodynamic interface plane which is an imaginary surface between the end of subsonic diffuser and the engine. Supersonic inlets commonly consist of nose, external supersonic diffuser (ramp), throat, subsonic diffuser, aerodynamic interface plane (AIP) and cowl. Nose is a sharp angled structural part of foremost of the inlet. At the supersonic diffuser, which is also called ramp, the flow is slowed down as near as speed of sound. Multiple oblique shocks are originated at ramp to keep total pressure losses as low as possible. At the throat region, a terminal normal shock is generated to decrease air speed to subsonic. After the throat, similar to the subsonic inlets, air speed decreases along subsonic diffuser to the engine face [1]. Cowl is structural part that supports inlet integrity. The oblique shocks generated on the ramp are generally directed to front sharp part of the cowl called cowl lip. In addition, inlet's flow control devices; bypass doors, bleed plenum and exits can be placed in the cowl. Simple sketch of a supersonic inlet is given in Figure 1.1.

2
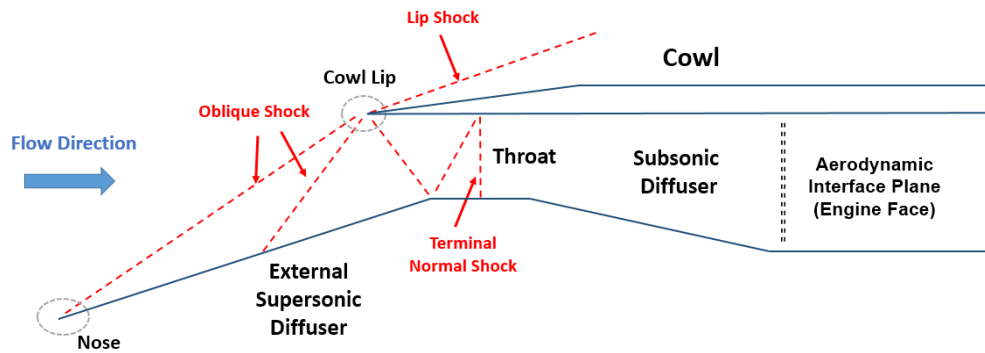
Figure 1.1 Simple Sketch of a Supersonic Inlet

Test model of an axisymmetric mixed compression inlet is given in Figure 1.2.
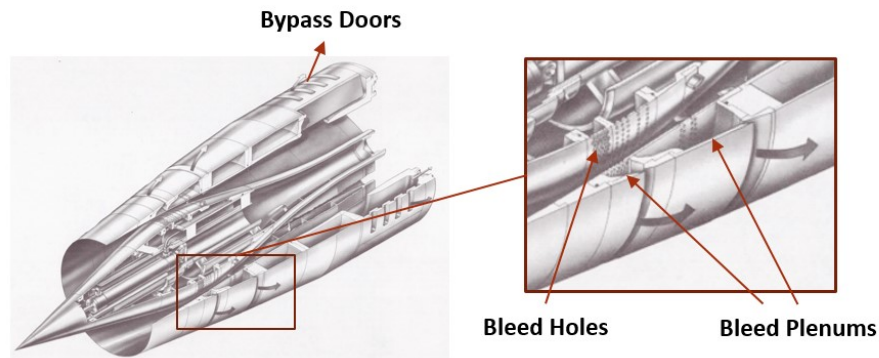
Figure 1.2 Test Model of a Mixed Compression Inlet [3]

1.1.1. Inlet Performance Parameters

Inlet performance parameters are mostly defined as pressure recovery, distortion, mass flow, capture area ratio and drag.

Total pressure recovery is a parameter which defines the efficiency of diffusion and compression process through the inlet. The efficiency of inlet can be defined as the ratio of average stagnation pressure at the AIP to freestream stagnation pressure [1]. This ratio is either calculated using a mass-averaged or an area-averaged basis. The area averaged calculations are usually preferred. The total pressure losses can be caused by friction losses, shock losses, losses caused by turbulence generation [2].

$$PR = \frac{P_{t2}}{P_{t0}} \tag{1.1}$$

Distortion parameter is related with the distribution of the pressure at the AIP. Non-uniform flow at the engine face can decrease engine performance and large variation on total pressure can cause instabilities on propulsion system also the engine can surge in severe cases. Nevertheless, there is no general expression of distortion coefficient and the definition can vary according to engine manufacturers. One of the definitions is given below:

$$DC = \frac{P_{t2,max} - P_{t2,min}}{P_{t2,ave}} \tag{1.2}$$

Capture area ratio, which is also called mass flow ratio, is defined as the ratio between captured flow area of the stream tube at far upstream (A_0) to the inlet cowl cross sectional area (A_c). Capture area is determined by air requirements for propulsion system, engine, bleed, secondary flow [1]. When evaluating the characteristics of inlet and performance, capture area ratio is a preliminary parameter and strongly related with inlet external drag. In supersonic speeds capture area ratio is less than or equal to 1 [2]. The capture area ratio can be expressed as

$$A_0/A_C \tag{1.3}$$

Inlet drag is a fundamental parameter that strongly affects aircraft overall performance. Inlet drag should be minimized as much as possible. Spillage, cowl, bleed, and friction are the main contributors of inlet drag [4].

$$C_d = \frac{F_d}{\frac{1}{2}\rho V_\infty^2 A_{ref}} \tag{1.4}$$

The margin between last stable point (LSP) and operation point (OP) is defined as the stability margin (SM). Minimum stability margin is determined according to provide safe flight, due to the uncertainties and flow disturbances can be encountered in all operational condition of aircraft [4].

$$SM = 1 - \left(\frac{PR_{LSP}}{\dot{m}_{corr,LSP}} / \frac{PR_{OP}}{\dot{m}_{corr,OP}} \right) > SM_{min} \qquad (1.5)$$

1.1.2. Classification of Supersonic Inlets

Supersonic inlets can be classified according to supersonic diffuser shape (axisymmetric, two dimensional, three dimensional, bifurcated), supersonic diffuser compression complexity (isentropic, single, double cone, …), where supersonic compression process takes place (external, internal, mixed), etc [1]. Based on supersonic compression process, inlet working behavior changes significantly. In this section, supersonic inlets are investigated with focus on where the supersonic compression process takes place; external and mixed compression that are mostly used in practical applications.

External compression inlets compress air at the external part of the inlet. At the entrance of the duct, a normal terminal shock forms as illustrated in Figure 1.3. It is a simple choice up to 2.5 Mach number. Since the total pressure recovery at the supersonic diffuser is closely related to the engine efficiency, it is intended to keep the total pressure recovery high by creating more than one oblique shock at the ramp section instead of a single oblique shock. However, the wedge angle on the ramp increases with the flight speed that increases the angle of rotation in the throat region resulting high cowl drag and long diffuser to avoid flow separation [5].
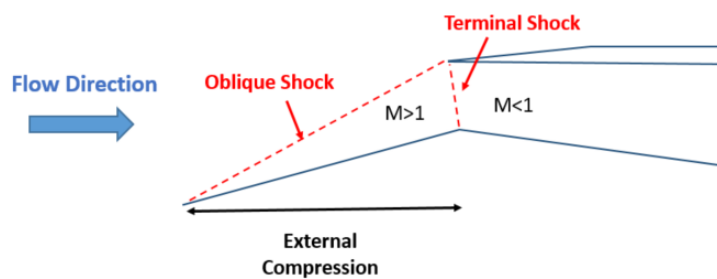
Figure 1.3 Simple Sketch of an External Supersonic Compression

Mixed compression inlets compress air both externally and internally at supersonic speeds. Oblique shocks are impinged into the duct and maintained compression process internally. Throat section needs acceptable amount of flow turning due to the

internally compression above speeds Mach 2.5. However, mixed compression inlets have unstart problem. Complex flow structure in the inlet needs to be handled with adjustable devices and flow control techniques which makes aircraft more expensive and heavier [2]. Simple sketch and shock structure of mixed compression inlet is illustrated in Figure 1.4
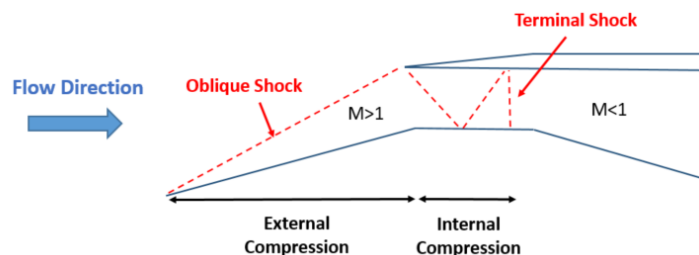
Figure 1.4 Schematic of Mixed Compression Inlet

1.1.3. Operation Characteristics

A supersonic inlet can operate in three modes: critical, subcritical and supercritical are determined according to where the terminal shock wave is formed. Inlet operation modes are illustrated in Figure 1.5.
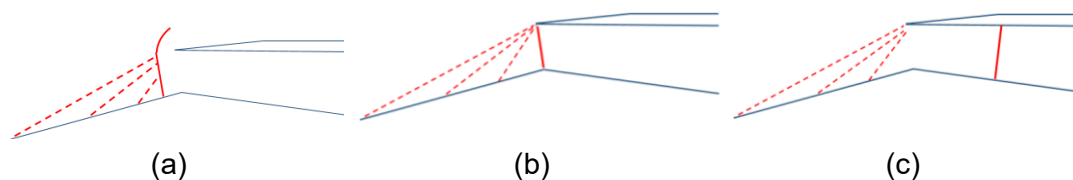
Figure 1.5 (a) Subcritical (b) Critical (c) Supercritical Operating Modes of Supersonic Inlet

Critical operation is defined as the condition in which the terminal shock located in the throat section. This is the best operational point, in terms of total pressure recovery, capture area ratio, distortion and drag. Inlets are desired to operate critically at design condition.

Supercritical operation is observed when the terminal shock is positioned downstream of the throat section. In some circumstances, the shock can moves along to the

subsonic diffuser such as when a decrease is desired in engine thrust, the fuel to air ratio should be decreased at the same time. At this condition, the terminal shock moves downstream with decreasing back pressure. In the subsonic diffuser, diverging geometry of diffuser leads to increase the flow speed. At some point, a strong terminal shock develops that causes decrease on the total pressure recovery. In addition, adverse pressure gradient effects related with shock/boundary layer interaction can trigger flow separation and decrease the uniformity of the flow. Whereas supercritical operation decreases performance of the inlet, it is a stable operation. When disturbances are disappeared, the terminal shock moves forward and repositions on the throat [1].

In the subcritical operation, the terminal shock is moved forward (upstream) of the throat. This condition is generally referred to as the inlet unstart condition. The shock can move upstream from the throat plane due to viscosity effects, some disturbances such as wind gusts, combustor pressure oscillations, error in metering fuel flow (instrumentation), and ablation of thermal protection material. In this region total pressure recovery is close to the critical point and the inlet supplies require flow with low distortion. But an amount of flow spills from inlet around cowl, so this adds rapid and dramatic increase in drag to aircraft. In the subcritical operation, the stability problem can occur and there is a potential to lost flight control at unstart point [2]. As a historical incidence, SR-71 aircraft which is equipped with a mixed compression inlet suddenly decelerated and caused the pilot's helmet hit to the cockpit canopy due to unstart event [6].

1.1.4. Viscosity Effects and Stability Problem

The stability problem is closely related with viscosity of the fluid. The flow can separate where the adverse pressure gradient effects are strong enough; such as along short designed ramp, the interior of the duct and along subsonic diffuser [1].

In the supersonic diffuser, boundary layer devices could use to provide transition from laminar to turbulent flow as a remedy for boundary layer separation. However,

transition is natural or by control devices; boundary layer separation could not prevent if adverse pressure gradient exceeds critical value. Figure 1.6a illustrates the pressure increase in the supersonic diffuser [1].

In the throat, the terminal normal shock wave is formed. Boundary layer and shock wave interact with each other. Abrupt change of the pressure behind the shock wave causes boundary layer separation. Furthermore, boundary layer could cause a series of shock discontinues along throat section called shock train that effects the health of flow behind throat and on subsonic diffuser [1]. For mixed compression inlets, oblique shocks are reflected into the duct. Similar to the terminal normal shock, oblique shocks interact with boundary layer at some downstream location. Shock wave/boundary layer interaction is illustrated in Figure 1.6b.

(a)   (b)
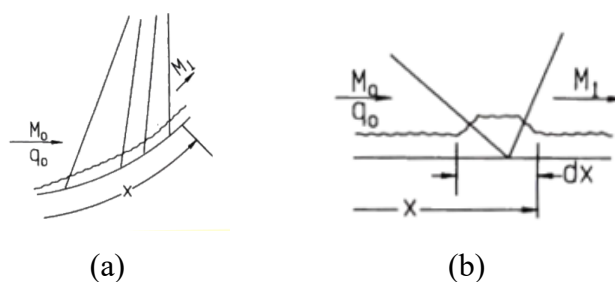
Figure 1.6 (a) Adverse Pressure Gradient at Supersonic Diffuser (b) Shock
Wave/Boundary Layer Interaction [1]

In addition, boundary layer could separate subsonic diffuser with highly divergent curvature angle. Flow could not adhere to surface with decreasing energy and adverse pressure gradient effects as shown in Figure 1.7.
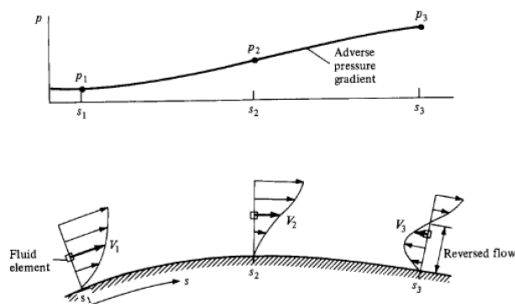
Figure 1.7 Adverse Pressure Gradient Effects at Subsonic Diffuser [7]

8

The characteristic of a supersonic inlet according to capture area ratio and the total pressure recovery is given in Figure 1.8. This diagram also named as "mass flow characteristic curve" or referred to "cane curve". As can be seen in the Figure, the critical operation point is favorable due to high total pressure recovery and capture area ratio performance. Since an aircraft is desired to operate in the critical operation. However, if boundary layer separates from surface, the flow area behind the interaction region reduces and prevents the desired amount flow move downstream. With increasing back pressure, the terminal shock moves from the throat region to the ramp section and an amount of flow spills from inlet around cowl which causes rapid increase on drag of aircraft. If the flow rate drops below a certain value which is last stable point in the Figure; low frequency, high amplitude pressure oscillation called "Buzz" phenomena occurs. At this unstable region, the terminal shock moves forward and backward [8]. If the situation that cause "buzz" is not eliminated, this cycle will continue until the engine is damaged. "Buzz" is usually related with a large amount of flow separation [2].
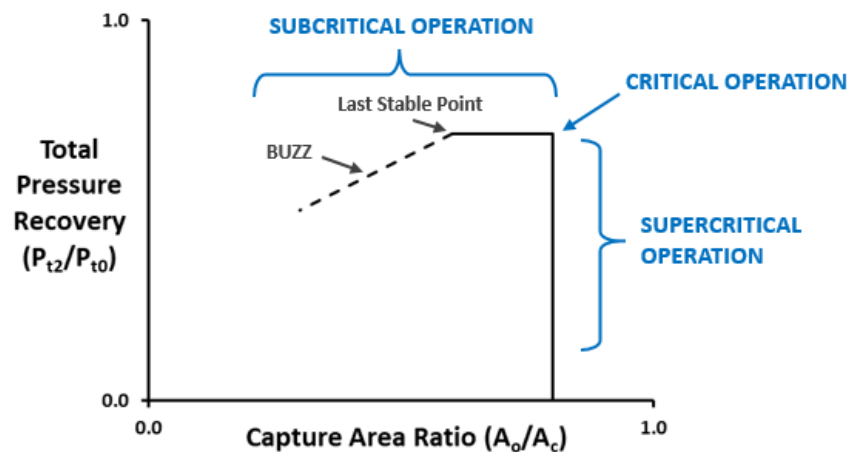
Figure 1.8 Operation Modes for Supersonic Inlet [1]

Designers especially working on mixed compression inlets prefer to avoid subcritical operation and set stability margin as large as possible to avoid unstable operation. Inlets are typically designed to operate in the supercritical region by adjusting throat

Mach number slightly greater than speed of sound. Therefore, a margin of safety is provided to inlet unstart [9].

Even if sufficient stability margin is provided, additional measures should be taken for mixed compression inlets due to the unstart problem, mixed compression inlets cannot swallow the terminal normal shock back to the throat section. There are some countermeasures to re-start the inlet: fast reactive bypass doors, adjustable throats or fuel flow adjustment at combustor [5]. But these solutions increase unit cost and weight of the aircraft; and also, decrease thrust and controllability of aircraft [2].

1.2. Boundary Layer Bleed Systems

Boundary layer separation can be overcame with an increase in length of the supersonic diffuser, the throat section and decrease in the divergence curvature angle of subsonic diffuser. However, aircraft geometrical and weight constraints restrict overall length of the inlet for design process in industrial applications [1].

Boundary layer bleed systems have traditionally been used in supersonic inlets to increase stability margin and efficiency of a supersonic inlet in order to prevent flow separation from adverse pressure gradient. Bleed systems remove the lower momentum part of the boundary layer in the areas where the boundary layer is thickened and under influence of the adverse pressure gradient. Bleed flow taken into plenum section can be used for subsystem of aircraft or discharged to overboard [2]. In Figure 1.9, typical bleed positions for a mixed compression inlet are shown.
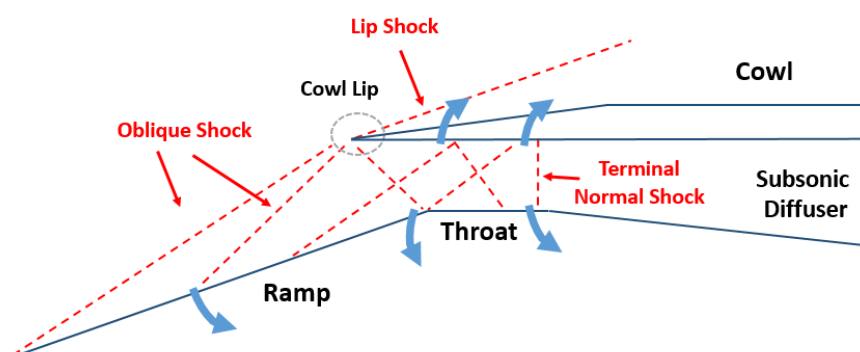
Figure 1.9 Typical Bleed Positions for Supersonic Inlet

In literature, there are many other flow control techniques; such as standard or micro vortex generators, tangential blowing, inlet wall cooling, plasma actuators, passive cavities/slots and air-jet vortex generators. Reviewing literature did not bring any information indicating these techniques have been employed in industrial applications, except vortex generators. In addition, these techniques considerably increase complexity, cost and weight of inlet [10]. Whereas vortex generators are commonly used for re-energizing the boundary layer flow and remediation of subsonic diffuser performance, there is high risk of damaging propulsion system by structural fatigue if vortex generators are used on areas like supersonic diffuser and throat section where high pressure oscillations occur [11].

Boundary layer bleed systems also have two advantages over other flow control alternatives. Firstly, engine-inlet matching problems cause movement of the terminal shock back and forth in the inlet. Movement of the shock position can be slightly suppressed by adjusting bleed mass flow. Also, especially for mixed compression inlets, boundary layer thickening can cause over-contraction and subcritical operation in severe cases. Boundary layer bleed system can diminish the boundary layer displacement effects [10].

In Figure 1.10, wind tunnel test data collected for typical mixed compression inlet configurations from literature [12]–[16] are shown. Digitized data are sketched as percentages of bleed over total pressure recovery. Although inlet configurations have different performance characteristics with percentage of bleed flow, at low values of bleed mass flow only 1% bleed flow increases total pressure recovery of the inlet by 10%. The further increase in bleed flow increases the efficiency of the inlets. But the rate of increase is slower. Moreover, as can be seen in the Figure, a number of inlets do not operate without bleed flow.
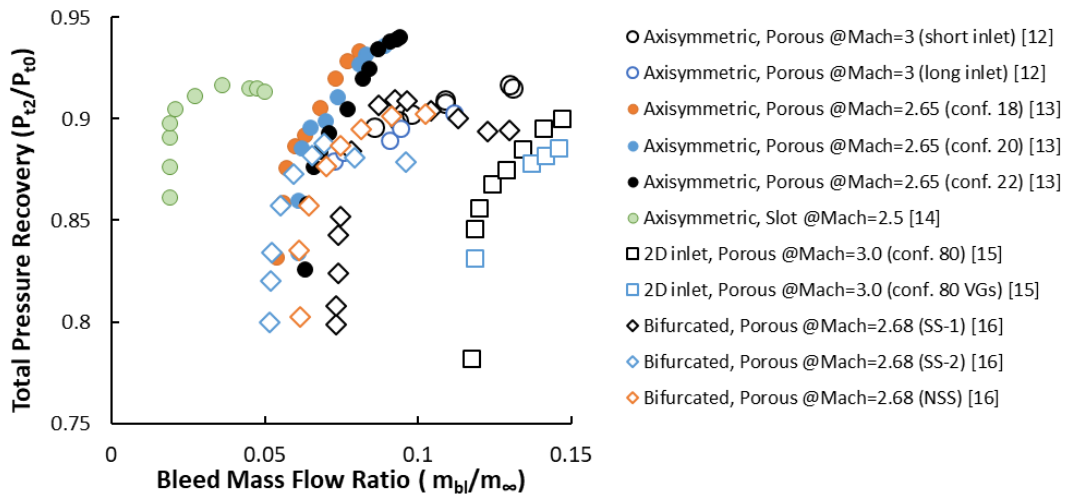
Figure 1.10 Effect of Bleed Flow on Inlet Performance

The presented wind tunnel test data are not based on systematic exploration of all independent parameters of bleed design. Hence type of inlet configuration and different combination of bleed parameters can lead to significant change on inlet efficiency.

1.2.1. Classification of Bleed Systems

Bleed systems can be classified as performance and stability bleed according their role and positions on the inlet. Performance bleed systems are used for suppressing shock boundary layer interaction effects and inlet instabilities by reducing the effective inlet contraction ratio. Stability bleeds reside just downstream of throat and primary role is stabilize the terminal shock position on inlet by using as a shock trap [9].
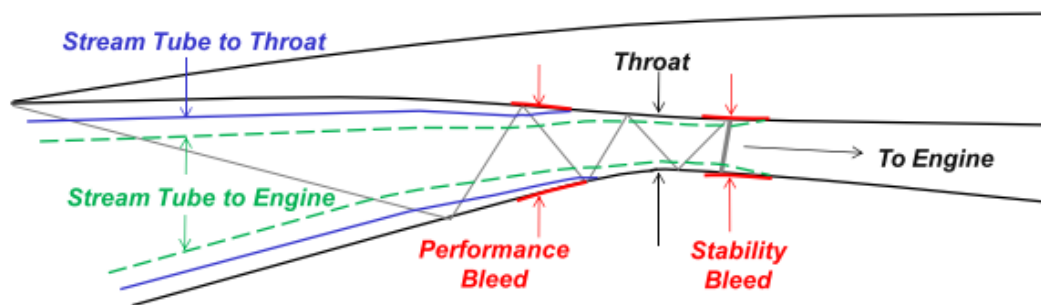
Figure 1.11 Performance and Stability Bleeds [9]

In addition, boundary layer bleed systems can be broadly classified into three types; slot, ram and porous bleed. The visualization of bleed types is given in Figure 1.12a, Figure 1.12b and Figure 1.12c, respectively. Flush slot bleed is generally used as a shock trap in throat section, increase stability by controlling terminal shock position to avoid buzz. Although bleed flow rate is higher over porous bleed holes, slot bleed position could not be effective in wide area where shock/boundary layer interactions can occur. Ram bleed type, which is also called scoop bleed, has similar application with slot bleed. However, there is possibility to ingest more than required bleed flow with ram bleed at off design conditions [1]. Porous bleed type, which is also called distributed bleed, is widely used due to its ease of geometrical modification. Bleed holes can be specified any size, and pattern modification (switch on-off with a simple dental plaster) can be done easily during wind tunnel tests [1]. In addition, porous bleed is favorable using as a stability bleed to control flow on large area if the shock / boundary layer interaction area changes with operation. Therefore, it is commonly used in mixed compression systems to prevent the effects of the final terminal shock and shock reflection [2].
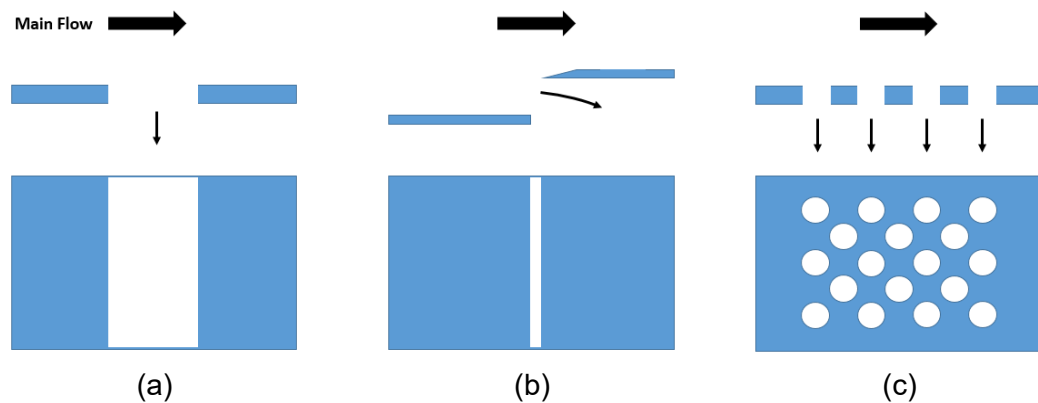
Figure 1.12 Side and Top Views of (a) Slot, (b) Ram and (c) Porous Bleed Systems

In early times of development of supersonic inlets, external compression inlet tests were conducted with preferring slot and ram bleed configurations. The bleed types were used as a shock trap at the well-known position of the terminal shock wave. Ongoing studies show that distributed bleed using as a shock trap can give high

performance as good as slot and ram bleed. In addition, porous bleed systems were preferred in the design of mixed compression inlets that have complex flow structure along duct. Nowadays, inlet designers tend to prefer porous bleed over slot and ram bleeds, because of advantage on usage flexibility of porous bleed configuration and slot and ram bleed has also negative effect on structural integrity [10].

The study is focused on the investigation of porous bleed configuration because of strengths on boundary layer control over other flow control options. In addition, in the field of porous bleed system, there are still unclarified issues and areas to be investigated and improved.

1.2.2. Sonic Flow Coefficient

Amount of bleed flow extracted by the bleed system is typically represented by the sonic flow coefficient, Q_{sonic}. Sonic flow coefficient is defined as the ratio of the actual bleed flow rate to the mass flow rate at choked condition which defines the maximum mass flow rate. The sonic flow coefficient represented by;

$$Q_{sonic} = \frac{W_{bl}}{W_{sonic}} \qquad (1.6)$$

General form of mass flow rate is designated as

$$W = \rho \, A \, V \qquad (1.7)$$

To express mass flow rate equation with Mach and total properties of freestream, ideal gas law, isentropic relations and speed of sound relation are used.

İdeal gas law:

$$P = \rho R T \qquad (1.8)$$

Isentropic flow relations:

$$\frac{T_t}{T} = 1 + \frac{\gamma - 1}{2} M^2 \tag{1.9}$$

$$\frac{P_t}{P} = \left(1 + \frac{\gamma - 1}{2} M^2\right)^{\frac{\gamma}{\gamma-1}} \tag{1.10}$$

Speed of sound can be expressed as

$$a = \sqrt{\gamma R T} \tag{1.11}$$

Rearranging the equation (1.7) with combining the equations (1.8)-(1.11), the general form of mass flow rate can be described as

$$W = A\, P_t\, M \left(\frac{\gamma}{R\, T_t}\right)^{1/2} \left(1 + \frac{\gamma - 1}{2} M^2\right)^{\frac{-(\gamma+1)}{2(\gamma-1)}} \tag{1.12}$$

W_{bl} is actual bleed mass flow rate through the entire bleed holes:

$$W_{bl} = A_{bl}\, P_{t,bl}\, M_{bl} \left(\frac{\gamma}{R\, T_{t,bl}}\right)^{1/2} \left(1 + \frac{\gamma - 1}{2} M_{bl}{}^2\right)^{\frac{-(\gamma+1)}{2(\gamma-1)}} \tag{1.13}$$

W_{sonic} is a reference flow rate calculated by assuming isentropic conditions through the bleed holes with sonic flow *(M = 1)* within the bleed holes based on flow properties at total condition:

$$W_{sonic} = A_{bl}\, P_{t,e} \left(\frac{\gamma}{R\, T_{t,e}}\right)^{1/2} \left(\frac{\gamma + 1}{2}\right)^{\frac{-(\gamma+1)}{2(\gamma-1)}} \tag{1.14}$$

The flow coefficient is commonly evaluated against plenum total pressure ratio coefficient which is the ratio between the plenum static pressure and the freestream stagnation pressure. Figure 1.13 shows the general behaviour of Q_{sonic} along the plenum total pressure ratio. The trend is generally resembled and called "cane curves" like the characteristic of the supersonic inlet. The range of plenum pressure ratio decreases with plenum pressure and Q_{sonic} increased until levelling up to the choked value.
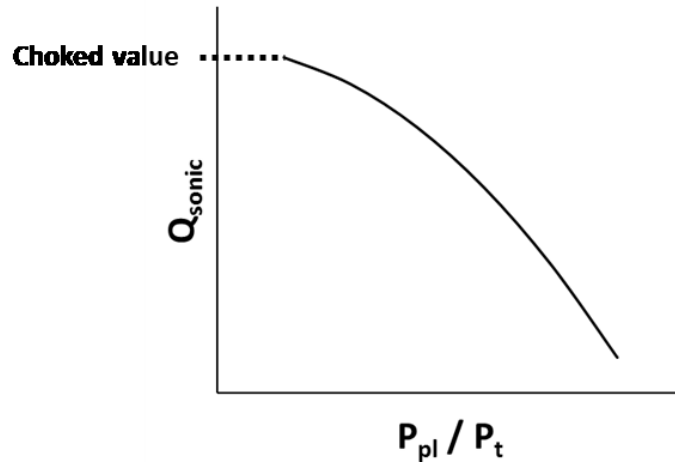
Figure 1.13 Q_{sonic} versus Plenum Total Pressure Ratio

1.2.3. Effective Parameters on Porous Bleed Systems

The effective parameters can be assigned in two subgroups: aerodynamic and geometrical parameters. Aerodynamic parameters can be counted as free stream conditions, approach boundary layer characteristics, and plenum static pressure which influence the flow properties in the vicinity of bleed holes. The list of aerodynamic parameters are given below.

Table 1.1 Aerodynamic Variables

$P_{t,\infty}$	freestream total pressure
P_∞	freestream static pressure
M	Mach number
P_{pl}	plenum static pressure
δ^*/θ	health of the boundary layer
Re	Reynolds Number

In addition, geometrical variables such as bleed shape, bleed porosity influence the amount of bleed flow. General description of geometrical parameters are illustrated in Figure 1.14.

16

	L/D: hole aspect ratio
	α: hole inclination angle
	R: hole corner radius
	Y/D: transverse spacing
	Y'/D: intercolumn spacing
	X/D: streamwise spacing
	A/A': entrance area to exit area ratio

(a) Porosity parameters   (b) Shape paremeters
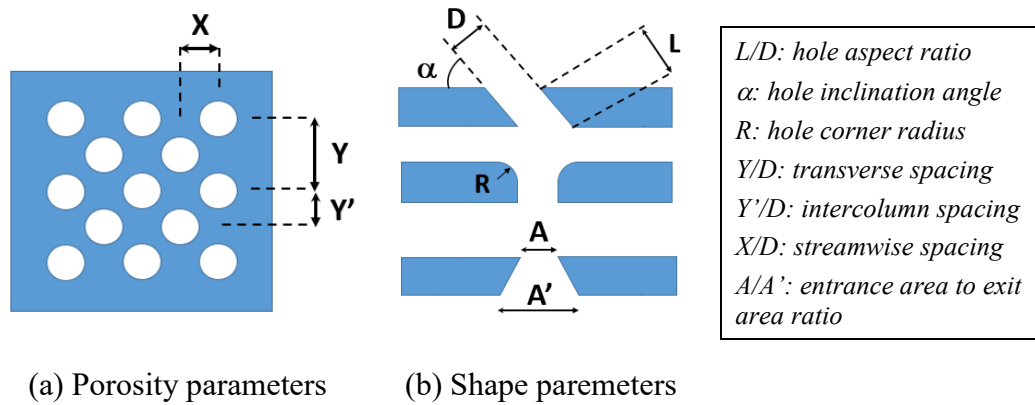
Figure 1.14 Geometrical Parameters on Bleed Holes [6]

The experimental studies [6], [17]–[20] are not sufficient to examine the effects of all parameters on the bleed flow. The studies mainly concentrate on Mach number, plenum static pressure, Reynolds number, hole aspect ratio, inclination angle of the hole axis and hole spacing (porosity).

The preliminary flow parameters that drive bleed flow is boundary layer edge Mach number and total plenum pressure ratio for a given hole geometry. As given experimental data [6] in Figure 1.15, the Q_{sonic} values increase significantly as Mach number decreases regardless of the hole inclination angle. The greatest level of Q_{sonic} occurs at the lower Mach numbers (e.g., Mach 1.27). The secondary effective parameter is inclination angle of the hole axis. In the Figure given below, in addition to the effect of Mach number on the amount of bleed, comparison of normal bleed hole, which is inclined 90° to surface, and 20° inclined hole test data are also performed. The 20° inclined hole configuration has almost three times of maximum Q_{sonic} than the normal bleed configuration. However, Q_{sonic} data is very sensitive to plenum static pressure and suddenly decreases at high total plenum pressure ratios. Sudden changes on Q_{sonic} makes difficult to obtain precious bleed flow and control propulsion system according to bleed rates. Furthermore, Eichorn [20] indicates that large flow instability occurs during testing of the 20° bleed holes. For these reasons, normal bleed hole configuration is investigated throughout the present study.
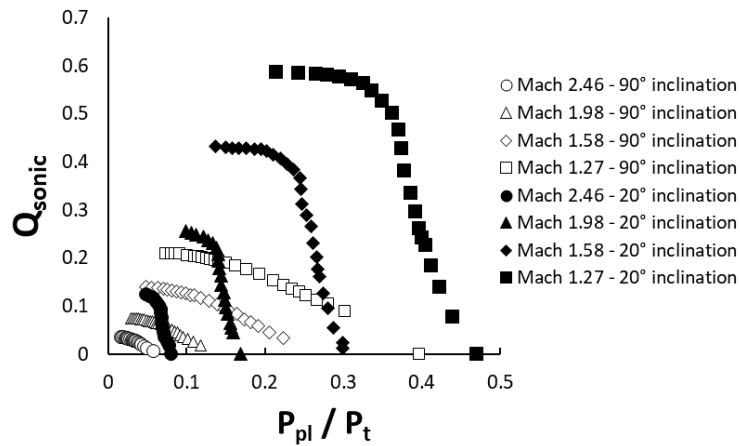
Figure 1.15 Q_{sonic} Variation According to Mach Number and Inclination Angle [6]

Bleed porosity is another effective parameter on bleed flow. Willis, et al. [6] stated that mutual interaction around the holes exists and this influence is not only about hole to hole interactions, but rather each row of holes is influenced by a different flow field. Also CFD analyses [21] show that local pressure increases at the downstream row of holes. In Figure 1.16, Q_{sonic} trends of single and multiple holes are plotted at Mach 2.0 and 2.46. As Bodner [18] pointed out that multiple hole interaction are negligible at Mach 2.46 whereas the test data for Mach 2.0 shows multiple holes have slightly better performance on Q_{sonic}. It should be noted that non-dimensional Q_{sonic} data are similar at Mach 2.46, whereas the actual flow rate changes in the order of number of holes in a porous region.
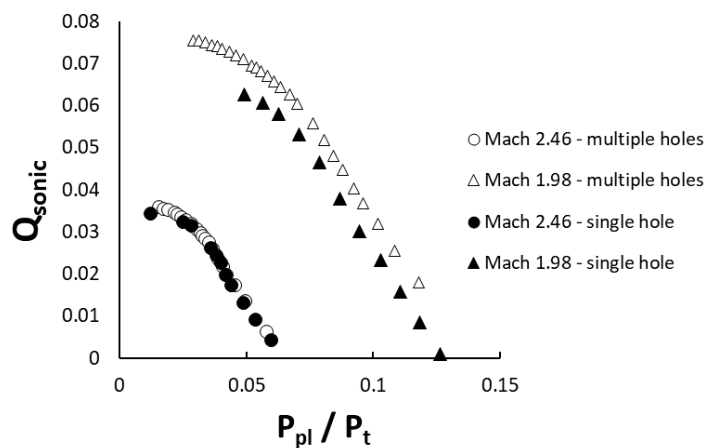
Figure 1.16 Q_{sonic} Variation According to Porosity [6]

18

Hole aspect ratio (*L/D*) can be counted as one of the secondary priority parameters on bleed flow. Previous tests [20] show that the characteristic of Q_{sonic} curves slightly change with hole aspect ratio. In the Figure below, hole aspect ratio comparison is done for normal bleed hole configuration using digitized data. Although the choked value of Q_{sonic} does not significantly change for normal bleed holes, the angle of rotation and trend of the curves vary with hole aspect ratio. It should be emphasized that for 20° inclined holes the behavior is different.
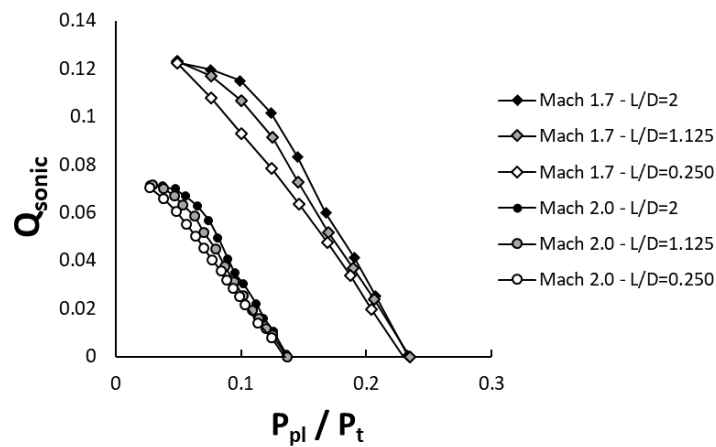
Figure 1.17 Q_{sonic} Variation According to Hole Aspect Ratio [20]

Reynold number effects are also investigated on bleed flow. Wind tunnel studies at Mach 1.3 show that Reynold number does not cause a remarkable change on Q_{sonic} data. In addition, CFD results [22] have shown that although Reynolds number has significant effect on stream-wise velocity profiles, the stagnation pressure distortion and secondary flow behind the bleed, no effect on sonic flow coefficient is observed.

1.2.4. Flow Structure around Bleed Hole

CFD simulations on bleed flow give opportunity to examine the flow structure, shock interactions effects in the vicinity of bleed holes. These flow data are very valuable to understand flow physics behind the bleed phenomena and give insight to develop BBC modeling.

The first study in CFD which is introduced shock structure in the bleed hole is performed by Shih, et al. [23]. The schematic diagram of flow structure of bleed hole is given in Figure 1.18a. A sample Mach contour through bleed hole obtained from CFD analysis [24] is also shown next to the diagram. As the flow moves on flat plate rotates downward into the hole when it reaches the forward part of the hole. This leads to formation of Prandtl-Meyer expansion waves and the flow accelerates into the hole. Accelerated flow impacts with back side wall of the hole. By compression-corner effects, some part of the flow moves on inside the bleed hole according to turning angle and forms one segment of the barrier shock, while other part of the flow leads to formation of second barrier shock above the flat plate. This formation is generally called "two segment shock system". The trailing vortices are generated on both forward and back lip of the hole. Turning angle is strongly dependent on plenum static pressure and flow properties around the bleed region. If the turning angle is not large enough, both segments do not form, and subsonic flow regions are observed.

(a)   (b)
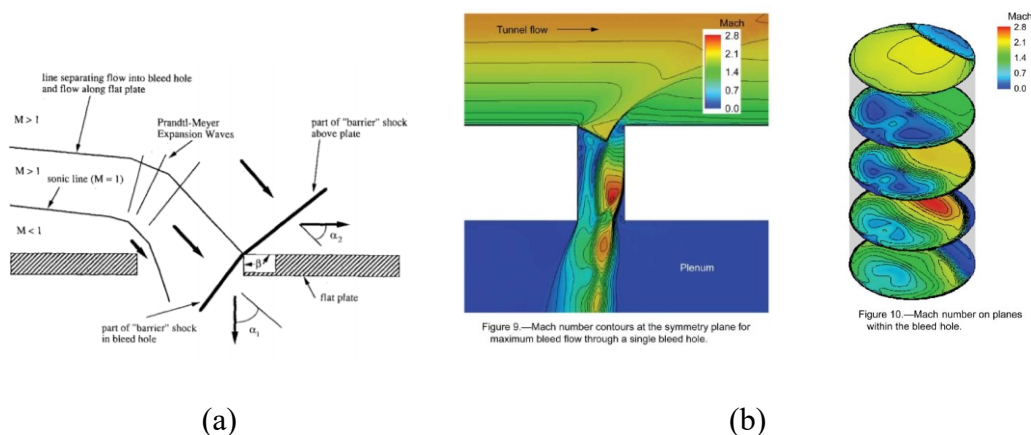
Figure 1.18 (a) Schematic Diagram the Flow Structure of Around Holes [23] (b) Mach Number Contours at the Symmetry Plane and within the Holes [24]

1.2.5. Design of Boundary Layer Bleed Systems

The inlet design is evaluated by considering the aircraft's operational flight envelope and performance requirements. Because modern aircraft systems do not allow optimization at a single operational point, optimization of propulsion sub-system

design especially boundary layer bleed system is one of the most challenging problems to find good compromise for providing adequate overall performance work on whole operation conditions. Bleed systems have an essential role in the performance of the supersonic inlets which should supply convenient airflow to the engine to obtain required thrust at low speeds and operate safely at high altitudes [4].

The proper amount of bleed flow suction is important for the overall performance of the inlet. If more than the required amount of flow is discharged, high momentum flow in the boundary layer is removed and total engine performance losses occur. In addition, the bleed system weight and drag force increase with over bleeding. Thus, the correct estimation of the amount of bleed and position is needed for the bleed system design process. Especially, the process becomes highly complicated for inlets, shock/boundary-layer interaction occurs at the internal part of the inlet [5].

Furthermore, efficiently overboard the bleed flow from the inlet increases the complexity of the problem. Bleed system requires lower exit static pressure over inlet's local surface pressure to maintain bleeding, else blowing phenomena occurs. Lower exit pressure is obtained by converging-diverging nozzle connecting plenum to freestream with the choked flow at the nozzle throat and the size of the nozzle throat area determines the plenum static pressure. Adequate plenum pressure is determined with bleed position and area related to the flow structure of the inlet. So, in order to prevent the recirculation of holes, bleed plenums are connected freestream separately. For design simplicity, the bleed holes can be adjusted to operate continuously at choked condition in order to keep bleed rates under control. However, this can cause an unnecessary increase in bleed drag. To provide the desired amount of bleeding effectively, keeping plenum pressure at a constant level is an improved method. In addition, controlling the bleed flow by adjusting the exit nozzle area is another way to control bleed rates. However, this technique increases complexity, cost and weight and require more space for the bleed system [25].

Studies related evaluation of bleed systems have been carried out over the past 60 years. In early examples, little information about bleed flow was known and wind tunnel testing was unique for inlet design and performance assessment of bleed system. Baseline of the inlet geometry and bleed locations were determined by means of theoretical calculations. To determine the adequate bleed location, translating supersonic diffuser or cowl was employed. In addition, to find best performance, testing a set of different bleed configurations was an customary procedure to evaluate bleed system performance [3], [12]–[15]. This method has also been used in a relatively recent test study [16].

However, wind tunnel testing is costly and requires a lot of time for preparation and conduction. Besides these, the optimization of the bleed system is highly iterative. Hence, analytical methods were introduced to the design of a bleed system [26]. The methods were based on empirical calculations which are a combination of theoretical assumptions and experimental data. But test models based on empirical data were very complex, and could not cover all topics about the bleed flow physics and effect on supersonic inlet [3]. Although analytical methods have provided improvements in defining the initial geometry and estimating the preliminary performance of an inlet, extensive wind tunnel testing was still required to evaluate accurately bleed system performance and fine-tuning the geometry [27].

Furthermore, much simpler bleed model tests were conducted to examine the flow around the hole and obtain more detailed information about the bleed flow. The first test, particularly on the bleed system, was conducted by McLafferty and Ranard [17]. The test data is used in analytical methods to explain basic behavior of the bleed flow for many years. However, the test model has only two rows of holes and any hole to hole interaction could not be observed in the flow [6].

The development of computer technology and advances in computational fluid dynamics (CFD) have provided the opportunity to calculate and visualize complex inlet flow fields. In this field, a number of numerical simulations have been carried

out to investigate bleed flow phenomena [23], [28]–[31]. But, CFD codes were limited with computational storage and speed of hardware to solve each discrete bleed hole. Another difficulty was the lack of accurate turbulence models. In that period, early empirical boundary condition studies for bleed flow were performed and numerical solutions were investigated [27], [31], [32]. Unfortunately, experimental data was not sufficiently available in detail especially local bleed rates to verify the accuracy of the computational methods. Also, these tests were used primarily to check for the two-dimensionality of the flow [33]. Thus, there was a need to increase test data that can be used in validation studies and cover the more issues in bleed flow.

In the 1990s, researchers at the NASA Lewis Research Center initiated an experimental program within the scope of the High-Speed Research Program to investigate the porous bleed systems [6], [18], [34], [35]. It is aimed to investigate effective parameters and flow structure in the bleed systems [6], and obtain data for verification and validation studies in computational fluid dynamics (CFD) [18]. These wind tunnel test results are widely used in CFD studies with many researchers [21], [24], [36]–[38].

Despite of successful studies in CFD, since the porous surfaces can be composed of hundreds of small holes, the design and optimization of bleed systems with modelling the bleed plenum chamber and cavity details demands high computer resources and it is not feasible even with the current computer capabilities. Therefore, CFD studies have been carried out to define a realistic boundary condition to predict bleed flow rate and simulate overall effect on the flow field where the bleed holes are located. These models are combination of theoretical and empirical approaches which are based on flow properties of the bleed regions or individual bleed holes.

1.3. Bleed Boundary Condition Modeling

The most commonly studied approaches are to assume the hole region as a single surface without modeling the hole cavity and the plenum [27], [31], [32], [39]–[42]. Local bleed rates and velocity components are calculated according to flow properties

at the solution points in the bleed region. The distributed hole effects of the entire bleed region are obtained instead of the individual effects of the holes [24]. Hence the flow structure around the bleed holes and effects on boundary layer are not considered in the simulations. Also, blowing phenomena is generally omitted in these models.

One of the first investigations of BBC on individual hole openings was studied by Benson, et al. [43]. In the study, four different boundary condition were applied to hole openings without model hole cavity and plenum details. The flow structure and Mach, Pressure contours of simulation results were evaluated with comparing fully resolved model (FRM) simulations which refers to analyses are performed with modelling the plenum and the hole cavity details. One except other three BBC models gained success for the prediction of Mach and Pressure distribution in flow domain. "Avg W BC" which refers to a boundary condition implied constant velocity profile over each bleed opening captures well the barrier shock formation. The method's main drawback is all boundary condition need priori knowledge about amount of bleed flow. Although the study gives very useful information about several boundary condition alternatives for bleed flow, the preliminary aim of bleed boundary condition modelling, estimation of bleed flow rates, is not covered and clarified.

Bunnag [25] developed a BBC model based on Prandtl-Meyer expansion theory which is an analytical representation of the flow structure within the hole. The model predictions are matched well with experimental data except for the choked flow rates and the data obtained near sonic conditions. Despite these progress, Bunnag's method assumes static pressure of the flow is equals to the plenum static pressure after expansion process and the analytical model only takes into account on vertical direction of turning flow into the hole, lateral effects are omitted. The model also omits blowing effects when the turning flow impacts with the back side corner of the hole. Furthermore, Morell [44] improved the model by taken into account these assumptions. CFD simulations on the case without shock interaction accomplish improvement on predictions however shock interaction effects in the bleed region still is not captured well. Nevertheless, both methods require modeling of some part of

hole cavity in order to perform the analytical approach and this increases grid size and complexity of modeling.

Since, in the present thesis, it is aimed to develop BBC model to estimate bleed rates and simulate the flow structure in the bleed regions as effortless as possible, the studies on bleed boundary condition modelling is concentrated on the approaches in which the BBC can be defined without need to model any detail of the hole cavity. Thus, Bunnag or Morell's methods are not evaluated for the further studies. The efforts on new BBC modeling in this study is based on two significant method that should be emphasized. In the following sections, detailed information about the two method is given and discussed.

1.3.1. Mayer and Paynter Bleed Boundary Condition Model

Mayer and Paynter [31] introduced a new BBC to evaluate bleed performance. Past studies on BBC modeling had been performed with omitting the unsteady effects on mass flux change when a shock moves over bleed region [32], [27]. Effects of shock position is important because static pressure increases ahead of the shock and consequently mass flow rate increases across the bleed holes. Mayer and Paynter developed a method for BBC modeling and AIP boundary condition to investigate unsteady effects on inlet flow. The local bleed rate is calculated according to boundary layer edge flow properties shown in Figure 1.19, a lookup table based on past experimental data [17], [26] and pre-defined constant plenum pressure [45].
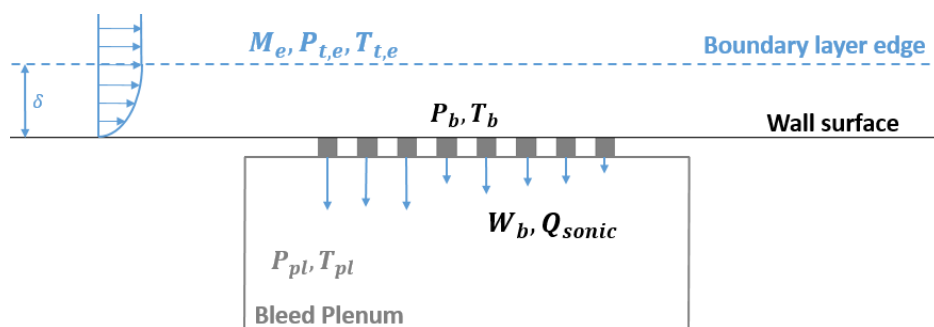
Figure 1.19 Schematic View of a Porous Bleed System

A supersonic inlet study [46] performed in 2005 is an example of the usage of this method. The method is implemented to Wind-US CFD code and CFD analysis results compared with experimental data which are well matched with each other. In addition, the implementation improved to fixed exit bleed plenum model rather constant pressure bleed model which requires complex control system to adjust pressure with changing the bleed plenum nozzle exit area [45].

The main difficulty of using the method is that it is required to obtain boundary layer edge flow properties (M_e, $P_{t,e}$, $T_{t,e}$) correctly for bleed rate calculations. However, a bleed region significantly affects the flow around it and boundary layer edge flow properties. In addition, it is very complex to determine the location of each grid on boundary layer edge especially if bleed region is under influence of a shock wave. Also unstructured grid modeling increases the difficulty [24]. Thus, bleed rate calculation based on lookup table gives incorrect estimations if the boundary layer cells are not determined correctly. One other drawback is that this method does not allow injection (blowing) when plenum static pressure is greater than the static pressure of the bleed surface [45].

In Figure 1.20, the validation study [45] performed using Mayer and Paynter method with fixed exit modification is given. The validation studies were performed on well-known experimental test cases. Open symbols refer to experimental data for different test conditions and curves with solid symbols show the method's results. Simulation results are sufficiently accurate except for zero bleed boundary conditions and the results for Mach 1.27. Slater illustrates Q_{sonic} estimations using lookup routine for Mach 1.27 and Mach 1.38 with dashed curves. Although experimental data at Mach 1.27 fit with the lookup routine, it is understood that the boundary layer edge flow properties are more compatible with Mach 1.38. In the porous bleed case with an oblique shock interaction, Figure 1.20b shows that the method estimates lower bleed rates at the choked condition. In addition, the method cannot produce reliable data at high plenum total pressure ratio conditions. As mention before, blowing phenomena is not taken into account in this method.

Figure 1.20 Mayer and Paynter Method Validation Study on (a) Porous Bleed System (b) Porous Bleed System with Shock Interaction [45]

1.3.2. **Slater Bleed Boundary Condition Model**

In 2009, Slater published the study about improved boundary condition method for 90° bleed holes [24]. The improvement in the method is that bleed flow velocity components at each grid point in the bleed region is estimated according to local surface flow properties instead of the boundary layer edge values. Since local flow properties can be obtained more easily and accurately, the implementation of the method to a solver is simpler and simulations are performed more efficiently compared to Mayer-Paynter method. Another improvement in the method is that Slater used relatively recent wind tunnel test data which have more detail information about bleed flow. Also, this method allows flow injection to the main flow according to local static pressure values.

W_{sonic} parameter is commonly calculated using flow properties at stagnation condition of the freestream, whereas Slater's method references sonic flow coefficient based on the static pressure and temperature at the local surface or boundary. The subscript "b" refers to the boundary value.

$$W_{sonic,b} = A_{bl} P_b \left(\frac{\gamma}{R \, T_b}\right)^{1/2} \left(\frac{\gamma + 1}{2}\right)^{\frac{-(\gamma+1)}{2(\gamma-1)}} \qquad (1.15)$$

The boundary sonic flow coefficient can be defined as

$$Q_{sonic,b} = \frac{W_{bl}}{W_{sonic,b}} = \frac{W_{bl}}{W_{sonic}} \left(\frac{W_{sonic}}{W_{sonic,b}}\right) \qquad (1.16)$$

The equation (1.16) can be arranged with evaluation of equation (1.13) and (1.15):

$$Q_{sonic,b} = (\frac{P_{t,e}}{P_b})(\frac{T_b}{T_{t,e}})^{1/2} \qquad (1.17)$$

To calculate bleed flow rates according to surface flow properties, some assumptions are required to be made.

$$\frac{P_{t,e}}{P_b} \cong \left(1 + \frac{\gamma - 1}{2} M_e^2\right)^{\frac{\gamma}{(\gamma-1)}} \qquad (1.18)$$

$$\frac{T_b}{T_{t,e}} \cong 1 \qquad (1.19)$$

Lastly, the scaled parameters can be calculated with following equations:

$$Q_{sonic,b} = Q_{sonic} \left(1 + \frac{\gamma - 1}{2} M_e^2\right)^{\frac{\gamma}{(\gamma-1)}} \qquad (1.20)$$

$$\frac{P_{pl}}{P_b} = \frac{P_{pl}}{P_{t,e}} \left(1 + \frac{\gamma - 1}{2} M_e^2\right)^{\frac{\gamma}{(\gamma-1)}} \qquad (1.21)$$

Figure 1.21 shows comparison between original parameters based on boundary layer edge flow properties and the scaled parameters using equation (1.20) and (1.21).

As can be seen in Figure 1.21b, inflow Mach number dependency are eliminated by the scaling operation, $Q_{sonic,b}$ data collapse for the various Mach numbers.
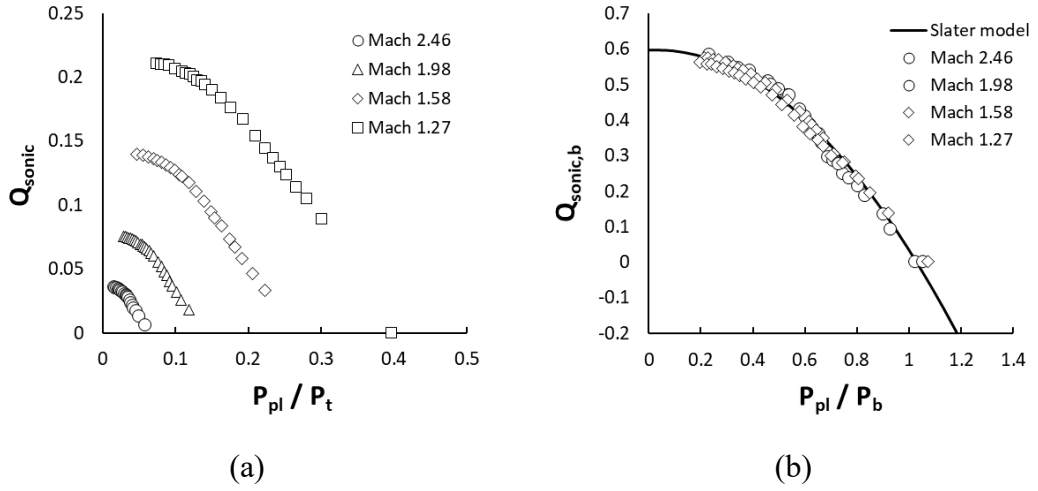
Figure 1.21 Scaling of Q_{sonic} (a) Original coefficients (b) Scaled Coefficients [24]

Moreover, the following 2nd order quadratic polynomial curve fitting, which is only a function of the ratio of plenum static pressure to the surface static pressure, is applied to $Q_{sonic,b}$ data in Figure 1.21b.

$$Q_{sonic,b} = -0.593614 \left(\frac{P_{pl}}{P_b}\right)^2 + 0.030693 \left(\frac{P_{pl}}{P_b}\right) + 0.597997 \qquad (1.22)$$

It should be noted that, the bleed flow rate becomes zero at a static pressure ratio of approximately 1.03 where the surface static pressure is slightly lower than the plenum static pressure. These phenomena can be addressed to dynamic or ram effect of the holes [24].

In addition, the method can calculate blowing mass flow rate along negative $Q_{sonic,b}$ values according to the fitted curve. Even though any wind tunnel data is not available to evaluate the scale parameters for blowing phenomena, negative mass flow rates can be obtained by using equation (1.22) with unknown accuracy.

Validation studies for the method are carried out by Slater [24] for the bleed systems with and without shock interaction and the results are compared with Mayer-Paynter method simulation results [24]. In Figure 1.22, The Mayer-Paynter bleed model results

are denoted by the solid symbols and the open symbols show the results for Slater bleed model that implemented to CFD simulations using the curve fitting model.

(a)

(b)

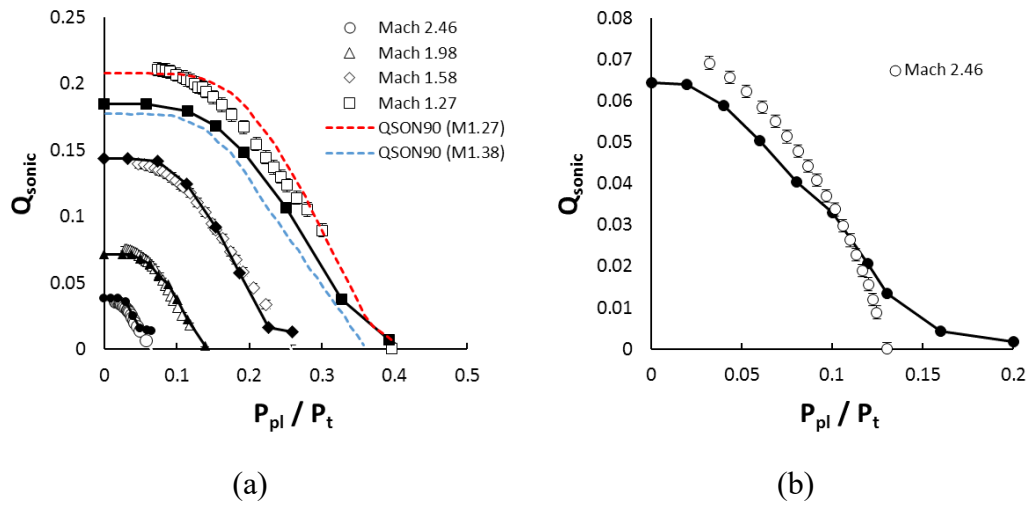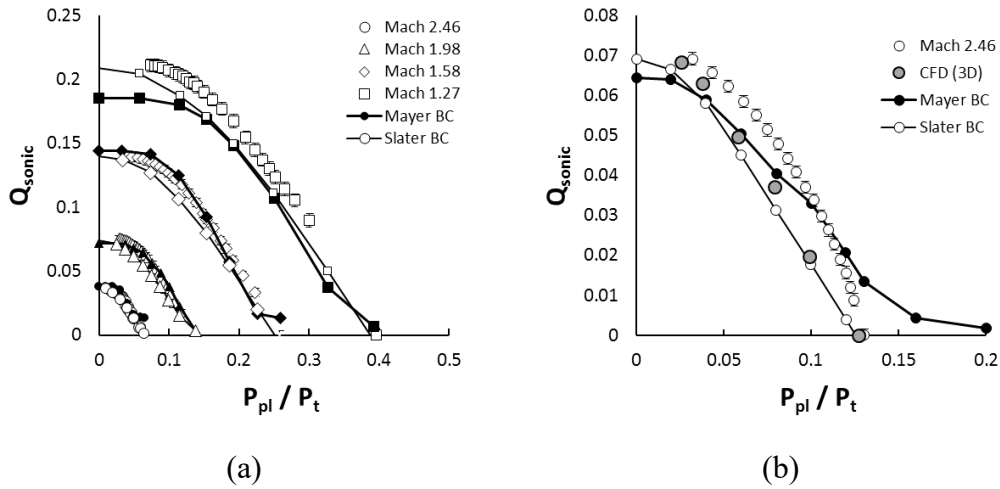Figure 1.22 Comparison of Mayer and Slater's Method Validation Study on (a) Porous Bleed System (b) Porous Bleed System with Shock Interaction [24]

The most noticeable improvement of Slater method is better prediction of the bleed rates near to the zero bleed conditions. In addition, Slater method estimates the choked bleed rates close to the experimental results. The results of the case with an oblique shock show that Slater's BBC results are compatible with three-dimensional solutions although the three dimensional simulations give lower bleed rates. Slater indicates that turbulence modeling may be the cause of the differences with the wind tunnel data.

The model is implemented to Wind-US CFD code [24], VULCAN Navier-Stokes code [47] and Overflow CFD solver [48]. CFD analysis results are generally matched well with the experimental data. In addition, an optimization study [49] is conducted by applying Slater method using surface patches on cowl and throat sections. Although the study lacks comparison with a wind tunnel data, baseline inlet model efficiency is increased up to 5%.

Although Slater model has achieved considerable success on BBC modeling, the method neglects the individual effects of bleed holes and flow expansion effects are

30

weaker through the main flow. Hence, neither three-dimensional bleed effects on downstream region nor surface pressure distribution around the holes are not correctly captured.

Wukie, et al. [48] evaluated three different boundary conditions on bleed flow: mass flow outlet, pressure outlet and Slater model. In addition, for all boundary conditions discrete hole and distributed applications are investigated and simulation results are compared. The analysis results show that if boundary conditions implied on discrete holes; downstream effects in terms of vorticity, total pressure and boundary layer turbulence quantities are matched well with full resolved CFD solutions on the contrary of distributed hole modeling. Illustrations of velocity contours given in Figure 1.23 and Figure 1.24 taken from the study shows that Slater method cannot capture the expansion and barrier shock formation at the downstream of the bleed region and within the bleed holes as fully resolved simulations. The effort on implementing Slater method to discrete hole openings did not succeed while the approach underestimates bleed rates approximately by 25%.
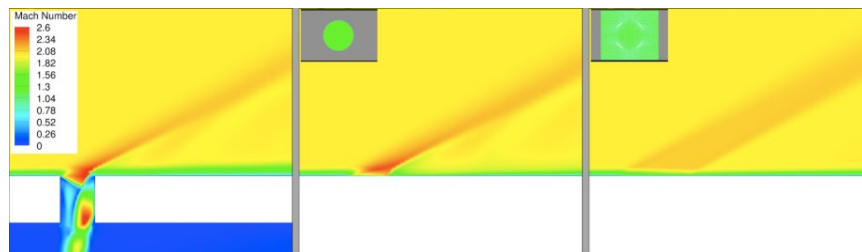
Figure 1.23 Comparison of Mach Contours on Symmetry Plane for P/P_∞=0.254 [48]

Figure 1.24 Comparison of Velocity Contours in the Vicinity of Bleed Hole for P/P_∞=0.254 [48]

1.4. Objectives of the Thesis

In this thesis, first objective is to obtain and present detailed information about the effects of the bleed flow to the supersonic inlets and understand physics on bleed flow control. Secondly, it is aimed to assess the success of the CFD method and the unstructured grid modeling technique on simulation of the porous bleed systems. Lastly, the major objective of the thesis is to introduce a new boundary bleed condition model to predict bleed flow rates correctly and simulate the flow structure in the vicinity of the holes and downstream of the bleed region without model bleed plenum and cavity details.

1.5. Outline of the Thesis

The first chapter is devoted to general information of the supersonic inlets; compression types, operation characteristics, viscous effects and stability problem. Literature survey is carried out about bleed boundary layer control systems; performance effects on supersonic inlets, types of bleed configuration, effective parameters on typical design process and the flow structure around bleed holes to understand the flow physics related with the thesis topic. In addition, the bleed system performance evaluation and analyses are discussed with emphasis on how analysis techniques are developed and applied on bleed systems.

In Chapter 2, the methodology used in validation and bleed boundary condition modeling studies in computational fluid dynamics (CFD) is presented. Firstly, general and integral form of the conservation equations are informed. Solid modeling, grid generation steps and solution strategy of CFD are explained in detail. Then, methodology about development and implementation of new bleed boundary condition models to the solver is explained. Finally, the approach on estimation accuracy and uncertainty of the CFD simulations are described.

In Chapter 3, CFD analyses are performed on full resolved models (FRMs) of the single and porous bleed systems for validation of the engineering approach. Due to the ease of modeling on complex geometries, it is intended to evaluate the unstructured

grid modeling. Grid converge study is conducted to find optimal grid resolution and turbulence model for bleed flow. CFD analysis results are compared with wind tunnel test data and reference CFD simulations. End of the chapter the analysis results and the flow structure around the bleed region are discussed to understand the physics behind the bleed flow.

In Chapter 4, three new bleed boundary condition (BBC) models are introduced. Additional CFD analyses on the porous bleed case are performed including blowing effects to examine the correlation between mass flow rate and flow properties at the reference boundaries. For each reference boundary, the data are collected and discussed according to scaled parameters. The deviations between the data and curve fitting models are calculated to select the best model for implementation to the solver.

In Chapter 5, In order to evaluate the validity of BBC modeling alternatives, CFD studies are performed on the porous bleed systems with and without shock interaction with the implementation of new BBC models to the solver. Approaches on solid modeling, grid generation studies for the BBC models are described. The analysis results for the BBC models are plotted along with the test data and the FRM simulation results. For examining flow structure around the bleed holes, visualizations of flow domain are presented. The deviations between the FRM and the BBC model results are calculated to measure the accuracy of the predictions.

Lastly, in the conclusion chapter, the summary of the present study is explained. The new BBC models are discussed considering strengths and drawbacks in terms of potential application opportunities. In addition, possible improvement areas in the bleed modeling are presented as future works.

CHAPTER 2

METHODOLOGY

In this chapter, the methodology used in the validation and bleed boundary condition modeling studies in CFD is explained. Firstly, general and integral form of the conservation equations are informed briefly. Solid modeling, grid generation steps and solution strategy of CFD are explained in detail. Then, the methodology of implementation of new BBC models to the solver is explained. Finally, approaches on estimation accuracy and uncertainty of the CFD simulations are described.

2.1. Governing Equations

In this thesis, CFD simulations are performed with using commercial ANSYS FLUENT software. The analyses are solved as steady-state, compressible form of Reynolds-Average Navier-Stokes equations. Methodology of flow solver will be described in the following sections.

2.1.1. Fluid Dynamics

Numerical solution is mainly based on conservation of mass, momentum and energy equation. General forms of conservation of mass also referred continuity is given below.

$$\frac{\partial \rho}{\partial t} + \nabla \cdot (\rho \vec{v}) = S_m \tag{2.1}$$

where ρ is the density, t is the time, $\vec{v}$ is the velocity vector and S_m is the source term represent addition of mass caused by vaporization or used defined sources, etc. This form is acceptable for both compressible and incompressible of flows [50].

Conservation of momentum can be written as

$$\frac{\partial(\rho\vec{v})}{\partial t} + \nabla \cdot (\rho\vec{v}\,\vec{v}) = -\nabla p + \nabla\,(\bar{\bar{\tau}}) + \rho\,\vec{g} + \vec{F} \qquad (2.2)$$

In the equation, p represents the static pressure, $\bar{\bar{\tau}}$ is the stress tensor, $\vec{g}$ is the gravitational acceleration and $\vec{F}$ is the external body force that contains other source terms related porous media or user defined sources, etc. also covers other source terms[50].

The stress tensor is described as

$$\bar{\bar{\tau}} = \mu\left[\,(\nabla\vec{v} + \nabla\vec{v}^T) - \frac{2}{3}\nabla.\vec{v}\,I\,\right] \qquad (2.3)$$

where μ and I represent the molecular viscosity, the unit tensor, respectively.

Conservation of energy can be expressed as

$$\frac{\partial(\rho E)}{\partial t} + \nabla.\left(\vec{v}(\rho E + p)\right) = \nabla.\left(\sum_j h_j \vec{J}_j\right) + S_h \qquad (2.4)$$

Where h_j and $\vec{J}_j$ represent the entalphy and the diffusion flux of species j. S_h is the source term contains the energy contributions such as the chemical reactions or user defined heat sources, etc [50].

Partial differential form of system of equations (2.1)-(2.4) is known as Navier Stokes equations. Since Navier-Stokes equations consist of five equations, the system of equations have seven unknowns which are *ρ, u, v, w, E, p and T*. Two additional definition are necessary to solve the problem. In the simulations, the flow is specified as compressible. Therefore, ideal gas assumption is applied to flow. The equation is stated as;

$$P = \rho RT \qquad (2.5)$$

For second equation, dynamic viscosity μ is calculated by mean of Sutherland's law;

$$\mu = \frac{1.45 \, T^{0.75}}{T + 110} 10^{-6}$$

(2.6)

2.1.2. Turbulence Modeling

ANSYS FLUENT solver includes various turbulence models; such as Reynold averaged Navier-Stokes (RANS) models, Reynold Stress models, detached and large eddy simulation models. There is no general acceptance on a single turbulence model for all types of fluid problems, the choice of turbulence model depends on physics of the flow problem, and adequate method should be determined by considering the limitations and capabilities of the models.

RANS models solve time averaged (ensemble-averaged) Navier-Stokes equations. For industrial fluid problems, RANS models are widely used and preferred over other methods with trade off between the level accuracy and computational cost. Brief information about Spalart-Allmaras (S-A), the two-equation Realizable k-ε and SST k-ω turbulence models are given in the following sections.

2.1.2.1. Spalart-Allmaras Model

The Spalart-Allmaras is one equation turbulence model. For the kinematic turbulent viscosity, additional transport equation are solved by the model [51]. The model is originally introduced for general aerospace problems. The model is particularly successful for flow simulations that subjected to adverse pressure gradients and preferred commonly in turbomachinery applications. However, the model is not developed for general industrial fluid problems. Especially for plane and round jet flows, large errors can be observed [50].

2.1.2.2. Two-equation Realizable k-ε Model

The Standard k-ε is two equation turbulence model based on model transport equation for turbulent kinetic energy (k) and turbulent dissipation rate (ε). Two separate transport equations are solved to determine a turbulent length and time scale [52]. The model is widely used for simulation of practical engineering flow applications due to

robust, inexpensive and relatively accurate predictions of the model. The standard model is only valid for fully turbulent flows because model neglects the effects of molecular viscosity. Therefore, the model is improved with modifications to improve performance. Realizable k- ε model is one of the modified versions of the original form [53]. With the approach on certain mathematical constraints on the Reynolds stress, the model is titled as "realizable". Realizable k- ε model has superior performance over other available k- ε model in the solver for separated flows and flows subjected to complex secondary flow features. Whereas for axisymmetric jet flows, the spreading rate is predicted poorly [50].

2.1.2.3. Two-equation k-ω SST Model

The Standard k-ω turbulence model solves transport equations for turbulent kinetic energy (k) and specific dissipation rate (ω). Hence the model is classified as two equation turbulence model. The standard model in the solver based on the Wilcox model [54]. The model has satisfactory performance on simulation of low Reynolds number effects, compressibility and shear flow spreading. But the standard model is very sensitive to freestream flow outside of the shear layer.

The shear-stress transport (SST) k-ω model is improved version of the standard model [55]. The model is a combination of the k-ω model and k-ε model that uses k-ω formulation in the near-wall region with k-ε model in the far field away from surface. With this modification, the model has becomes reliable for use in wider area of industrial applications [50].

2.2. Numerical Tools and Numerical Simulation Methodology

In this section, solid modeling, grid generation methods, boundary condition definitions and solution strategy for CFD simulations are explained in detail.

2.2.1. Solid Modeling, Grid Generation and Boundary Condition Definitions

The solid models of the bleed cases are generated with GAMBIT version 2.4.6 commercial meshing program. For the single hole bleed system, to match inflow

approaching boundary layer flow properties in the reference line of wind tunnel, the distance between the inlet surface and the reference line is changed iterative until matching is accomplished. The matched model is used for validation studies performed on the single hole bleed system. For the porous bleed cases, preliminary studies are carried out on similar flat plate model to match the flow properties much easier. The matched flow profiles are imposed as inlet boundary condition in the solver and grid sizes are is reduced.

Grid generation is performed with using commercial GAMBIT version 2.4.6 and TGRID version 15.0 software. One of the motivations of this thesis is to evaluate the unstructured grid modeling on bleed system analysis. GAMBIT is used to generate surface and volume mesh; boundary mesh is modeled with TGRID. Surface mesh is generated by using triangular elements. Boundary layer mesh is modeled with 25 layers of triangular prism cells for viscous wall surfaces by adjusting first height and setting growing rate to 1.10. First height is determined to provide y^+ values close to 1.0. The first 10 of prism cells grow exponentially and the growing ratio of the other 15 layers is adjusted to provide that aspect ratio of last layer is 50%. After boundary layer meshing, volume grid is generated using tetrahedral elements and grow rate is preserved as 1.10. Maximum element size of volume elements is determined as 0.4 diameter of holes.

(a) Triangle   (b) Triangular Prism   (b) Tetrahedron
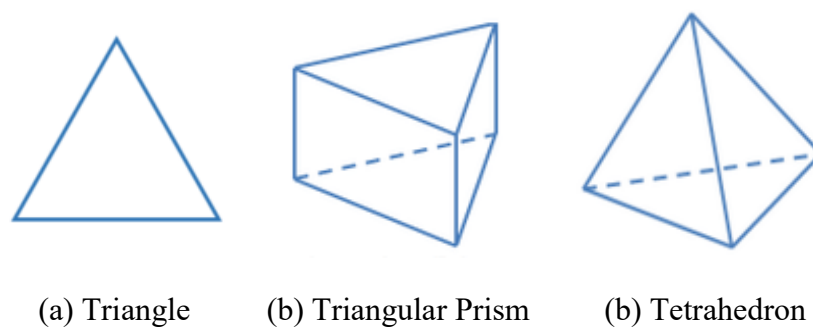
Figure 2.1 Grid Element Types

Grid sensitivity analyses are carried out on different size of grids for each validation cases. Minimum element size of the grids is defined dependent to the hole diameter.

CFD studies are performed using three turbulence models that are given detail information in Section 2.2.2. Converged CFD simulations on different level of grids are presented. Optimal grid size and turbulence model are determined for bleed flow. Neither additional converge study, nor turbulence model comparison is performed for CFD analyses of new BBC models. The determined grid size and turbulence model is used for the further analyses.

Boundary conditions are defined similarly for the CFD simulations, whereas different approaches are applied for some special cases. As mention before, boundary layer grows naturally in the wind tunnel test section and matching inflow flow properties with the reference line is required. Hence pressure inlet boundary condition is defined on the inlet surface for single hole bleed case. Total pressure and static pressure are adjusted iteratively to match approaching boundary layer flow properties. For the porous bleed cases, matched inflow profile determined from preliminary studies on similar flat wall is imposed as inlet boundary condition to decrease computational time and grid size. Pressure outlet boundary condition is identified to the outlet and the plenum exit. Defined static pressure on the outlet is not taken into account by the solver. Due to the flow speed is greater than the speed of sound, the solver judges as a supersonic outflow boundary condition. On contrary, defined static pressure on the plenum exit leads to vary the overall bleed flow through the plenum. Desired bleed mass flow rate is obtained by adjusting the pressure on the plenum exit. Wall boundary condition is identified for bottom surface, where bleed openings are placed; top surface, bleed sides and plenum surfaces. It is considered that top surface has no influence on bleed flow, so inviscid wall boundary condition is applied. All other wall surfaces are specified as adiabatic, no-slip wall boundary condition.

In addition, the suitable boundary condition on bleed openings are studied before evaluation of the BBC models. In the solver, several outlet boundary conditions can be defined: velocity-inlet, pressure-outlet, mass-flow outlet. Velocity-inlet boundary condition can be applied as an outlet boundary condition but it is not suitable for compressible flow and leads to a nonphysical result [56]. In addition, defining pressure

outlet boundary condition on bleed opening requires unreasonable solution process to match desired flow rates. Because the BBC models are estimated bleed flow rate using average static pressure value on the reference boundary. As all outlet boundary condition alternatives are examined, the mass flow outlet boundary condition is considered the most appropriate method and BBC modeling studies are carried out defining mass flow outlet boundary condition on bleed openings. As details given in Section 2.3, the BBC models are implemented ANSYS FLUENT with user defined functions (UDF) and mass flow outlet boundary condition is applied by imposing desired bleed mass flow rate on bleed hole openings.

2.2.2. Computational Fluid Dynamics Solver

CFD analyses of the porous bleed case are performed with using commercial ANSYS FLUENT software version 15.0 with Reynolds-Average Navier-Stokes equation solver. Three dimensional, compressible, steady state, Reynolds-Averaged Navier-Stokes equations are solved by density based finite volume method. Solver setting are adjusted Roe flux difference-splitting method based on node based calculation. The simulations are performed using Spalart-Allmaras (S-A) or the two-equation Realizable k-ε or SST k-ω turbulence models.

For validation studies on fully resolved models (FRM), a similar solution procedure described by Slater [24] is preferred to converge simulations more smoothly. The initialization in all domain cells is done by inlet flow properties. At the beginning, plenum exit surface boundary condition is specified as wall. Hence zero bleed flow is imposed. The analyses are initially started with first order discretization then switch to second order discretization after a certain solution iteration. After domain flow properties is settled down and plenum exit surface pressure approaches to bottom wall pressure, pressure outlet boundary condition is applied on the plenum exit surface. Finally, plenum exit pressure is decreased step by step and the bleed flow rates are obtained for different plenum total pressure ratios.

A different solution strategy is applied for the BBC modeling simulations. Since bleed holes and the plenum are not modeled, the solution behavior is much stable. To obtain bleed rates for different plenum total pressure ratios, the analyses are started with adjusting desire plenum pressure value in the UDFs. In the solution process, UDFs are compiled after the initialization, and mass flow rate is evaluated and imposed to the bleed openings for each solution iteration according to the reference boundary properties. As similar to validation studies, the analyses are started with first order discretization then switch to second order discretization after a certain solution iteration.

Convergence criteria for validation studies are specified as residual levels reduced to 10^{-3} levels and the percent change of mean of bleed flow is dropped below to %1 in the last 10000 iterations. CFD analyses of the BBC models are much stable and the analyses require less solution iterations. Hence percent of change of mean bleed flow is monitored in the last 1000 solution iterations to check that the convergence criteria is met.

2.3. Implementation of New Bleed Boundary Condition Models to the Solver

ANSYS FLUENT allows to utilize custom fluid properties by user-defined function (UDF) implementation. Standard features of FLUENT can be enhanced with using UDFs. For instance, user can customize a boundary condition, material properties, source terms of transport equations, specify time dependent parameters, perform initialization, post processing [57].

UDF coding structure is compatible with C programing language. Source file can include a single or multiple UDFs. In addition, single or multiple source files can be either interpreted or compiled in FLUENT. Predefined macros supplied by FLUENT are accessed with include statement of inclusion directive of "udf.h" header file. UDFs can be executed either at the beginning or at the end of the iteration while solution process is ongoing.

In Chapter 4, three new BBC models are introduced and correlations between boundary properties with bleed mass flow are presented based on CFD solutions of the porous bleed case. For each definition, 3rd order polynomial curve is fitted to collapsed data for implementation to the solver. The implementation of these models are accomplished by means of UDFs. In order to illustrate UDF implementation, a simple representation is given in Figure 2.2 for a porous bleed region containing six holes in a row. The figure shows the working steps of UDFs for the bleed region boundary (BRB) model which uses boundary flow properties on the bleed region around the holes to predict bleed flow rate. The other models are similar in terms of UDF implementation. Detail information about BRB and other two models can be found in Chapter 4.
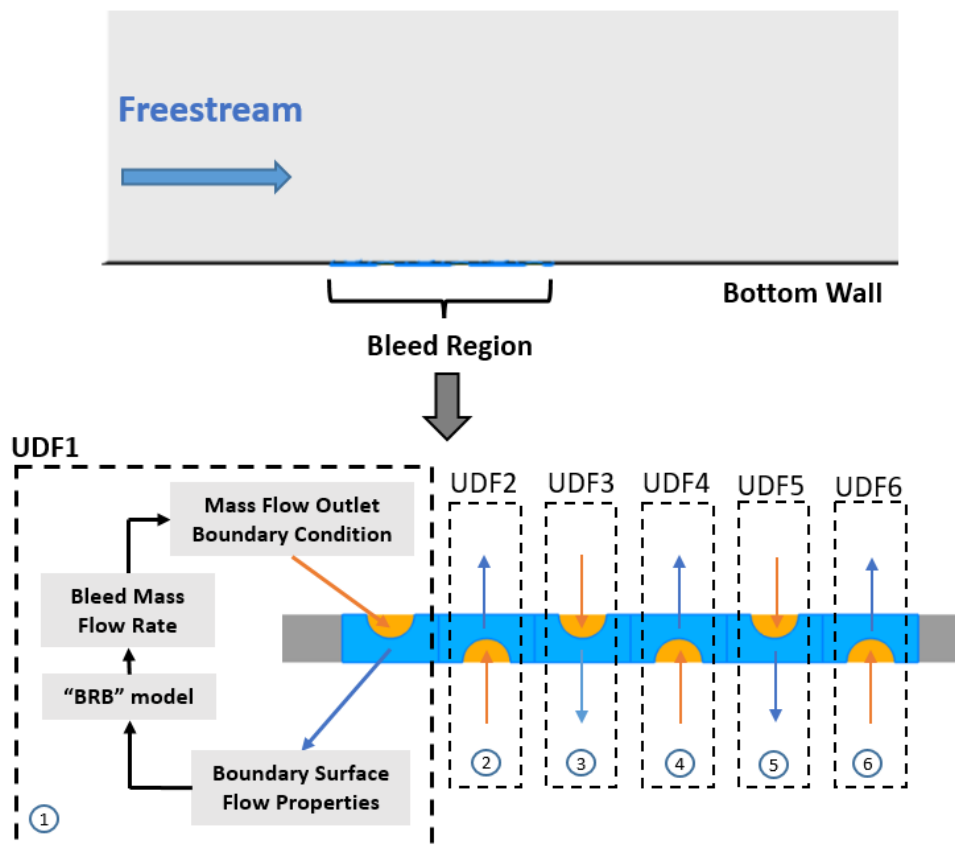

Figure 2.2 Scheme of UDF implementation

Firstly, the desired plenum static pressure should be predefined as an input parameter in UDF code. After the compilation of UDF in the solver and the simulation is started. For each solution iteration, area and surface flow properties of the reference boundary are obtained for each grid cell and area weighted average of P_b and T_b is calculated. Plenum pressure ratio (P_{pl}/P_b) and $W_{sonic,b}$ parameter (see Equation (4.1)) are determined. Then $Q_{sonic,b}$, which is a function of plenum pressure ratio, is calculated using the polynomial fitting models developed in Chapter 4. Multiplication of $Q_{sonic,b}$ and $W_{sonic,b}$ (see Equation (4.2)) gives bleed (or blow) mass flow rate. Lastly, mass flow outlet boundary condition on the bleed opening is adjusted by imposing determined mass flow rate to the solver. The mass flow rate calculation can be resulted negative (blowing) or positive (bleeding) according to the reference boundary flow properties and the plenum static pressure. The solver does not allow to impose negative value to mass flow outlet boundary condition, so mass flow direction on the bleed opening is required to be changed. Phases of UDF processing described above are performed for each solution iteration until the converged solution is obtained. It should be noted that multiple UDFs are required to implement for a porous wall. Since each hole is threated individually according to the reference boundary flow properties of the hole.

To decrease the computational time of the simulations, UDF code is parallelized by means of predefined macros in the solver. A sample UDF code developed for the BBC model is presented in Appendix A.

2.4. Evaluation of the Numerical Simulation Accuracy

In the literature, there are a number of accuracy evaluation techniques. Mean Absolute Deviation (MAD), Mean Squared Deviation (MSD) and Root Mean Squared Deviation (RMSD) are can be counted the foremost of these methods. The RMSD metric is widely used in the literature and the metric is preferred for evaluating the accuracy of the numerical simulations in the thesis. The main distinction of the RMSD

44

method to others, the difference between reference data and estimated data are squared before averaging, and a relatively high weight is applied to large deviations.

Root Mean Square Deviation (RMSD) can be expressed as following relation:

$$RMSD = \sqrt{\frac{1}{n}\sum_{i=1}^{n}\left|X_{reference} - X_{estimated}\right|^2} \qquad (2.7)$$

where X is the parameter being evaluated (Q_{sonic} or PR), and n is the total number of cases or samples.

To evaluate Q_{sonic} values in the order of the maximum bleed flow rate, the RMSD values are normalized with the choked flow rate according to the wind tunnel test data. The normalized root mean square deviation (NRMSD) is calculated as follows:

$$NRMSD = \frac{RMSD}{X_{max}} \qquad (2.8)$$

where X_{max} represents the choked bleed rate of the test data.

The percentage deviation between the reference and estimated data is calculated using the relation given below.

$$\% \ Deviation = \frac{\left|X_{reference} - X_{estimated}\right|}{X_{max}} * 100 \qquad (2.9)$$

Lower values of NRMSD and the percentage deviation indicate that a better agreement between the reference and estimated data.

2.5. Uncertainty Approach for CFD Analyses

In the CFD simulations for some cases especially near to zero bleed condition, residuals and bleed mass flow histories have an oscillatory behavior that address to unstable behavior of the physical condition since the complex flow structure and recirculation phenomena are observed around the holes. For this reason, as mentioned

in Section 2.2.2, variation of the mean value of last a certain solution iteration of the bleed flow rate evaluated as convergence criteria.

However, for data correlation studies for the new BBC models are based on the data of the last solution iteration. Necessity of introduce uncertainty variation on bleed flow is considered. Figure 2.3 shows a solution history of Q_{sonic} data for the case that oscillatory behavior is observed. The data is obtained from validations studies for the porous bleed case without shock interaction where pressure ratio parameter (P_{pl}/P_t) is 0.0580, detailed information can be found for the case in Section 3.3. As indicated in the Figure, the mean value is calculated according to the last 10^4 iterations. The converge criteria which is defined as percent different between the last 10^4 iterations to the previous 10^4 iterations is ensured less than 1%. Difference between maximum and minimum values of the last 10^4 iterations is defined as the uncertainty interval of Q_{sonic}. The percentage of uncertainty is calculated by dividing the difference to the mean value.

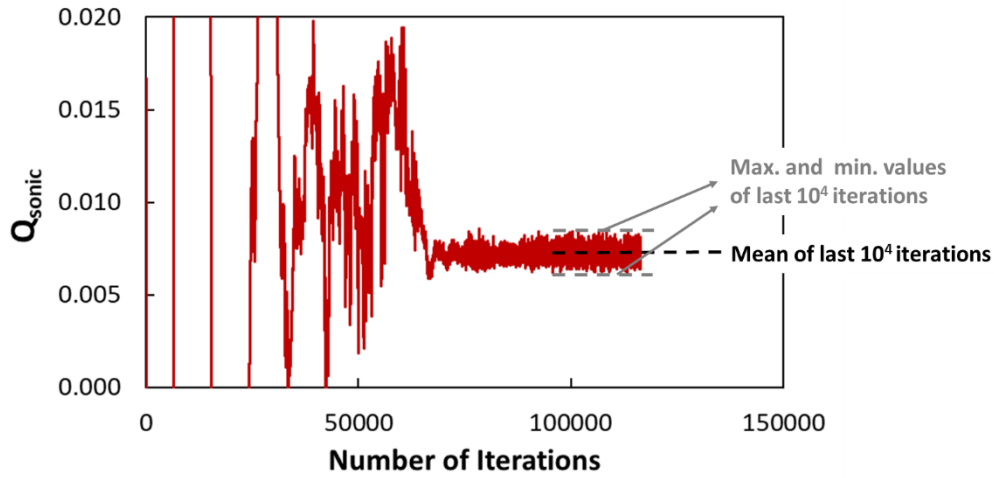Figure 2.3 Oscillatory Behavior of Q_{sonic}

The expression of uncertainty is given below:

$$\% \ Uncertanity = \left| \frac{Q_{sonic,max} - Q_{sonic,min}}{Q_{sonic,mean}} \right| * 100 \qquad (2.10)$$

46

The magnitude of uncertainty of each data is presented on graphs by the error bars. It should be noted that the error bars cannot be seen if the band is not bigger enough than the marker size.

CHAPTER 3

VALIDATION OF TEST CASES

In this chapter, CFD analyses are performed on single and porous bleed systems for validation of the engineering approach. Grid converge study is conducted to find optimal grid resolution and turbulence model for bleed flow. Due to the ease of modeling on complex geometries, it is intended to evaluate the unstructured grid modeling. Grids are generated with using commercial GAMBIT and TGRID software; and solution of the domain is performed with using commercial ANSYS FLUENT software. Details of the validation cases are given in the following sections.

3.1. Numerical Simulations of Bleed Flow through a Single Bleed Hole

In the Nasa-Lewis Research Center, wind tunnel tests were conducted to investigate the effects of the single bleed hole on a turbulent supersonic boundary-layer over a flat plate in supersonic speeds [18]. In the scope of this study, normal bleed hole configuration, which is inclined 90° to flat plate surface, is evaluated. Test section has dimensions of 15x15 cm and the bleed flow is discharged to the plenum which has dimensions of 7.3 cm diameter to 8.89 cm height. Bleed hole diameter is 6 mm and length is 12 mm; length to diameter ratio (*L/D*) is 2.
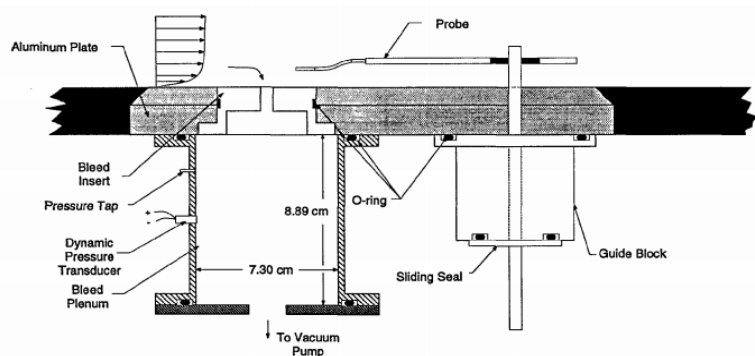

Figure 3.1 Schematic of Single Bleed Hole Test Section [18]

The boundary layer is naturally developed on the lower surface of the wind tunnel test section. The boundary layer parameters were measured with the translating pitot tube 6.25 cm upstream of the bleed hole center. Test conditions and approaching boundary layer parameters is given in Table 3.1.

Table 3.1 Test Conditions

Mach	2.46
P_t	172368 Pa
T_t	300 K
δ	1.29 cm
δ^*	0.34 cm
Re	1.69×10^7 /m

Test data uncertainty values were reported as 1.5% for total pressure measurements and 1% for sonic flow coefficient.

3.1.1. Solid Model, Grid Generation and Boundary Conditions

The geometry is modeled by defining the inlet boundary condition 91.5 cm behind the reference line, in order to match the boundary layer properties in the wind tunnel test reference line. The normalized speed profile comparison along the reference line is shown in Figure 3.6a. The solid model and the boundary conditions used in the analyses are shown in Figure 3.2. The symmetry surface is defined to reduce the total number of grid elements. The bottom, side, hole and plenum walls are defined adiabatic, no-slip wall boundary condition. It is assumed that the top wall has no effect on bleed flow, so inviscid boundary condition is applied.
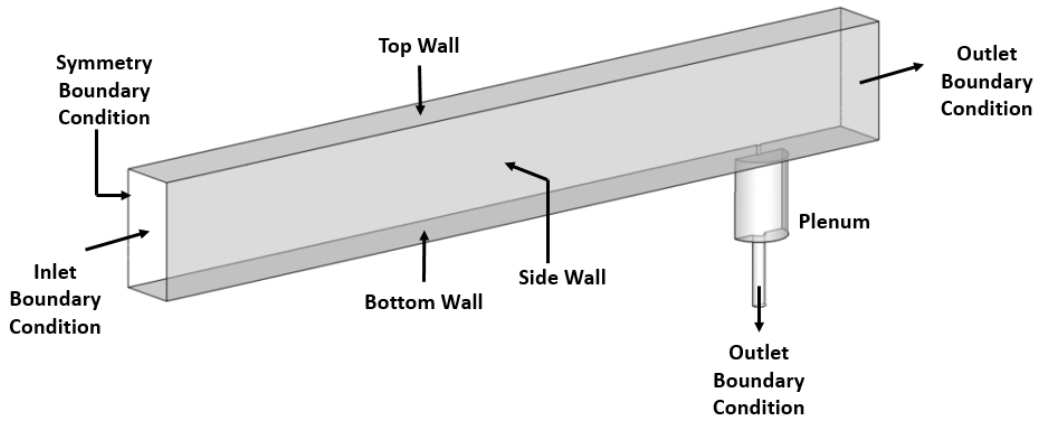
Figure 3.2 Solid Model of the Single Bleed Hole Case and Boundary Conditions

In the grid convergence study, four different grids are generated with unstructured tetrahedral elements. The total number of cells for solution domains are given in Table 3.2 and the grid structure around the hole according to mesh level is shown in Figure 3.3.

Table 3.2 Total Number of Cells of Solution Domains

	Min. Element Size [D]	Total Number of Cells
Course	0.06	0.6×10^6
Medium	0.04	1.3×10^6
Fine	0.03	2.2×10^6
Very fine	0.02	4.8×10^6

(a) Course

(b) Medium

(c) Fine

(d) Very Fine
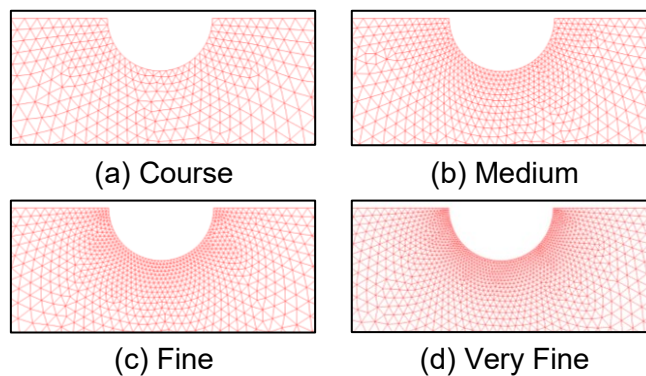
Figure 3.3 Grid Structure around the Hole According to Minimum Element Size

The grid convergence study and turbulence model comparisons are evaluated for the condition where the pressure ratio parameter (P_{pl}/P_t) is equal to 0.0348. In Figure 3.4, the change of the sonic flow coefficient according to the number of cells and the turbulence models are shown. Analyses performed using Realizable k-ε turbulence model reached only one reliable converged solution. Therefore, grid convergence study is not completed for Realizable k-ε model. In accordance with literature, it can be seen that SST k-ω turbulence model is in the best agreement with the experimental data. In addition, no noticeable differences are observed between the medium grid and the two finer grids. Thus, the medium grid is selected for further studies. The medium grid illustrations are given in Figure 3.5.

Figure 3.4 Variation of Sonic Flow Coefficient with Total Number of Cells

Figure 3.5 Grid Model of the Single Bleed Hole Case

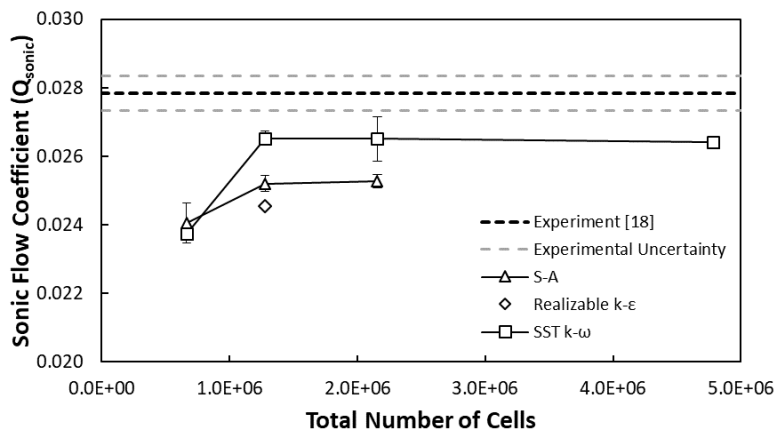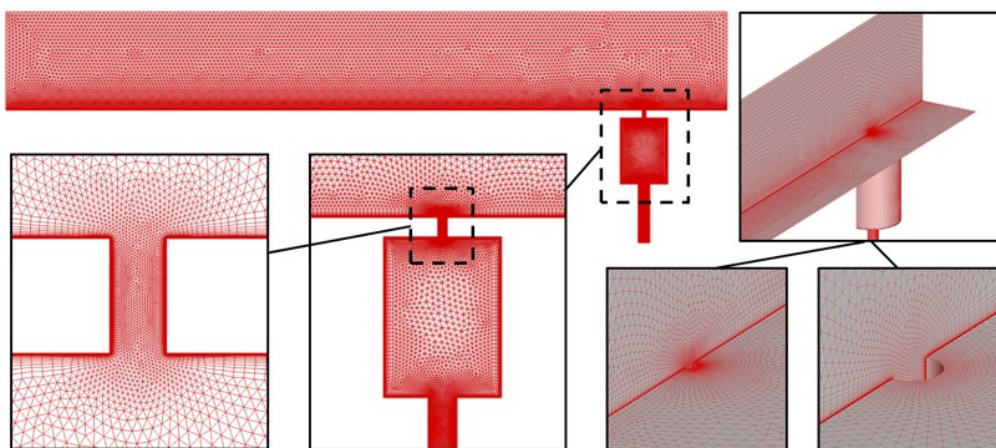The different levels of grids are modeled with a boundary layer formed in the prism-cells and unstructured tetrahedral elements. First height is determined as 0.0061 mm to obtain y^+ value around 1 for all grid models. The first height value is checked and validated from analysis results. y^+ obtained along the bottom wall for the medium grid is shown in Figure 3.6b.

(a)   (b)
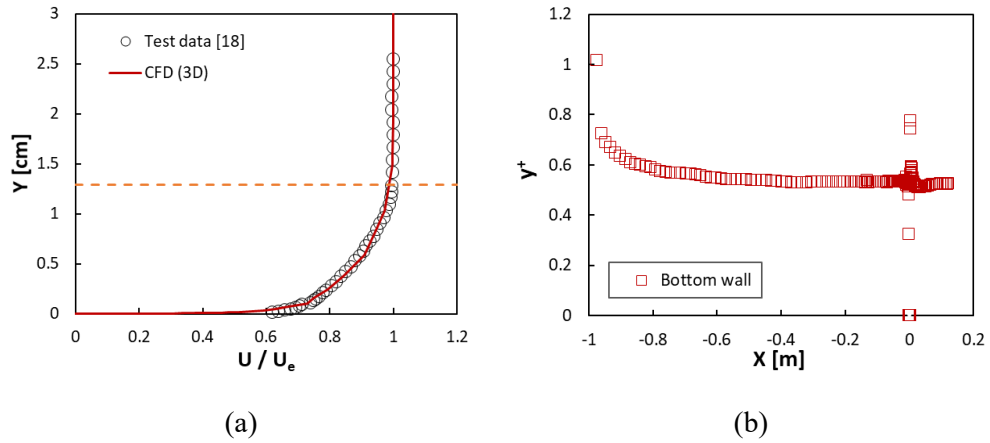
Figure 3.6 (a) The Speed Profile along the Reference Line (b) y^+ Values along Bottom Wall

3.1.2. Analysis Results

According to the grid convergence study and turbulence model comparisons, SST k-ω turbulence model and the medium grid size is determined as optimal solution method. Additional analyses are conducted for other total plenum pressure ratio points. The residuals and Q_{sonic} histories are given in Figure 3.7 for the condition where the pressure ratio parameter (P_{pl}/P_t) is equal to 0.0348. To satisfy the convergence criteria, *60K* solution iterations require for the simulation. The analysis results are plotted along with the test data and the reference CFD results as given in Figure 3.8. The CFD solutions are quite compatible with the wind tunnel test data. In addition, the percentage of deviations between CFD and experimental results are normalized with the choked value of the bleed flow and presented in Figure 3.9. In order to obtain the percentage of deviations between the test data and the CFD results, spline curves are generated for the experimental data to calculate bleed rates at the same plenum

pressure ratio condition of the analyses. The deviations are in the range of 2.1% to 8.9%, the analysis results of the case are very close to the experimental data. NRMD is calculated as 0.048 with using all the compared data points.

(a)   (b)
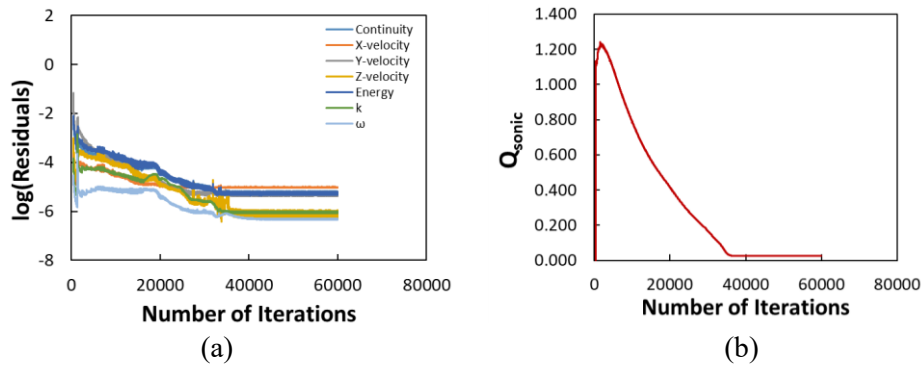
Figure 3.7 Solution Histories for (a) Residuals and (b) Q_{sonic}
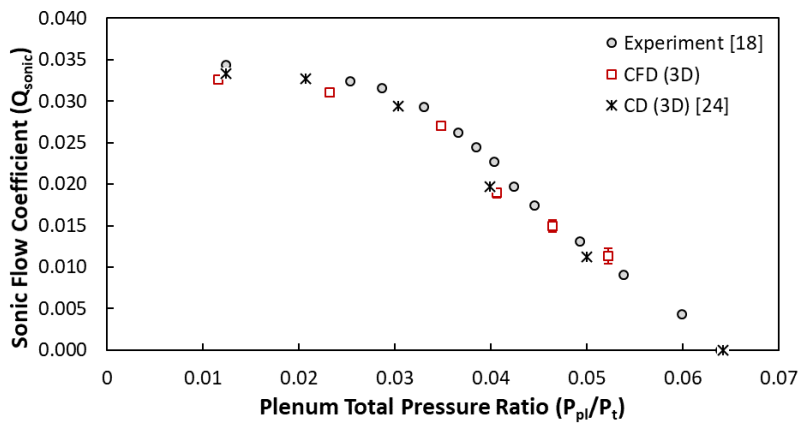
Figure 3.8 Comparison of the Results of the Single Hole Case
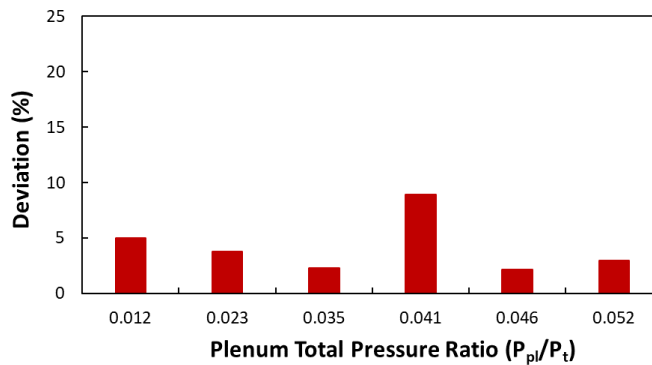
Figure 3.9 The Percentage of Deviations between Experimental [18] and CFD Results for the Single Bleed Hole Case

54

3.1.3. Flow Domain Visualizations

The pressure contours around the bleed hole for Q_{sonic}=0.0113 and Q_{sonic}=0.0326 is given in Figure 3.10. It can be seen that bleed mass flow significantly affects the pressure distribution at bottom surface. In addition, the symmetry plane Mach contours are shown in Figure 3.11. The two segment barrier shock structure is capture well and the Mach contours are in agreement with the reference CFD study [24] given in Figure 3.11c.

(a)   (b)
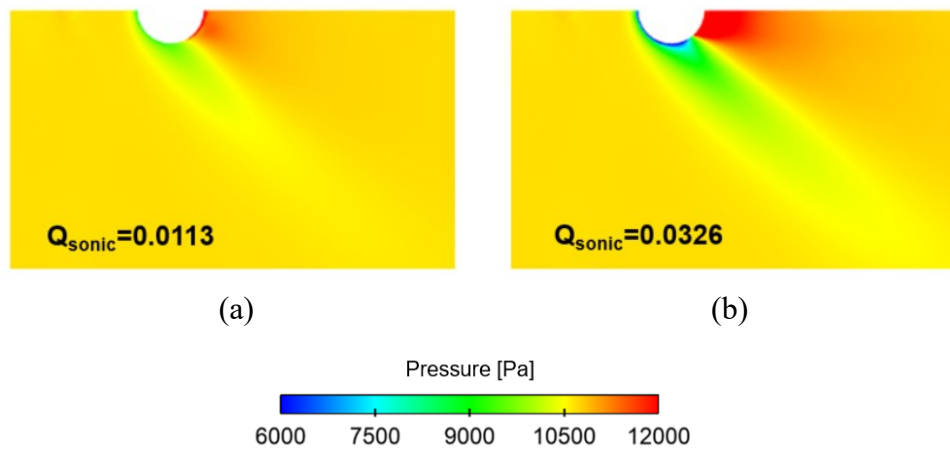
Figure 3.10 Comparison of Pressure Contours around the Bleed Hole for (a) Q_{sonic}=0.0113 and (b) Q_{sonic}=0.0326

(a)   (b)   (c)
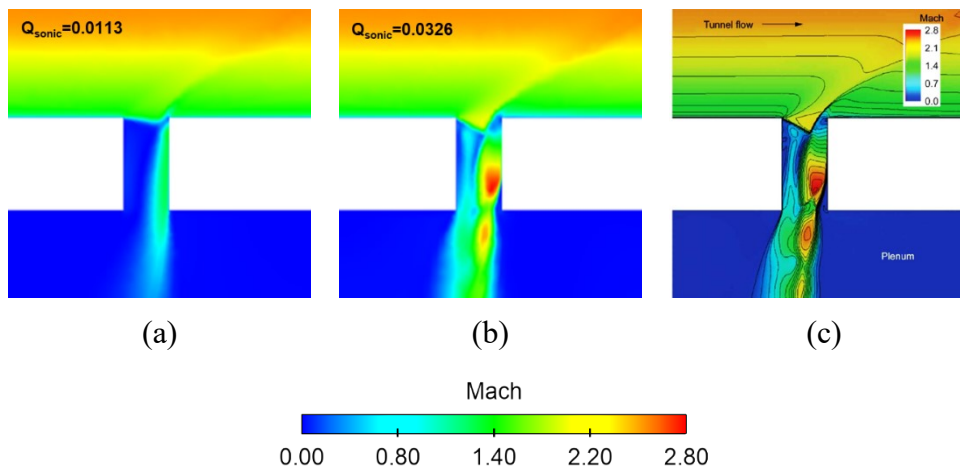
Figure 3.11 Comparison of Mach Contours at the Symmetry Plane for (a) Q_{sonic}=0.0113 and (b) Q_{sonic}=0.0326 (c) CFD study [24]

55

3.2. Numerical Simulations of Porous Bleed on a Flat Plate

In the Nasa-Lewis Research Center, wind tunnel tests were conducted to investigate the effects of the porous bleed on a turbulent supersonic boundary-layer over a flat plate in supersonic speeds [6]. Tests are conducted at Mach 1.27, 1.58, 1.98 and 2.46 on different bleed configuration and inclination angles with flat plate surface. In the scope of this study, normal bleed configuration (C1 model), inclined 90° to flat plate surface, is evaluated at Mach 2.46. Test section has dimensions of 30x30 cm and the bleed flow is discharged to the plenum. Tests schematic is illustrated in Figure 3.12. Diameter is 6.35 mm and length is 6.35 mm, length to diameter ratio (*L/D*) is 1 for all bleed holes. The bleed flow is discharged from six rows of twelve bleed holes on the bleed region.
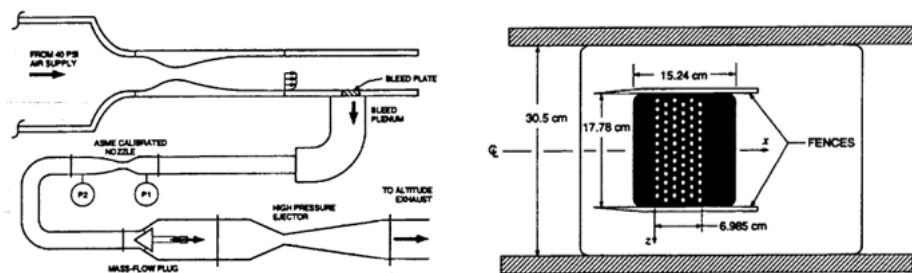
Figure 3.12 Schematic of Porous Bleed Test Section [6]

The boundary layer is naturally developed on the lower surface of the wind tunnel test section. The boundary layer parameters were measured with the translating pitot tube 81.915 mm upstream of the bleed region. Test conditions and approaching boundary layer parameters is given in Table 3.3.

Table 3.3 Test Conditions

Mach	2.46
P_t	172400 Pa
T_t	293 K
δ	2.63 cm
δ^*	0.717 cm
Re	1.75×10^7 /m

Test data uncertainty values were reported as 0.045 psi for total pressure measurements, 2.4% for sonic flow coefficient and 1.8% for plenum pressure ratio at Mach 2.46.

3.2.1. Solid Model, Grid Generation and Boundary Conditions

The solid model and the boundary conditions used in the analyses are shown in Figure 3.13. Symmetry planes are defined by taking advantage of repetitive hole pattern to decrease the number of grid cells. The bottom, side, hole and plenum walls are defined adiabatic, no-slip wall boundary condition. It is assumed that the top wall has no effect on bleed flow, so inviscid boundary condition is applied. Preparatory analyses are performed on a flat plate model to match the boundary layer properties in the wind tunnel test reference line. The normalized speed profile comparison along the reference line is shown in Figure 3.17a. The match profile with reference line boundary layer properties is imposed as inlet boundary condition for the bleed system model.

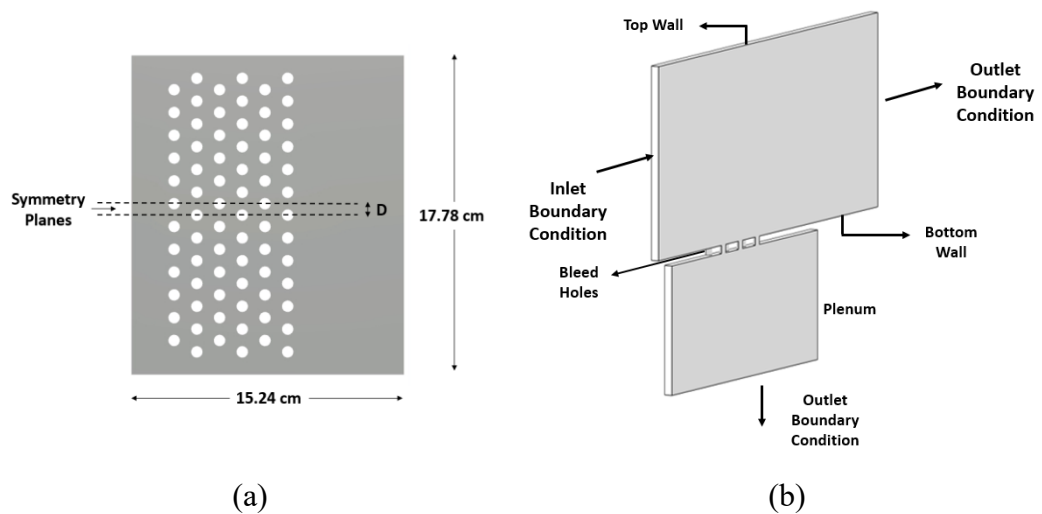(a)   (b)

Figure 3.13 The Porous Bleed System (a) Symmetry Planes (b) Solid Model and Boundary Conditions

In the grid convergence study, three different grids are generated with unstructured tetrahedral elements. The total number of cells for solution domains are given in Table

3.4 and the grid structure around the holes according to mesh level is shown in Figure 3.14.

Table 3.4 Total Number of Cells of Solution Domains

	Min. Element Size [D]	Total Number of Cells
Course	0.08	0.5×10^6
Medium	0.04	1.2×10^6
Fine	0.02	3.5×10^6

(a) Course

(c) Medium

(e) Fine
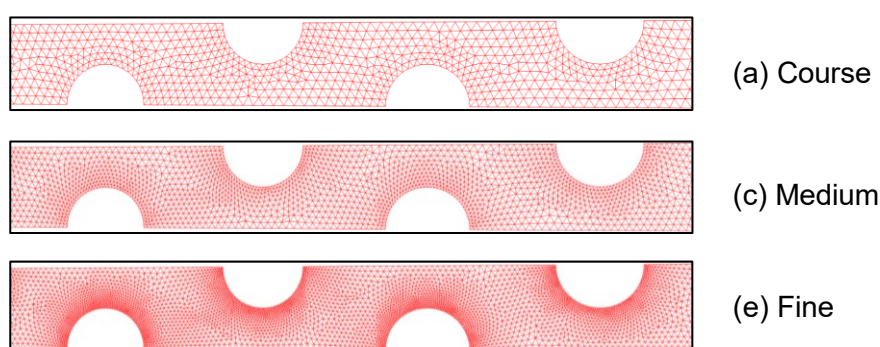
Figure 3.14 Grid Structure around the Holes According to Minimum Element Size

The grid convergence study and turbulence model comparisons are evaluated for the condition where the pressure ratio parameter (P_{pl}/P_t) is equal to 0.0348. In Figure 3.15, the change of the sonic flow coefficient according to the number of cells and the turbulence models are shown. Analyses performed using Realizable k-ε turbulence model could not reach a reliable converged solution. Therefore, Realizable k-ε is not shown in the graph. In accordance with literature, it can be seen that SST k-ω turbulence model is in the best agreement with the experimental data. In addition, no noticeable differences are observed between the medium grid and the two finer grids. Thus, the medium grid is selected for further analyses. The medium grid illustrations are given Figure 3.16.
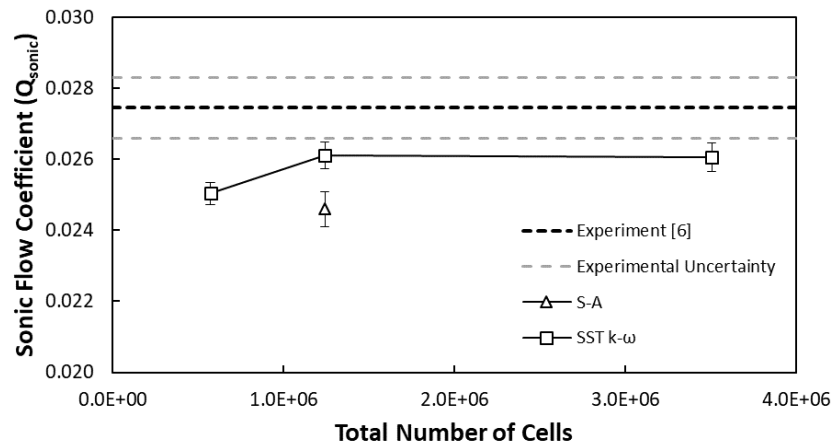
Figure 3.15 Variation of Sonic Flow Coefficient with Total Number of Cells
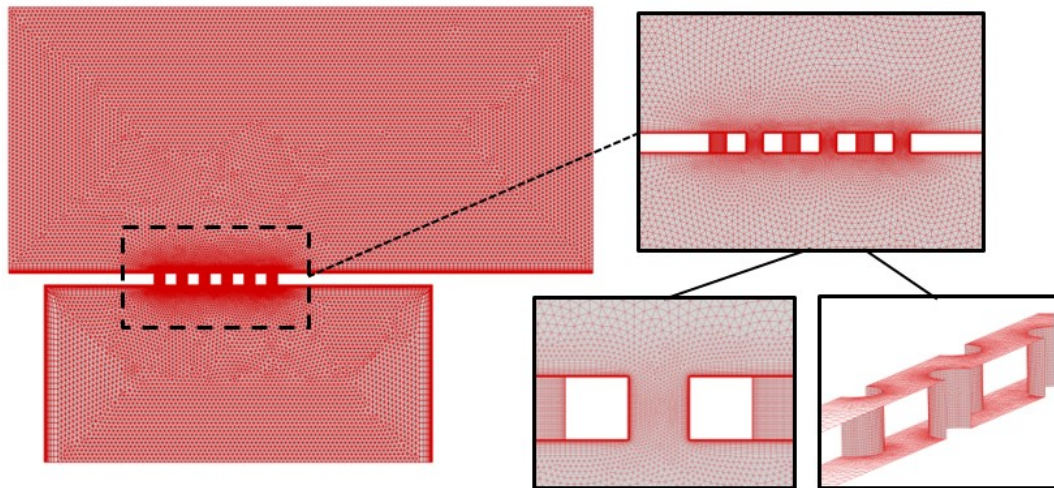
Figure 3.16 Grid Model of the Porous Bleed Case without Shock

The different levels of grids are modeled with a boundary layer formed in the prism-cells and unstructured tetrahedral elements. First height is determined as 0.007 mm to obtain y^+ value is around 1 for all grid models. The first height value is checked and validated from analysis results. y+ obtained along the bottom wall for the medium grid is shown in Figure 3.17b.
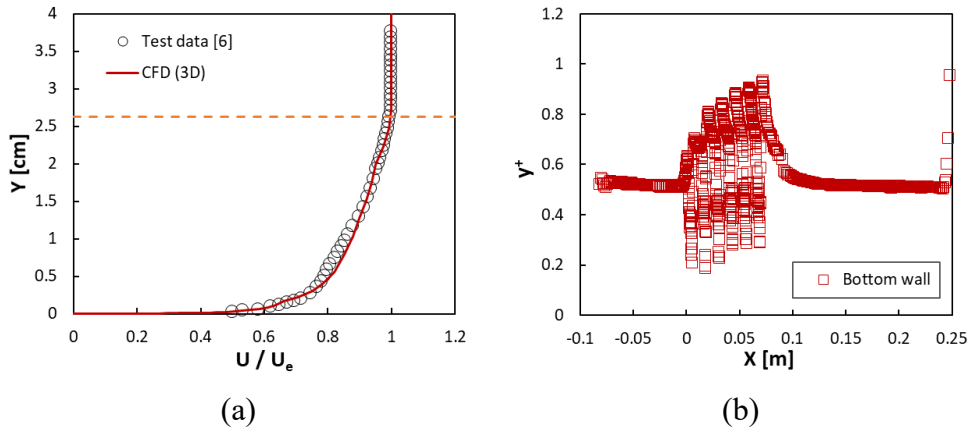
Figure 3.17 (a) The Speed Profile along the Reference Line (b) y^+ Values along Bottom Wall

3.2.2. Analysis Results

According to the grid convergence study and turbulence model comparisons, SST k-ω turbulence model and the medium grid size is determined as optimal solution method. Additional analyses are conducted for other total plenum pressure ratio points. The residuals and Q_{sonic} histories are given in Figure 3.18 for the condition where the pressure ratio parameter (P_{pl}/P_t) is 0.0348. To satisfy the convergence criteria, *80K* solution iterations require for the simulation. The analysis results are plotted along with the test data and the reference CFD results as given in Figure 3.19. The CFD solutions are quite compatible with the wind tunnel test data. In addition, the percentage of deviations between CFD and experimental results are normalized with the choked value of the bleed flow and presented in Figure 3.20. In order to obtain the percentage of deviations between the test data and the CFD results, spline curves are generated for the experimental data to calculate bleed rates at the same plenum pressure ratio condition of the analyses. The deviations are in the range of 0.7% to 3.6%, the analysis results of the case are considerably close to the experimental results. NRMD is calculated as 0.023 with using all the compared data points.

(a)   (b)
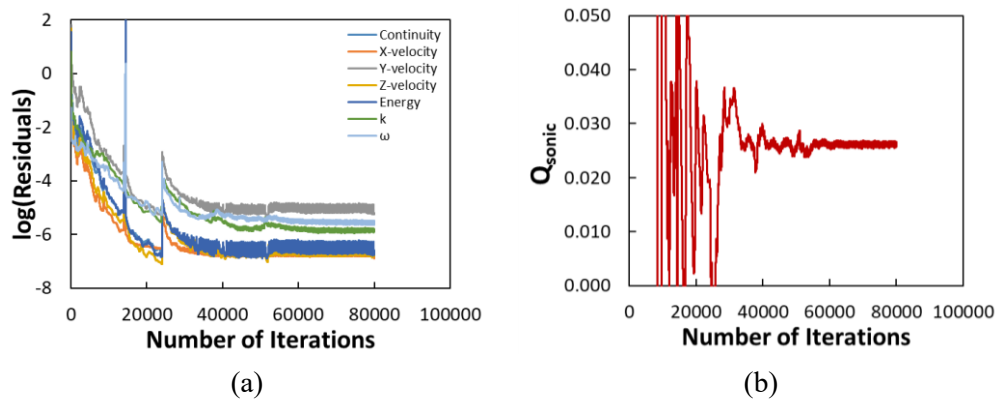
Figure 3.18 Solution Histories for (a) Residuals and (b) Q_{sonic}
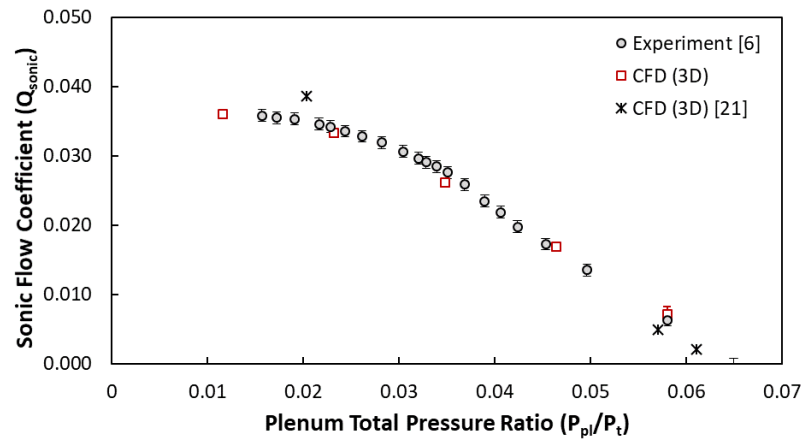
Figure 3.19 Comparison of the Results of the Porous Bleed Case without Shock
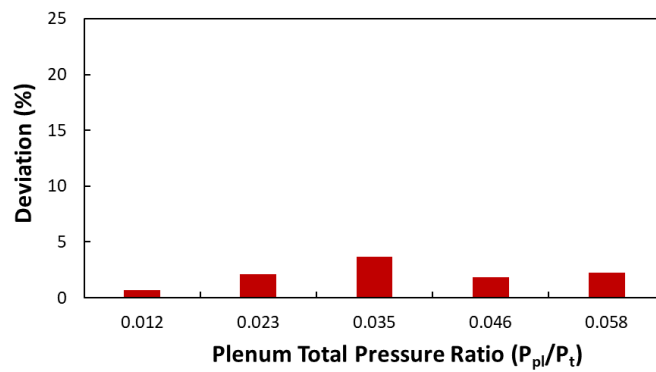
Interaction

Figure 3.20 The Percentage of Deviations between Experimental [6] and CFD

Results for the Porous Bleed Case without Shock Interaction

During the wind tunnel tests, total pressure profile measurements are taken for different mass flow rates at the downstream of the porous bleed region. Comparison of the experimental data [35] and the CFD analysis results are given in Figure 3.21. The analysis results are sufficiently accurate in capturing total pressure profiles.
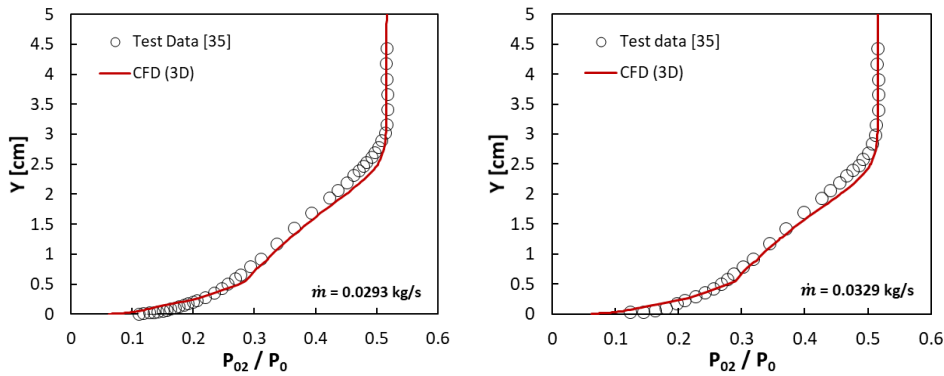
Figure 3.21 Comparison of Normalized Pitot Profiles

3.2.3. Flow Domain Visualizations

The pressure contours on the bottom hole around the porous bleed region for Q_{sonic}=0.0169 and Q_{sonic}=0.0340 is given Figure 3.22. In addition, the Mach contours at the solution domain are shown in Figure 3.23. The Figures show that the effects of shock and expansion waves around the bleed holes on the bottom wall and flow domain.

(a)

(b)
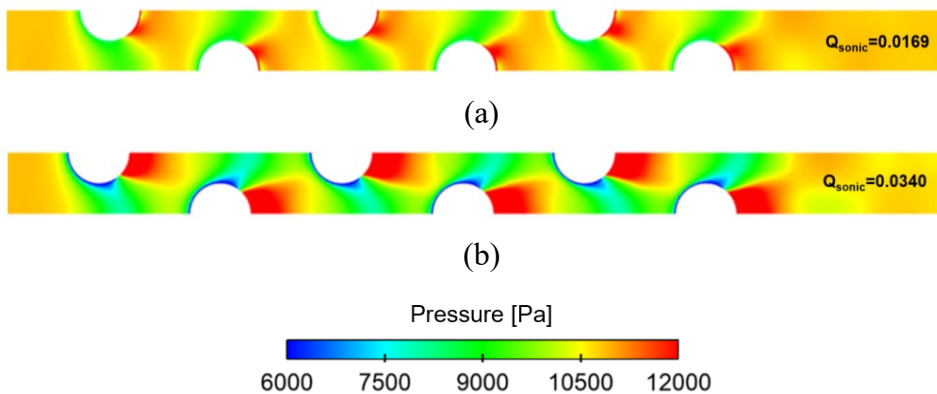
Figure 3.22 Comparison of the Pressure Contours over Porous Bleed Region for (a) Q_{sonic}=0.0169 and (b) Q_{sonic}=0.0340

(a)   (b)
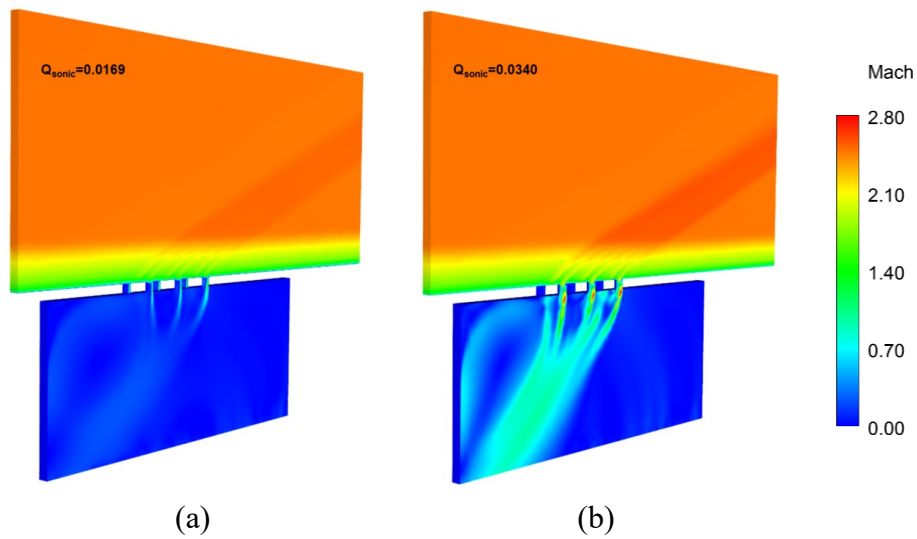
Figure 3.23 Comparison of the Mach Contours at the Symmetry Plane for (a)
Q_{sonic}=0.0169 and (b) Q_{sonic}=0.0340

3.3. Numerical Simulations of Porous Bleed on a Flat Plate with Oblique Shock Interaction

In the Nasa-Lewis Research Center, wind tunnel tests were conducted to investigate the effects of the porous bleed with interaction oblique shock over a flat plate at 2.46 Mach number [34]. Test section has dimensions of 30x30 cm and tests schematic is shown in Figure 3.24. The tests were conducted to investigate the effect of the bleed system distorted by an oblique shock wave on the flow profile. Diameter is 6.35 mm and length is 6.35 mm, length to diameter ratio (*L/D*) is 1 for all bleed holes. The bleed flow is discharged from eight rows of twelve bleed holes on the bleed region.
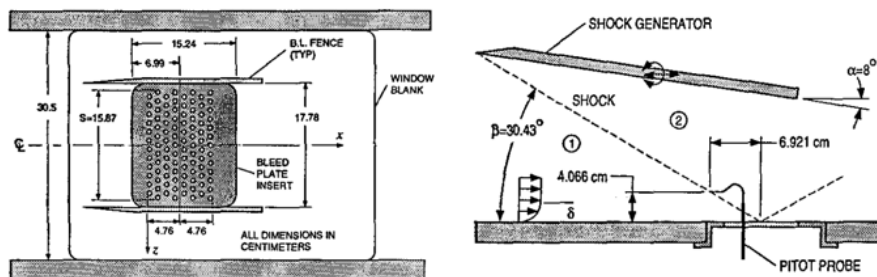
Figure 3.24 Schematic of Porous Bleed Test Section [34]

63

The boundary layer is naturally developed on the lower surface of the wind tunnel test section. The boundary layer parameters were measured with the translating pitot tube 81.915 mm upstream of the bleed region. Test conditions and approaching boundary layer parameters is given in Table 3.5.

Table 3.5 Test Conditions

Mach	2.46
P_t	172400 Pa
T_t	292 K
δ	2.63 cm
δ^*	0.727 cm
Re	1.81×10^7 /m

Test data uncertainty values were reported as 0.021 psi for total pressure measurements and 2.2% for sonic flow coefficient.

3.3.1. Solid Model, Grid Generation and Boundary Conditions

The solid model and the boundary conditions used in the analyses are shown in Figure 3.25. Symmetry planes are defined by taking advantage of repetitive hole pattern to decrease the total number of grid cells. The bottom, side, hole and plenum walls are defined adiabatic, no-slip wall boundary condition. It is assumed that the top wall has no effect on bleed flow, so inviscid boundary condition is applied. As similar to previous case, preparatory analyses are performed on a flat plate model to match the boundary layer properties in the wind tunnel test reference line. The normalized speed profile comparison along the reference line is shown Figure 3.28a. Matched profile with reference line boundary layer properties is imposed as inlet boundary condition for the bleed system model.

(a)   (b)
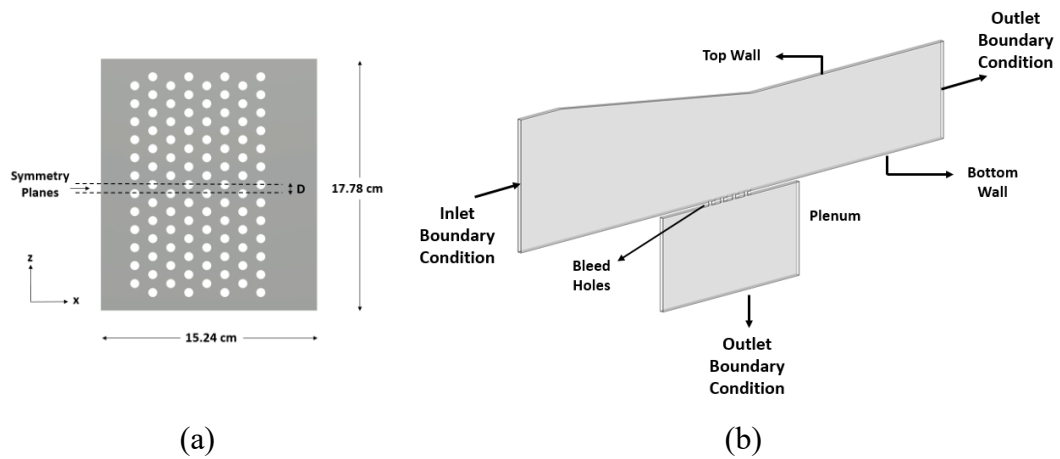
Figure 3.25 The Porous Bleed System with an Oblique Shock (a) Symmetry Planes
(b) Solid Model and Boundary Conditions

In the grid convergence study, three different grids are generated with unstructured tetrahedral elements. The total number of cells for solution domains are given in Table 3.6. Grid illustrations can be seen in Section 3.2.1 because meshing strategy and hole geometrical properties are similar with the porous bleed case.

Table 3.6 Total Number of Cells of Solution Domains

	Min. Element Size [D]	Total Number of Cells
Course	0.08	1.3×10^6
Medium	0.04	2.2×10^6
Fine	0.02	5.3×10^6

The grid convergence study and turbulence model comparisons are evaluated for the condition where the pressure ratio parameter (P_{pl}/P_t) is 0.0348. In Figure 3.26, the change of the sonic flow coefficient according to the number of cells and the turbulence models are shown. In accordance with literature, it can be seen that SST k-ω turbulence model is in the best agreement with the experimental data. In addition, no noticeable differences are observed between the medium grid and the two finer grids. So the medium grid is selected for further analyses. The medium grid illustrations are given in Figure 3.27.
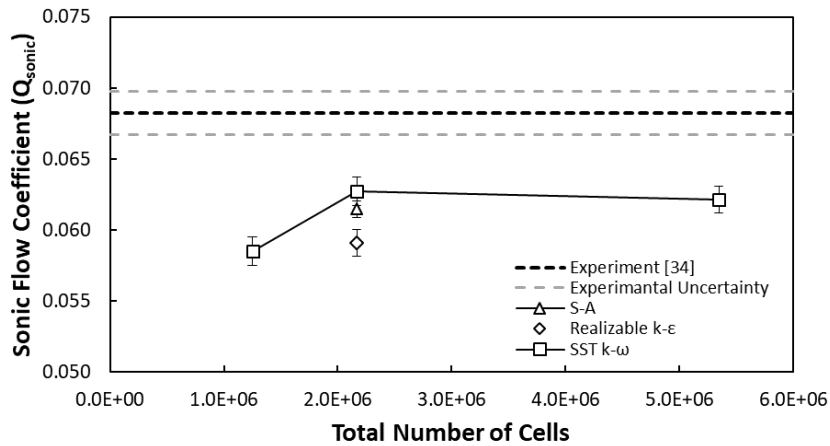
Figure 3.26 Variation of Sonic Flow Coefficient with Total Number of Cells
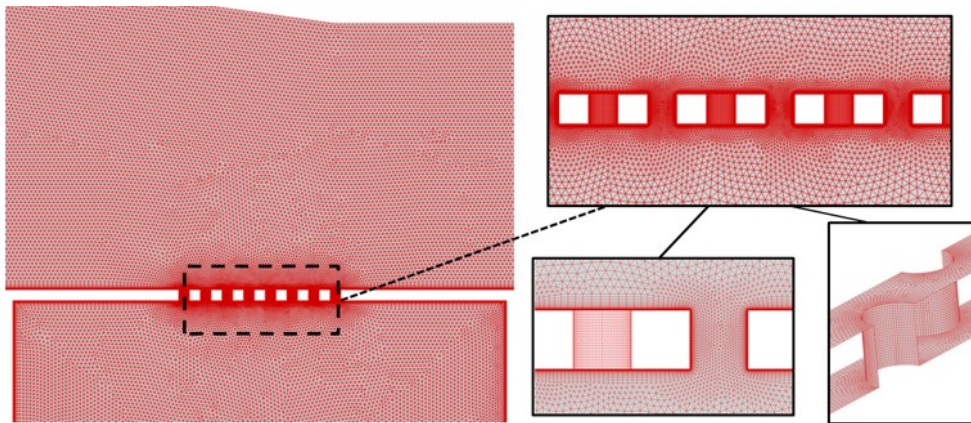
Figure 3.27 Grid Model of Porous Bleed Case with an Oblique Shock

The different levels of grids are modeled with a boundary layer formed in the prism-cells and unstructured tetrahedral elements. First height is determined as 0.007 mm to obtain y^+ values around 1 for all grid models. The first height value is checked and validated from analysis results. y+ obtained along the bottom wall for the medium grid is shown in Figure 3.28b.
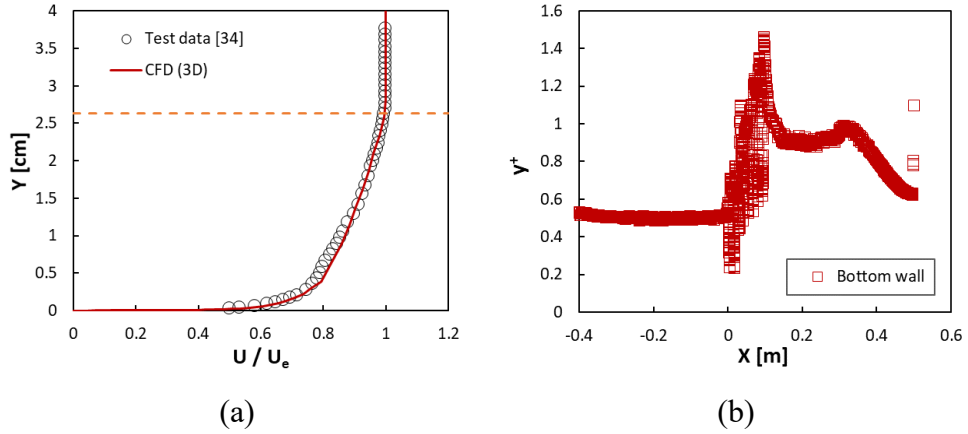
Figure 3.28 (a) The Speed Profile along the Reference Line (b) y^+ Values along Bottom Wall

3.3.2. Analysis Results

According to the grid convergence studies and turbulence model comparisons, SST k-ω turbulence model and the medium grid size is determined as optimal solution method. The residual and Q_{sonic} histories are given in Figure 3.29 for the condition where pressure ratio parameter (P_{pl}/P_t) is equals to 0.0348. To satisfy the convergence criteria, *90K* solution iterations require for the simulation. The analysis results are plotted along with the test data and the reference CFD results as given in Figure 3.30. The analysis results are quite compatible with the test data. In addition, the percentage of deviations between CFD and experimental results are normalized with the choked value of the bleed flow and presented in Figure 3.31. In order to obtain the percentage of deviations between the test data and the CFD results, spline curves are generated for the experimental data to calculate bleed rates at the same plenum pressure ratio condition of the analyses. The deviations are in the range of 2.6% to 10.4%, the analysis results of the case are compatible with the experimental data. NRMD is calculated as 0.065 with using all the compared data points.

67

(a)   (b)
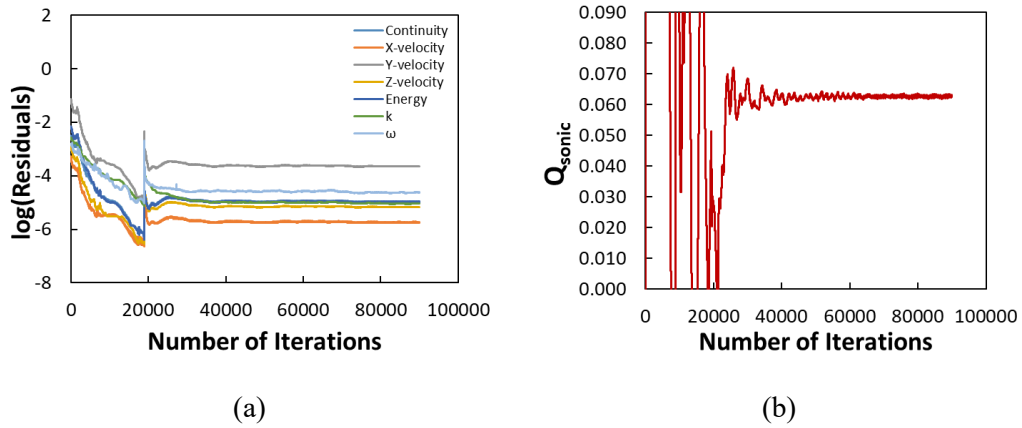
Figure 3.29 Solution Histories for (a) Residuals and (b) Q_{sonic}
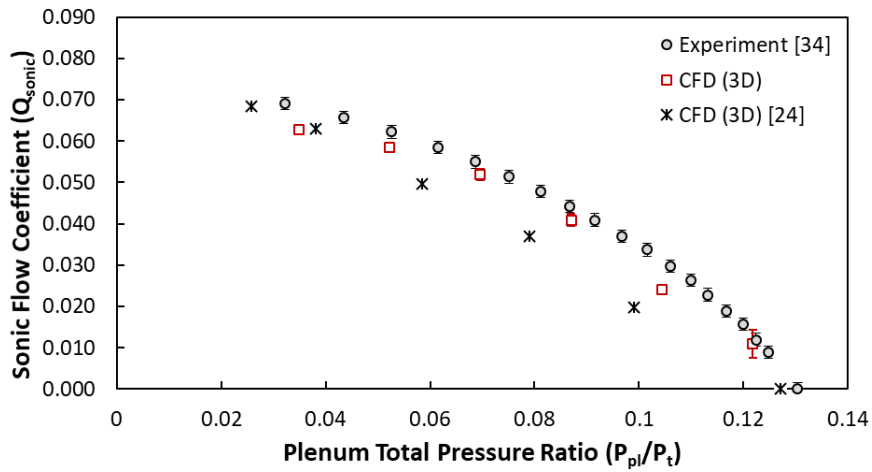
Figure 3.30 Analysis Results of the Porous Bleed Case with an Oblique Shock
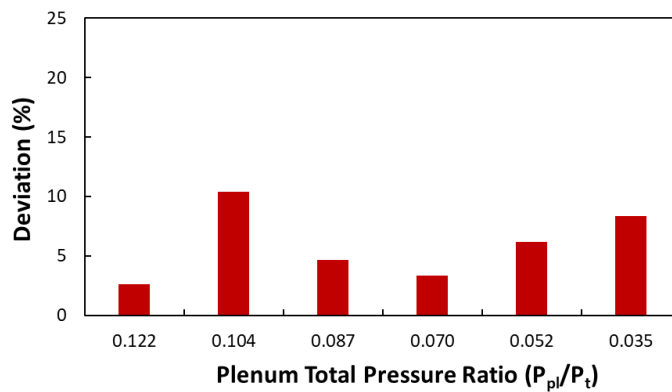
Figure 3.31 The Percentage of Deviations between Experimental [34] and CFD
Results for the Porous Bleed Case with an Oblique Shock

68

During the wind tunnel tests [34], total pressure profile measurements are taken for different mass flow rates at the downstream of the porous bleed region. The comparison of the experimental data and the CFD analysis results are given in Figure 3.33. The analysis results are sufficiently accurate in capturing total pressure profiles.
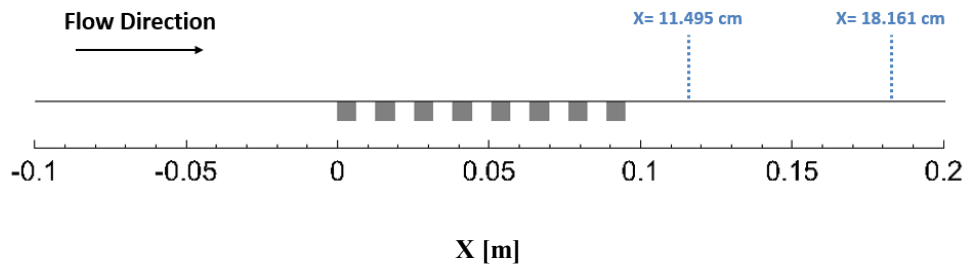
Figure 3.32 Schematic of Normalized Pitot Profile Stations
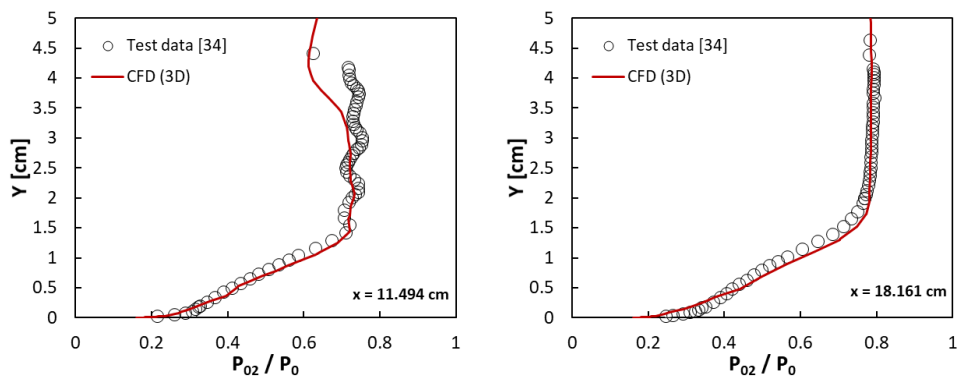
Figure 3.33 Comparisons of Normalized Pitot Profiles at Choked Condition

Comparison between the measured normalized surface pressure distributions [34] with CFD solutions at choked condition is performed in Figure 3.34. Since pressure measurements are obtained from just downstream of each bleed hole, the data are obtained for two lines along upstream to downstream on the bottom wall which are passing through the hole centers. Although, exact location of pressure tabs used in the experimental studies are not known, it can be seen in Figure 3.34 that CFD captures well pressure distribution along bleed holes however pressure values at downstream of bleed region (x=0.15 to 0.3 m) are underestimated.
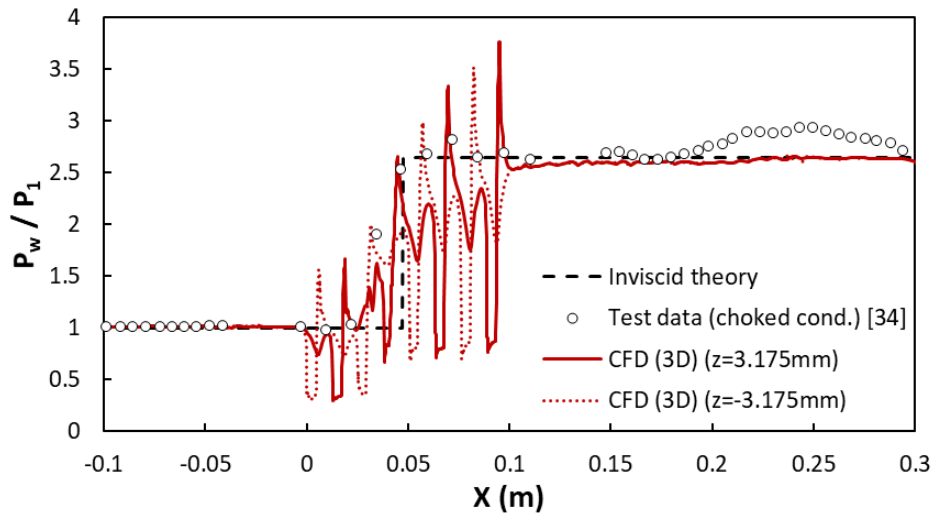
Figure 3.34 Comparison of Wall Pressure Distribution Profiles at Choked Condition

3.3.3. Flow Domain Visualizations

The pressure contours on the bottom wall for Q_{sonic}=0.0240 and Q_{sonic}=0.0635 is given in Figure 3.35. In addition, Mach contours at the solution domain are shown in Figure 3.36. The effect of bleed system on the boundary layer can be seen clearly on Mach contour visualizations. In Figure 3.36a, the flow separates from the bottom wall without a proper amount of bleed flow, and the flow reattaches to the surface with increasing bleed rates as can be seen in Figure 3.36b.
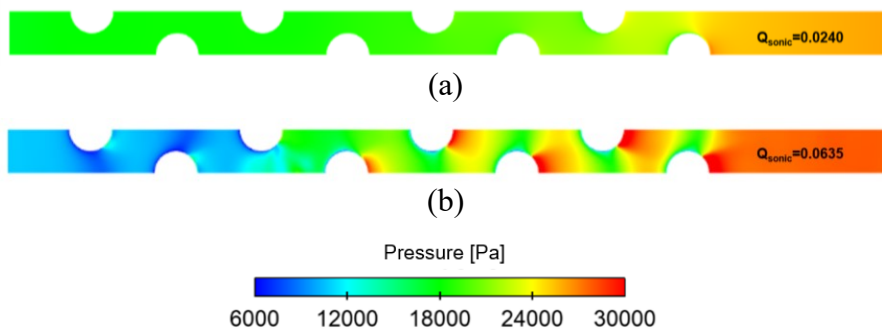
Figure 3.35 Comparison of Pressure Contours over Porous Bleed Region with an Oblique Shock Interaction for (a) Q_{sonic}=0.0240 and (b) Q_{sonic}=0.0635

70
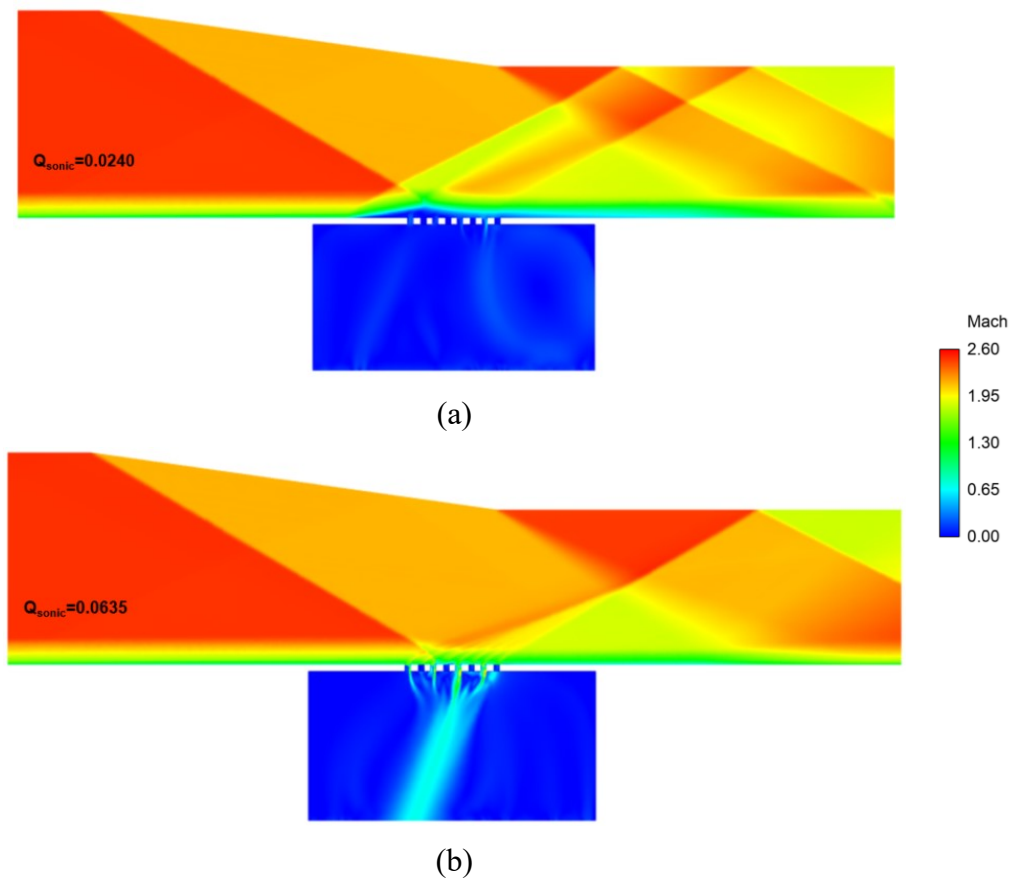
Figure 3.36 Comparison of the Mach Contours over Porous Bleed Region with an Oblique Shock Interaction for (a) Q_{sonic}=0.0240 and (b) Q_{sonic}=0.0635

3.4. Discussion on the Validation Studies

In this chapter, CFD analysis studies are performed for single and porous bleed systems (with/without shock) which are widely used in the literature. Different levels of unstructured grid are generated with using minimum element size, which is defined dependent to the hole diameter. As a result of the grid convergence studies, the medium grid resolution with a minimum element size of 0.04D is determined as optimal to model bleed flow around the holes for all cases. The simulations are performed for Spalart-Allmaras (S-A), the two-equation Realizable k-ε and SST k-ω turbulence models. SST k-ω turbulence model is selected to further analyses due to be in the best agreement with experimental data. CFD analyses are expanded for different plenum total pressure ratios (P_{pl}/P_t).

As a result of validation studies, the CFD results show good agreement with the wind tunnel test data. In addition, total pressure profile measurements downstream of the porous bleed region are compared with CFD results. The CFD approach is sufficiently accurate in capturing total pressure profiles. The pressure and Mach contours around the bleed flow are also investigated. Flow structure around the bleed holes for the single bleed hole case have similar Mach distribution with the reference CFD study from the literature. As a result, it is considered that the CFD is a reliable method to analyse the porous bleed systems where test data is not available.

CHAPTER 4

DEVELOPMENT OF NEW BLEED BOUNDARY CONDITION MODELS

Various bleed boundary condition (BBC) modeling techniques are discussed in Section 1.3. Slater [24] improved Mayer's boundary condition with defining Q_{sonic} and the plenum total pressure ratio parameter according to the reference boundary flow properties. Slater method supplies adequate Q_{sonic} data over entire bleed region. However, as similar to previous works, three-dimensional flow structure around the bleed holes and effects on boundary layer are not captured well with the method because discrete bleed hole effects are omitted. In addition, Benson, et al. [43] showed success on simulating the flow structure of the bleed flow by defining known mass flow rates on individual bleed openings without model hole cavity and plenum details.

In consideration of these studies, it is deduced that the flow properties around each bleed hole should be examined individually on a porous bleed region. If a correlation between bleed flow rates and flow properties on a boundary can be found, the bleed flow rates can be imposed easily on bleed openings and three dimensional effects on the main flow can be captured.

Hence, three new BBC models are introduced. Further CFD analyses on the porous bleed system are performed including blowing effects to obtain a correlation between bleed modeling and reference boundary flow properties. FRM analysis are collected on the reference boundaries for each BBC model. Collected data are presented and discussed according to the scaled parameters. The deviations between the data and curve fitting models are calculated to select the best model for implementation to the solver.

4.1. CFD Analyses for Data Correlation

The validation studies have been carried out for different models; the single bleed hole, the porous bleed cases with and without shock interaction in Chapter 3. To examine the effects of bleed mass flow rate on the reference boundary flow properties, the porous bleed case without shock interaction is determined for further studies. The experimental data of this case is also used by Slater while improving the Mayer's method. As the porosity effect on the flow properties cannot be obtained, the single bleed hole case is not evaluated although it is favorable in term of CFD solution process. In addition, the porous bleed case with shock interaction is considered inappropriate to evaluation, since shock effects on the flow may lead to a corruption on the data.

To evaluate effects of the freestream Mach number and the blowing phenomena around the holes, additional analyses are carried out on the porous bleed case. CFD analyses are performed using the information of optimal turbulence model and grid size which are determined during the validation studies. The boundary conditions also defined as similar to the FRM of the case. The detail information can be found in Section 3.2. The analysis results are compared with test data in Figure 4.1. In addition, the percentage of deviations are calculated based on the choked bleed rates of the test data and presented in Figure 4.2 In order to obtain the percentage of deviations between the test data and the CFD results, spline curves are generated for the experimental data to calculate bleed rates at the same plenum pressure ratio condition of the analyses. The analysis results of the case are quite compatible with the experimental data. The data for the blowing flow rates cannot be evaluated due to the lack of experimental data on this region.
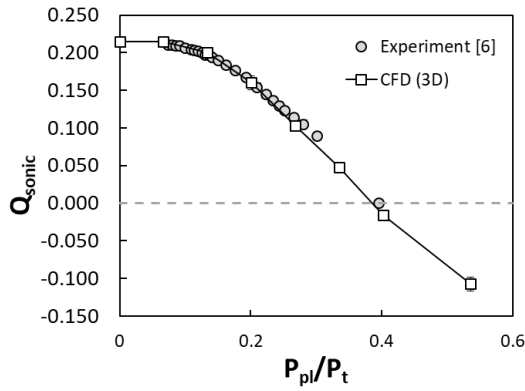
(a) Mach 1.27　　　　　　　　　　　　(b) Mach 1.58
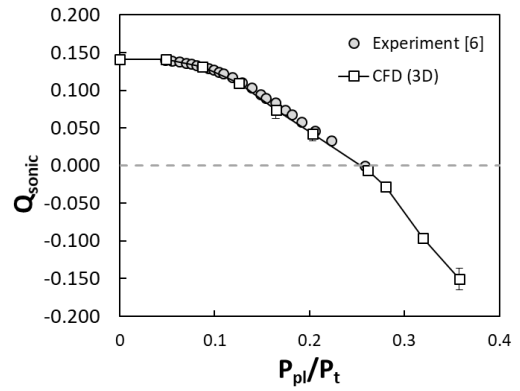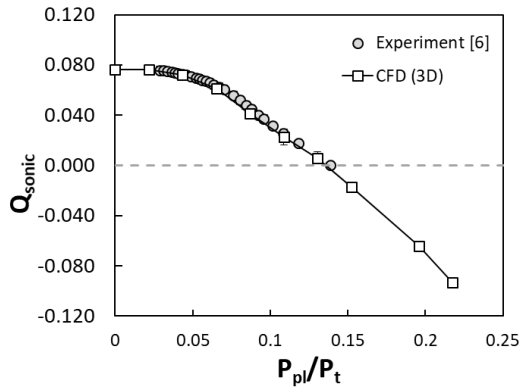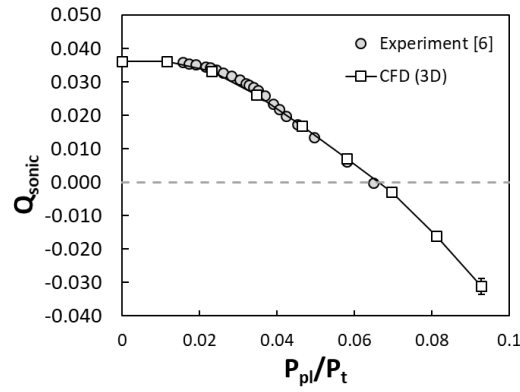
(c) Mach 1.98　　　　　　　　　　　　(d) Mach 2.46

Figure 4.1 Additional CFD Analysis Results of the Porous Bleed Case
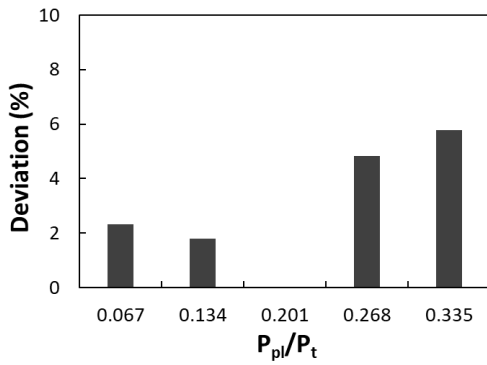
(a) Mach 1.27　　　　　　　　　　　　(b) Mach 1.58
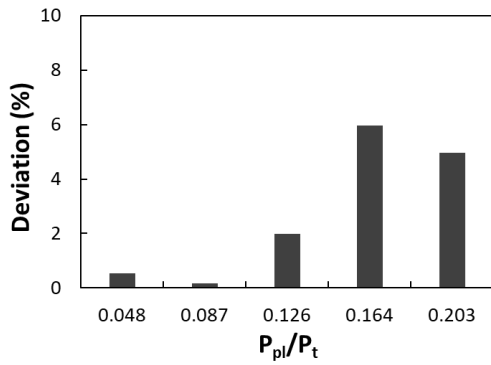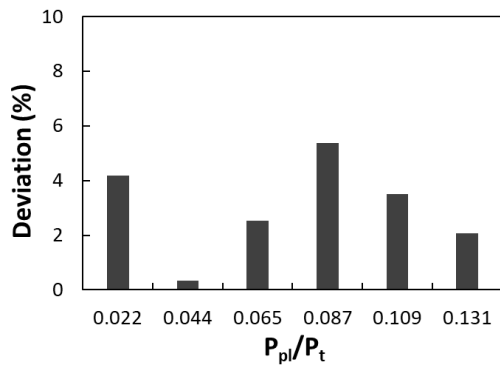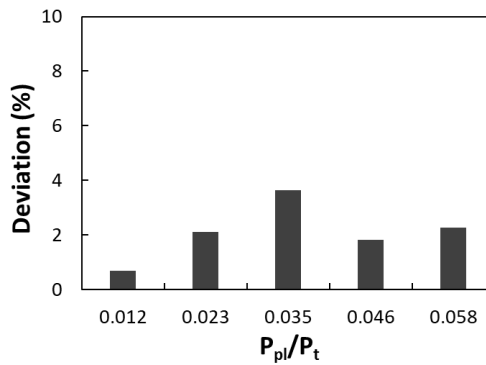
(c) Mach 1.98　　　　　　　　　(d) Mach 2.46

Figure 4.2 The Percentage of Deviations between CFD and the Experimental Results
[6] for the Porous Bleed Case without Shock Interaction

NRMSD are calculated using all available data points and presented in Figure 4.3. The
Figure shows that CFD method gives consistent accuracy on the case for different
freestream conditions.
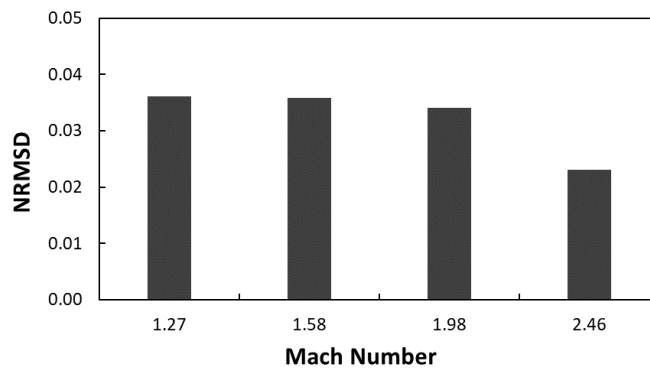
Figure 4.3 Variation of NRMSD Values with Mach number

4.2. Reference Surface Definitions

Three new BBC models are introduced to investigate the effects of bleed mass flow
rate on the reference boundary flow properties.

First of all, a reference boundary is defined on the bleed openings and it is named as
Bleed Hole Boundary (BHB) which is shown in Figure 4.4a. Secondly, the rectangular
area (not includes hole opening surfaces) around the bleed hole is defined as a

76

reference boundary. The boundary definition is called as Bleed Region Boundary (BRB) and representation of the model is given in Figure 4.4b. Finally, as similar to previous boundary definition, the diamond shaped area is defined as a reference boundary because the rectangular area cannot be defined as bleed region if the porosity is more than 20%. The diamond shaped boundary can be applied up to 40% porous regions. The third boundary condition is entitled as Bleed Region Diamond Boundary (BRDB) due to the surface shape that covered. Among the reference boundary definitions, the easiest and flexible way is to use the bleed openings as the reference boundary in terms of grid generation and solver implementation processes. Since the boundary condition specification on the bleed surface is already required for the bleed flow. For the other models, reference boundaries should be identified individually for each bleed hole.

The reference boundary illustrations and the numeration of bleed holes are given in Figure 4.4.

(a) Bleed Hole Boundary (BHB)

(b) Bleed Region Boundary (BRB)

(c) Bleed Region Diamond Boundary (BRDB)
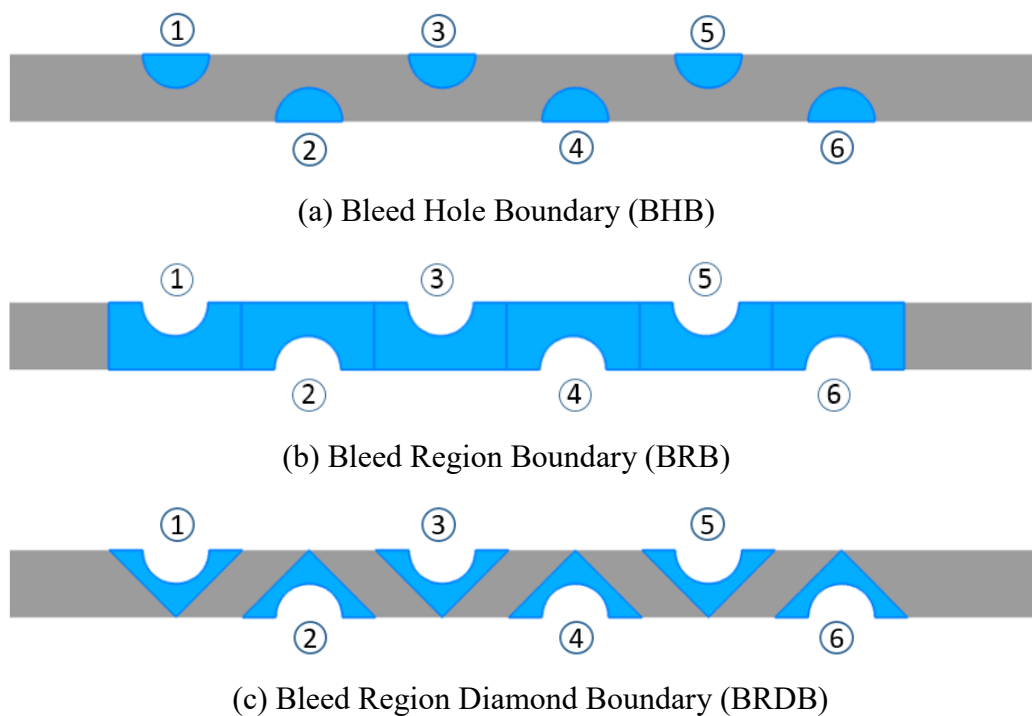
Figure 4.4 The Reference Boundary Models

77

4.3. Data Correlation

Data correlations studies for the three boundary definitions are given in the following sections. Firstly, the flow properties are collected according to reference boundary definitions. Non-dimensional flow properties are evaluated without required any assumptions which are described for Slater method. The subscript "b" refers to the related boundary value.

$$W_{sonic,b} = A_{bl} \, P_b \left(\frac{\gamma}{R \, T_b} \right)^{1/2} \left(\frac{\gamma + 1}{2} \right)^{\frac{-(\gamma+1)}{2(\gamma-1)}} \qquad (4.1)$$

The boundary sonic flow coefficient can be defined as

$$Q_{sonic,b} = \frac{W_{bl}}{W_{sonic,b}} \qquad (4.2)$$

Finally, plenum pressure ratio calculated according to the static pressure on the reference boundary.

$$\frac{P_{pl}}{P_b} \qquad (4.3)$$

For implementation to UDF, a simple polynomial curve fitting is required to be obtained. Thus, 2nd and 3rd polynomial curve fittings are applied to scaled data. In addition, it should be noted that using scaled values of negative mass flow rates (blowing) increases the deviations on bleed modeling for all boundary definitions and the scaled values of negative $Q_{sonic,b}$ is not collapse along plenum pressure ratio parameter for the BRB and BRDB models. Hence, the data of negative mass flow rates are removed from curve fittings.

4.3.1. Data Correlation for Bleed Hole Boundary

Mass flow rates and surface pressures are collected on the BHB by post processing the CFD analyses. The collected data is given in Figure 4.5.

Figure 4.5 Collected Data on the BHB

Non-dimensional flow properties are evaluated according to the reference boundary flow properties using Equation (4.1), (4.2) and (4.3). The Q_{sonic} coefficient is plotted against plenum pressure ratio based on boundary flow properties in Figure 4.6. As can be seen in the figure, the data collapse fairly well along scaled parameters. In addition, it has to be emphasized that freestream Mach number is no longer a factor that affects the Q_{sonic} parameter.

Figure 4.6 Scaled Data for the BHB Model

2nd and 3rd polynomial curve fitting models are applied to positive values of $Q_{sonic,b}$ data. As mentioned before negative values increase the deviations on modeling bleed flow. Thus, the negative flow rates are removed from the collected data.

Figure 4.7 Curve Fittings for the BHB Model

The NRMSD calculations are performed for the curve fitting models are given in Table 4.1. Normalized factor is determined as 1.0 according to maximum $Q_{sonic,b}$.

Table 4.1 NRMSD Values of the Curve Fittings for the BHB Model

	NRMSD
2nd Order Polynomial	0.0628
3rd Order Polynomial	0.0610

Since the 3rd order fitting model has lower NRMSD value, the model is selected for implementation to solver. In addition, the choked flow condition is obtained approximately at plenum pressure ratio equal to 0.4. The $Q_{sonic,b}$ value at choked condition is not expected to change along lower pressure ratios. 3rd polynomial fitting captures this behavior better. The tertiary equation of the curve fitting is given below:

$$Q_{sonic,b} = -0.803 \left(\frac{P_{pl}}{P_b}\right)^3 - 0.682 \left(\frac{P_{pl}}{P_b}\right)^2 + 0.396 \left(\frac{P_{pl}}{P_b}\right) + 0.974 \quad (4.4)$$

4.3.3. Data Correlation for Bleed Region Boundary

Mass flow rates and surface pressures are collected on the BRB by post processing the CFD analyses. The collected data is given in Figure 4.8.
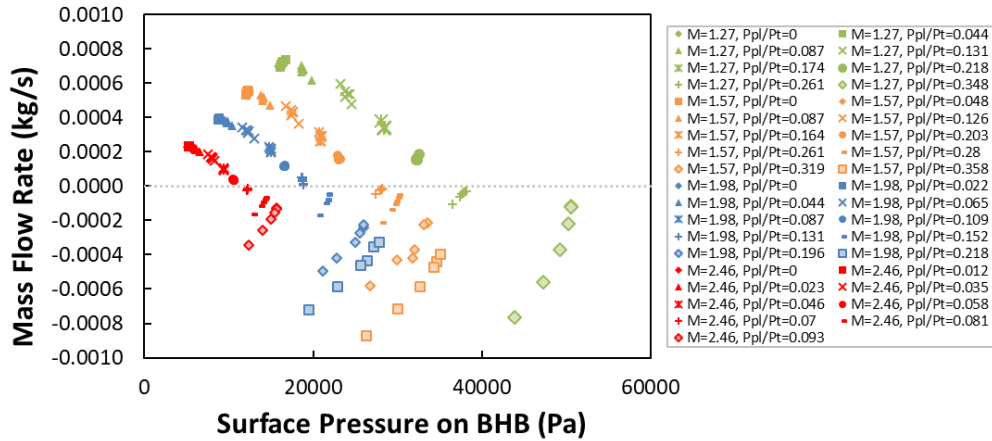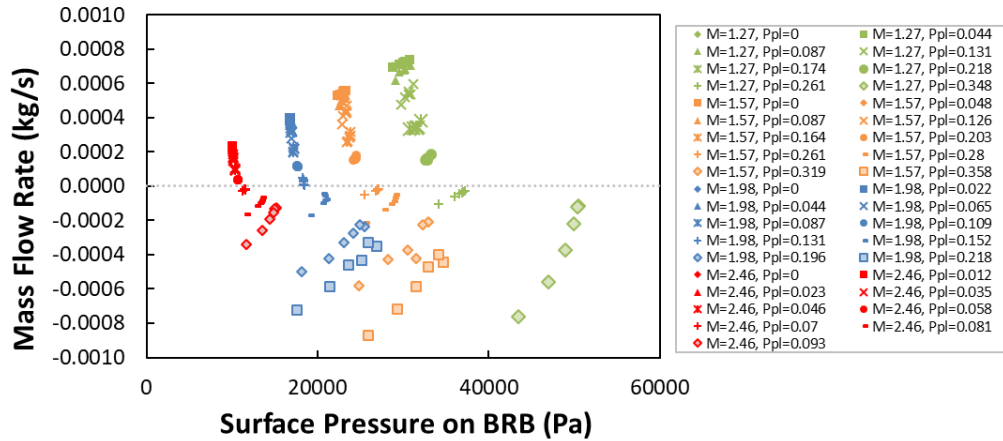

Figure 4.8 Collected Data on the BRB

Non-dimensional flow properties are evaluated according to the reference boundary flow properties using Equation (4.1), (4.2) and (4.3). The Q_{sonic} coefficient is plotted against plenum pressure ratio based on boundary flow properties in Figure 4.9. As can be seen in the figure, the data collapse fairly well along scaled parameters except negative $Q_{sonic,b}$ values. In addition, it has to be emphasized that freestream Mach number is no longer a factor that affects the Q_{sonic} parameter.
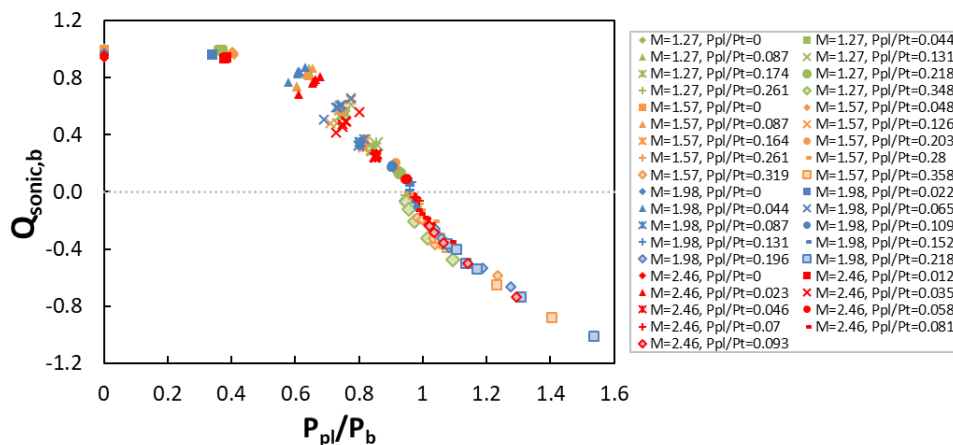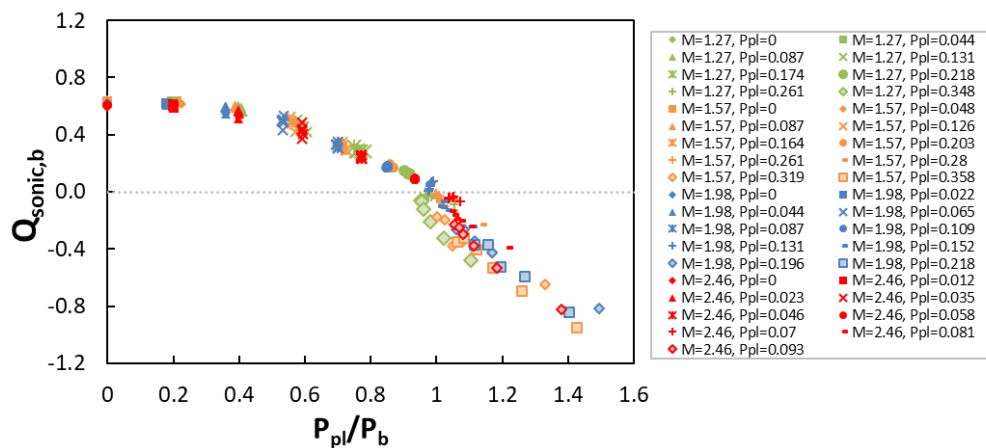

Figure 4.9 Scaled Data for the BRB Model

2nd and 3rd polynomial curve fitting models are applied to positive values of $Q_{sonic,b}$ data. As mentioned before negative values increase the deviations on modeling bleed flow. Thus, the negative flow rates are removed from the collected data.
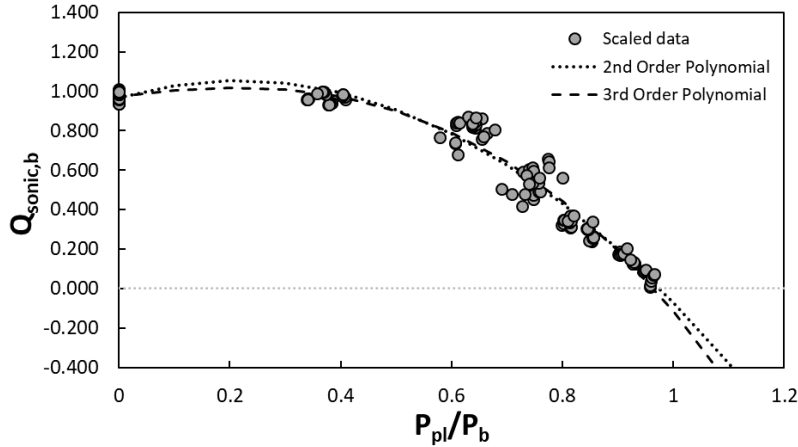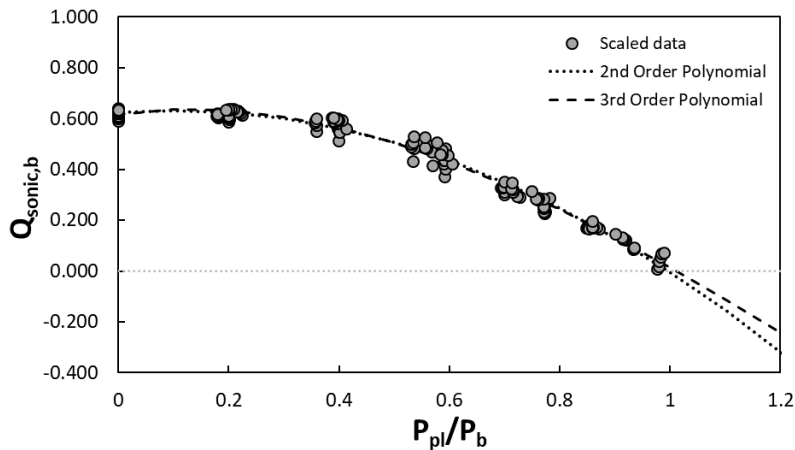

Figure 4.10 Curve Fittings for the BRB Model

The NRMSD calculations are performed for the curve fitting models are given in Table 4.2. Normalized factor is determined as 0.642 according to maximum $Q_{sonic,b}$.

Table 4.2 NRMSD Values of the Curve Fittings for the BRB Model

	NRMSD
2nd Order Polynomial	0.0361
3rd Order Polynomial	0.0347

Since the 3rd order fitting model has lower NRMSD value, the model is selected for implementation to solver. The tertiary equation of the curve fitting is given below:

$$Q_{sonic,b} = 0.289 \left(\frac{P_{pl}}{P_b} \right)^3 - 1.192 \left(\frac{P_{pl}}{P_b} \right)^2 + 0.299 \left(\frac{P_{pl}}{P_b} \right) + 0.617 \qquad (4.5)$$

4.3.4. Data Correlation for Bleed Region Diamond Boundary

Mass flow rates and surface pressures are collected on the BRDB by post processing the CFD analyses. The collected data is given in Figure 4.11.
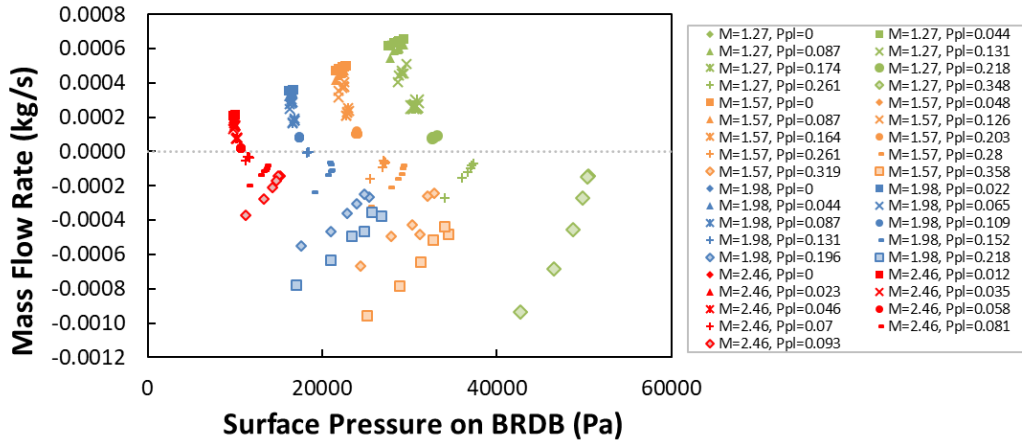
Figure 4.11 Collected Data on the BRDB

Non-dimensional flow properties are evaluated according to the reference boundary flow properties using Equation (4.1), (4.2) and (4.3). The Q_{sonic} coefficient is plotted against plenum pressure ratio based on boundary flow properties in Figure 4.12. As can be seen in the figure, the data collapse fairly well along scaled parameters except negative $Q_{sonic,b}$ values. In addition, it has to be emphasized that freestream Mach number is no longer a factor that affects the Q_{sonic} parameter.
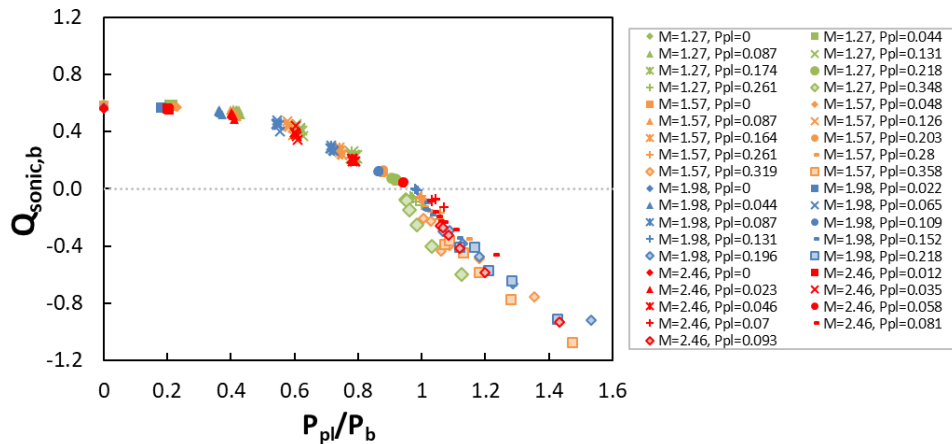
Figure 4.12 Scaled Data for the BRDB Model

2nd and 3rd polynomial curve fitting models are applied to positive values of $Q_{sonic,b}$ data. As mentioned before negative values increase the deviations on modeling bleed flow. Thus, the negative flow rates are removed from the collected data.
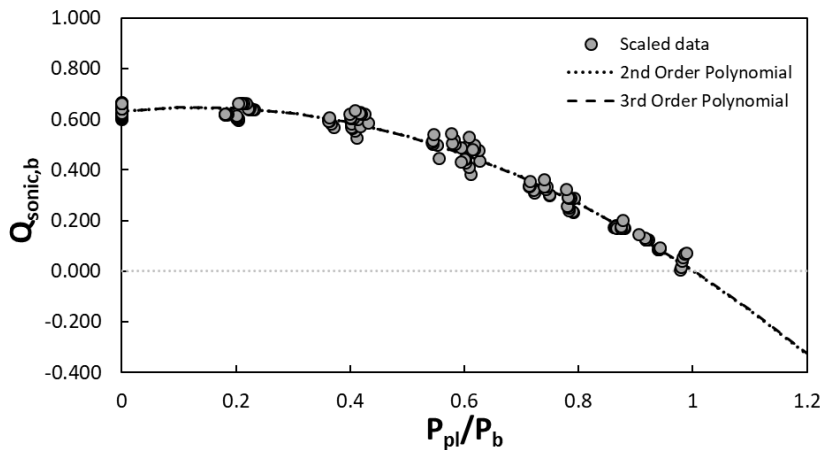
Figure 4.13 Curve Fittings for the BRDB Model

The NRMSD calculations are performed for the curve fitting models are given in Table 4.3. Normalized factor is determined as 0.668 according to maximum $Q_{sonic,b}$.

Table 4.3 NRMSD Values of the Curve Fittings for the BRDB Model

	NRMSD
2nd Order Polynomial	0.04013
3rd Order Polynomial	0.04012

The 2nd order and 3rd order fitting models have very close NRMSD values. 3rd polynomial is preferred for implementation to solver. The tertiary equation of the curve fitting is given below:

$$Q_{sonic,b} = 0.018\left(\frac{P_{pl}}{P_b}\right)^3 - 0.889\left(\frac{P_{pl}}{P_b}\right)^2 + 0.244\left(\frac{P_{pl}}{P_b}\right) + 0.631 \qquad (4.6)$$

4.5. Discussion

In this chapter, three new BBC models are introduced to investigate flow properties around each individual bleed hole. Additional CFD analyses on the porous bleed system is performed including the blowing flow rates.

Data correlations studies for the three reference boundary definitions are carried out with using collected data by post processing the FRM simulations. Non-dimensional flow properties are evaluated according to reference boundary flow properties.

For all the BBC models, the data collapse fairly well along the scaled parameters except the negative $Q_{sonic,b}$ values for the BRB and BRDB models. In addition, negative mass flow (blowing) increases the deviations on bleed modeling for all the reference boundary models. Hence, the data of negative mass flow rates are removed from curve fittings. 2nd and 3rd polynomial curve fitting models are applied to positive values of $Q_{sonic,b}$ data. Although 2nd and 3rd order polynomial fittings for the BRDB model are fairly close, the 3rd order fitting has lower NRMSD value for the other models. Since the 3rd curve fitting polynomials are preferred for implementation to solver.

The NRMSD values for the three reference boundary definitions is given below.

Table 4.4 NRMSD Values of the Best Curve Fittings for the BBC Models

	BHB	BRB	BRDB
NRMSD	0.0610	0.0347	0.04012

According to the NRMSD values, the scaled data used for curve fitting of BRB model are more compatible over other reference boundary definitions. Therefore, the success on prediction bleed mass flow rate of the model is expected to be superior to other models.

CHAPTER 5

EVALUATION OF NEW BLEED BOUNDARY CONDITION MODELS

In the previous chapter, new BBC models are developed and the correlations between the boundary properties and the bleed mass flow rates are presented based on CFD solutions of the porous bleed case.

In this chapter, in order to evaluate the validity of the BBC model alternatives, CFD studies are performed with implementation of UDFs using the optimal mesh size and SST k-ω turbulence model which are determined from CFD studies on the FRMs in Chapter 3. Solid modeling, grid generation studies for the BBC models are performed in the similar manner as the FRM simulations, whereas the reference boundaries are required to define on grid models for implementation of the BBC models to the solver.

The analysis results for the BBC models are plotted along with the test data and the FRM simulation results. For examining flow structure around the bleed holes, visualizations of flow domain are presented. The deviations between the FRM and the BBC model results are calculated to measure the accuracy of the predictions.

5.1. Numerical Simulations of Bleed Boundary Condition Models

The porous bleed cases with and without shock interaction are selected for the evaluation of the BBC models. General description of wind tunnel test section and test condition for these cases are stated in Section 3.2 and 3.3, respectively. CFD simulations are conducted at Mach 2.46 for both cases and the results are compared with the test data and the FRM solutions.

5.1.1. Solid Model, Grid Generation and Boundary Conditions

The solid models are generated as similar to the FRM whereas the side surfaces of the holes and the plenums are not modeled. The mass flow outlet boundary condition is

defined for the bleed flow on the hole openings and the other boundary conditions are defined similarly as in the FRM analyses shown in Figure 5.1. The bottom, side and plenum walls are defined adiabatic, no-slip wall boundary condition. It is assumed that the top wall has no effect on bleed flow, so inviscid boundary condition is applied. As used on FRM simulations, the matched inlet profiles are imposed as inlet boundary condition for both cases.

(a)   (b)
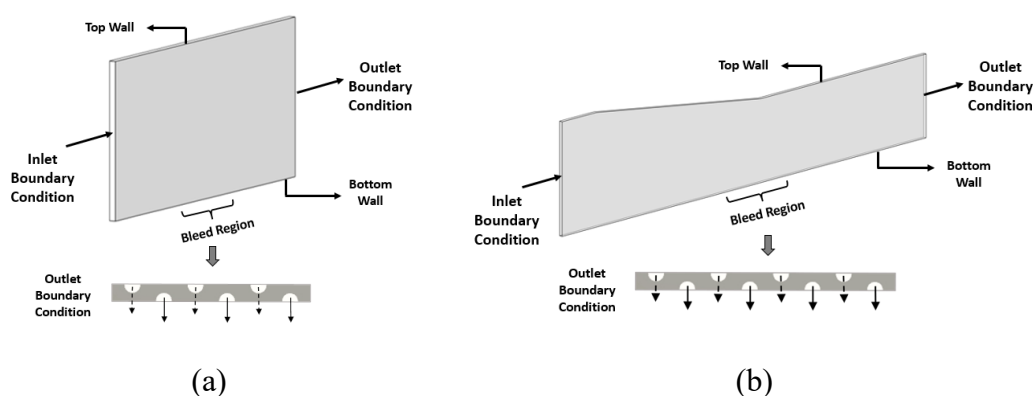
Figure 5.1 The Porous Bleed Systems (a) without Shock Interaction (b) with an Oblique Shock

Determined optimal mesh size for FRM analyses is applied to the new solid models. Thus, grid convergence study is not repeated. The grid size around the holes are adjusted as 0.04D. For implementation of BBC models to the solver, referenced boundaries are required to define on the grid models. Therefore, the generated grids differ from each other. In order to reduce grid generation efforts, no custom grid is prepared for the BHB model. The grid generated for the BRB model is used for the BHB implementation. The total number of cells for difference boundary models are presented in Table 5.1. The grid sizes are very close to each other. The BRDB model has slightly lower grid size. It is considered that the small difference on grid size may be caused by the grid generation algorithm. The grid size is reduced by about half compared to the FRM grids.

Table 5.1 Total Number of Cells for the BBC Models

	BHB	BRB	BRDB
Total Number of Cells (without shock interaction)	0.613×10^6	0.613×10^6	0.608×10^6
Total Number of Cells (with an oblique shock)	1.203×10^6	1.203×10^6	1.188×10^6

Since the images of grids are similar for both cases, the grid illustrations are given only for the case without shock interaction in Figure 5.2. Grid structure on different boundaries are shown in blue color. Boundary layer grid generation is conducted with the same methodology using in the FRM simulations. More information can be found in Section 3.2.1 and 3.3.1.
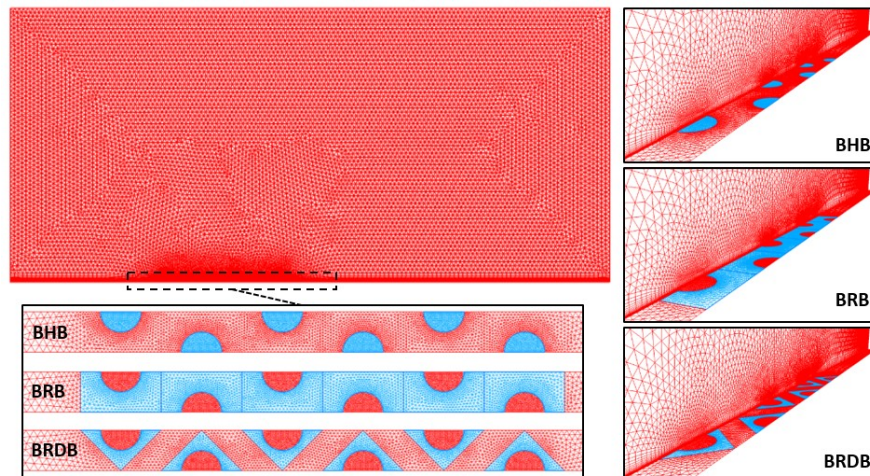
Figure 5.2 Grids of the BBC models

5.1.2. Analysis Results

CFD analyses are performed using SST k-ω turbulence model for the BBC models with UDF implementation. The details of this approach is stated in Section 2.3 and solution strategy is described in Section 2.2.2. To obtain the data for different pressure ratios, the plenum pressure parameter is specified to the desired value in the UDFs. The Q_{sonic} histories are obtained from the solutions of the porous bleed cases for the BRB model and the histories are plotted for the condition where the pressure ratio

parameter (P_{pl}/P_t) is equal to 0.0348. The simulation of the case without shock interaction requires much less solution iteration to achieve a converge solution. Although *13K* solution iterations are enough to obtain the solution in the absence of the shock interaction, the number solution iteration increases to a minimum of *30K* with shock interaction. The convergence behavior of the other boundary model simulations are very similar to the shown cases so the solutions of the other BBC model simulations are not presented. For all BBC models, an oscillatory solution behavior is not observed on histories and the uncertainty values are calculated less than 1% for all cases. Thus, the uncertainty approach mentioned in Section 2.5 has not been applied on to graphics.

(a)   (b)
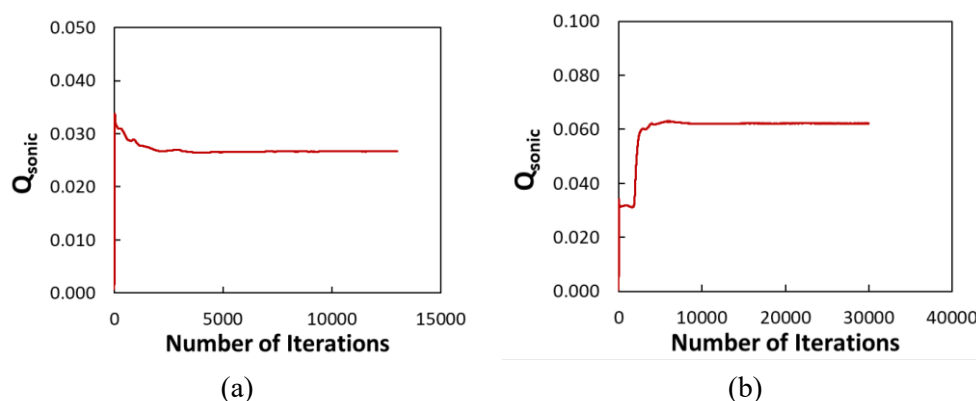
Figure 5.3 Solution Histories of Q_{sonic} for the Porous Bleed Cases (a) without Shock Interaction and (b) with an Oblique Shock

The analysis results of the BBC models are plotted along with the test data and the FRM simulation results in Figure 5.4. In addition, the percentage of deviations between FRM solutions and the BBC models are presented in Figure 5.5. Although the prediction of blowing mass flow rate is not objective of this thesis, the simulations are also performed for high plenum ratios. Hence, the graphs are splitted up into two region as bleeding and blowing to evaluate two phenomena separately. As can be seen in Figure 5.4, the BRB model is superior for the both cases on estimating bleed rates although the BRDB model predicts very close to BRB model on the case with an oblique shock. However, the BRDB model slightly overestimates the bleed rates for

the first case. The BHB model underestimates the bleed flow for the both cases and higher deviation values are observed. Also, it should be emphasized that the percentage of deviations increase with increasing the plenum pressure ratio and the greatest values are observed near to the zero bleed rates.
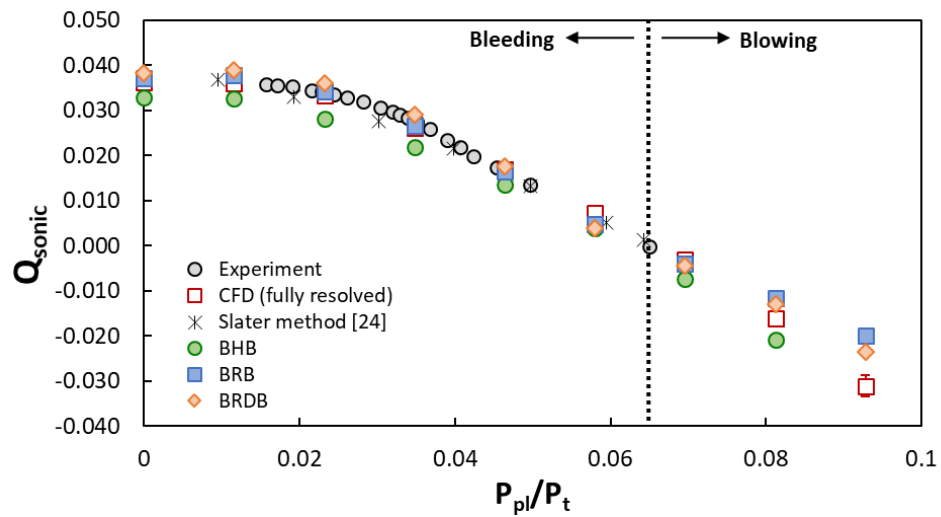
(a)
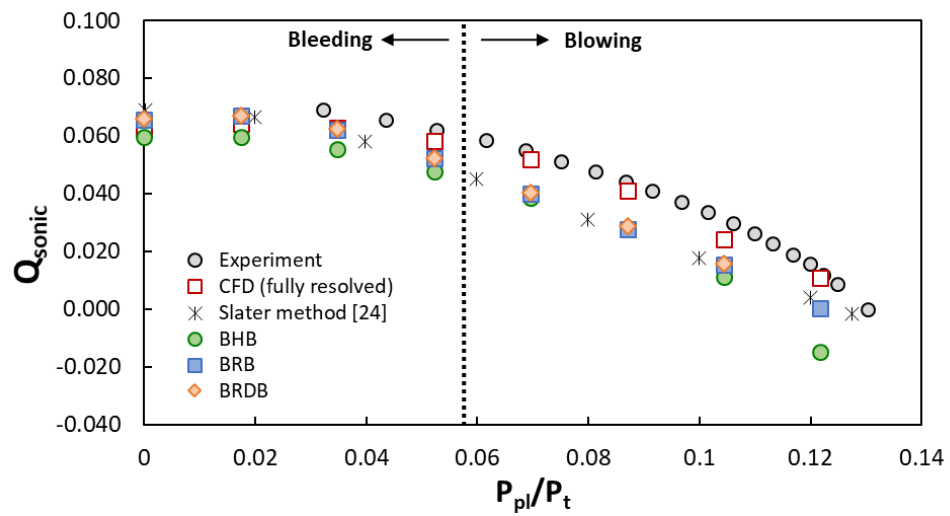
(b)

Figure 5.4 Analysis Results of the BBC Models for the Porous Bleed Cases (a) without Shock Interaction (b) with an Oblique Shock
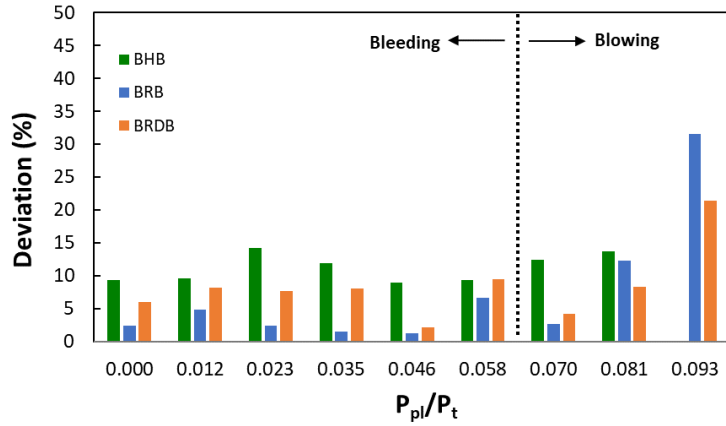
(a)
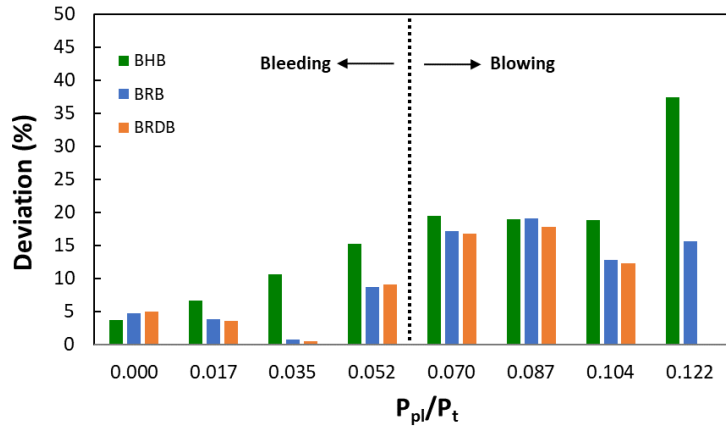
(b)

Figure 5.5 The Percentage of Deviations between the FRM and the BBC Models on Estimation the Bleed Flow Rate for the Porous Bleed Cases (a) without Shock Interaction (b) with an Oblique Shock

NRMSD values on estimation of Q_{sonic} data are presented in Table 5.2.

Table 5.2 NRMSD Values of the BBC Models on Estimation of Mass Flow Rate

	NRMSD on Q_{sonic} (without shock interaction)		NRMSD on Q_{sonic} (with an oblique shock)	
	Bleeding	Blowing	Bleeding	Blowing
BHB	0.107	0.130	0.100	0.250
BRB	0.037	0.196	0.053	0.163
BRDB	0.073	0.135	0.055	0.158

92

Area weighted average of total pressures on the outlet are collected to present total pressure recovery parameter for all CFD analyses even though there is no available PR data in the literature for these cases. PR values of bleed boundary approaches are compared with FRM solutions in Figure 5.6. The percentage of deviations between FRM solutions and the BBC models results are presented in Figure 5.7.
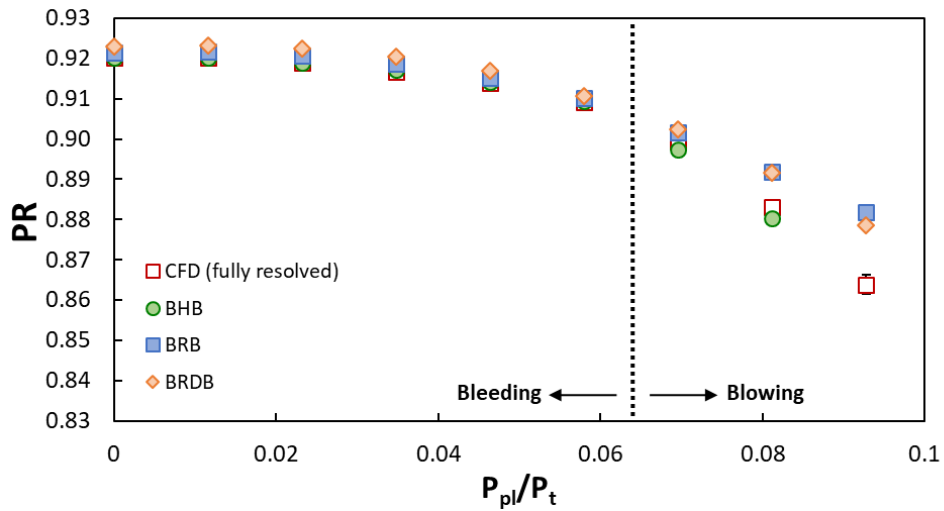
(a)
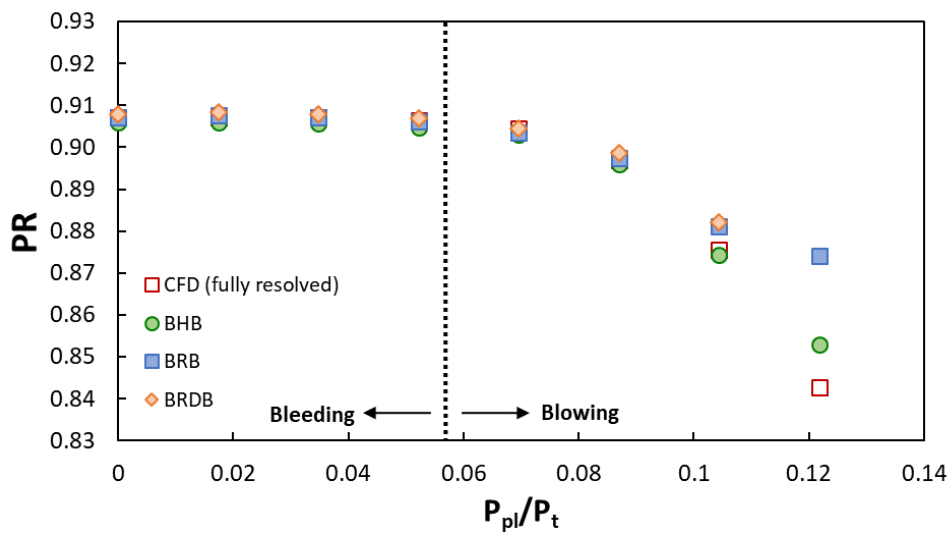
(b)

Figure 5.6 PR results of the BBC Models for the Porous Bleed Cases (a) without Shock Interaction (b) with an Oblique Shock
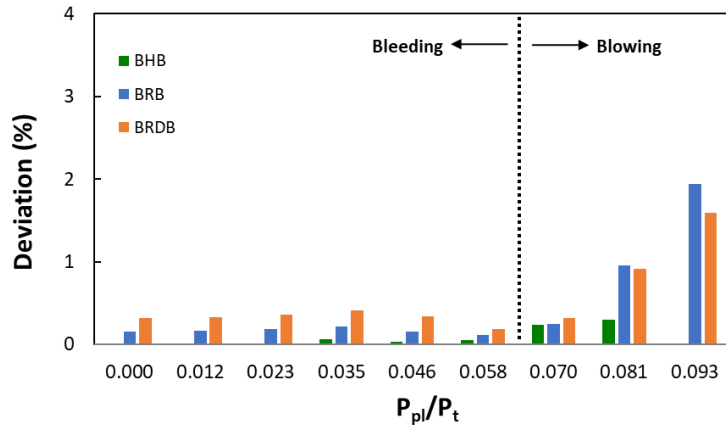
(a)
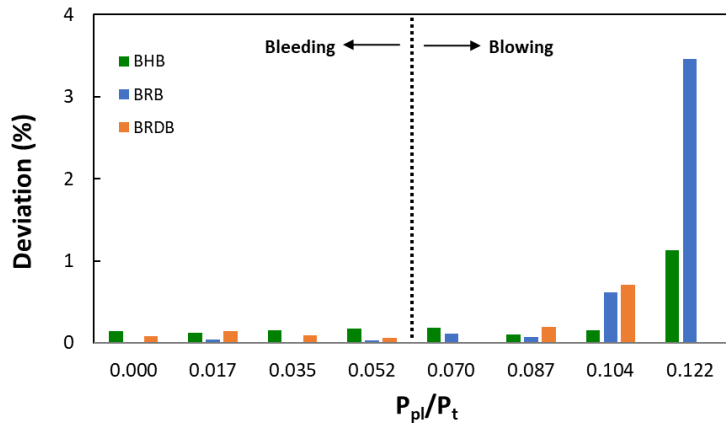
(b)

Figure 5.7 The Percentage of Deviations between the FRM and the BBC Models on Estimation the Efficiency for the Porous Bleed Cases (a) without Shock Interaction (b) with an Oblique Shock

As a result of PR comparison, the influence of porous bleed region on efficiency is captured very well with the BBC modelling. If the RMSD values in Table 5.3 is examined, the BHB model is surprisingly the best matched model with the reference results in both bleeding and blowing conditions for the case without shock interaction, although the model underestimates the bleed flow rates on bleed openings. It should be emphasized that PR decreases considerably decreasing bleed mass flow rate for the porous bleed cases.

NRMSD values on estimation of PR is presented in Table 5.3.

Table 5.3 NRMSD Values of the BBC Models on Estimation of PR

	NRMSD on PR (without shock interaction)		NRMSD on PR (with an oblique shock)	
	Bleeding	Blowing	Bleeding	Blowing
BHB	0.0004	0.0027	0.0015	0.0058
BRB	0.0017	0.0126	0.0003	0.0176
BRDB	0.0033	0.0108	0.0010	0.0042

5.1.3. Flow Domain Comparison for Porous Bleed Systems

The pressure contours on to the bottom wall of the cases without and with shock interaction for P_{pl}/P_t=0. 0348 is given in Figure 5.8 and Figure 5.9, respectively. Although, the pressure distribution of the BBC models are different over the bleed openings especially near corners where barrier shocks form, the bleed models capture well pressure distribution around the hole at the bottom surface. The BHB model provides flow estimation based on the pressure data in the bleed openings. Therefore the difference in this pressure distribution over the openings is considered as the cause of underestimation of the bleed rates.

(a) FRM

(b) BHB

(c) BRB

(d) BRDB

Pressure [Pa]

6000   7500   9000   10500   12000
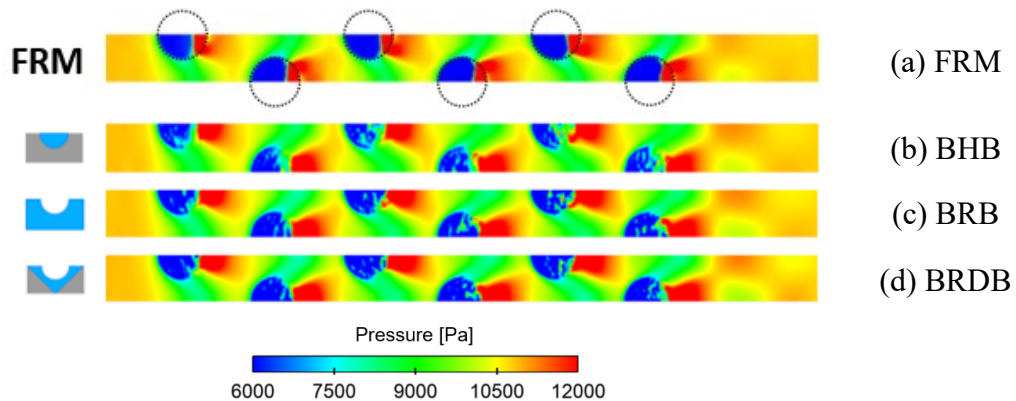
Figure 5.8 Comparison of Pressure Contours over Bottom Wall without Shock Interaction for P_{pl}/P_t=0.0348
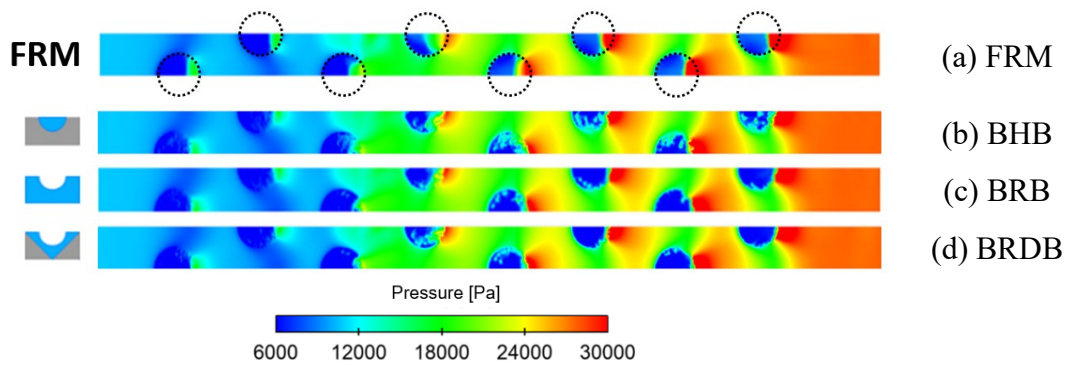
Figure 5.9 Comparison of Pressure Contours over Bottom Wall with an Oblique Shock Interaction for P_{pl}/P_t=0.0348

To demonstrate and compare downstream effects of bleed regions, domain spitted up by a number of cross planes. Pressure contours shows that the BBC models simulate the flow structure significantly similar as the FRM analysis solutions. Pressure contours for the cases without shock interaction and with an oblique shock are shown in Figure 5.10 and Figure 5.11, respectively.
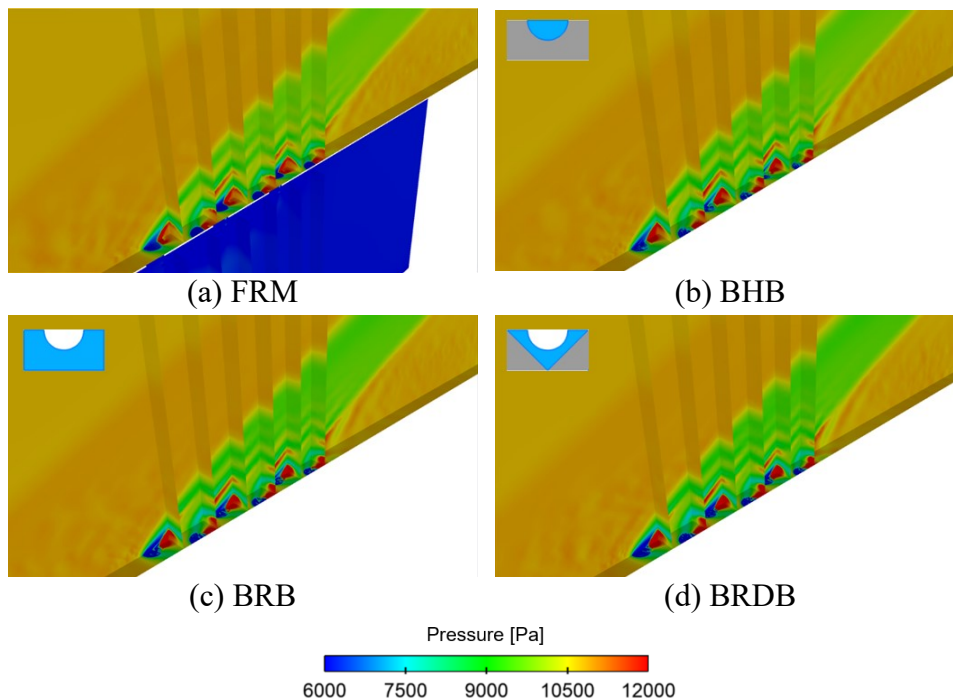
Figure 5.10 Comparison of Pressure Contours in the vicinity of Bleed Region without Shock Interaction for P_{pl}/P_t=0.0348
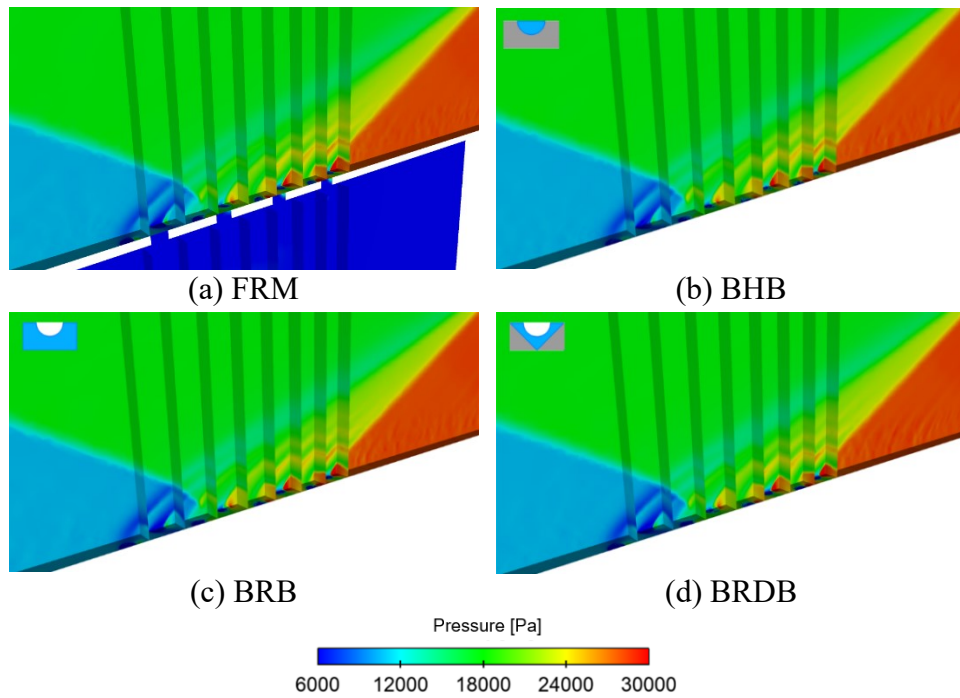
Figure 5.11 Comparison of Pressure Contours in the Vicinity of Bleed Region with an Oblique Shock Interaction for P_{pl}/P_t=0.0348

In addition, if pressure contours are viewed on larger representations around the holes (Figure 5.12 and Figure 5.13), the effects of shock expansions and barrier shocks to main flow are captured very similar to the FRM solutions.
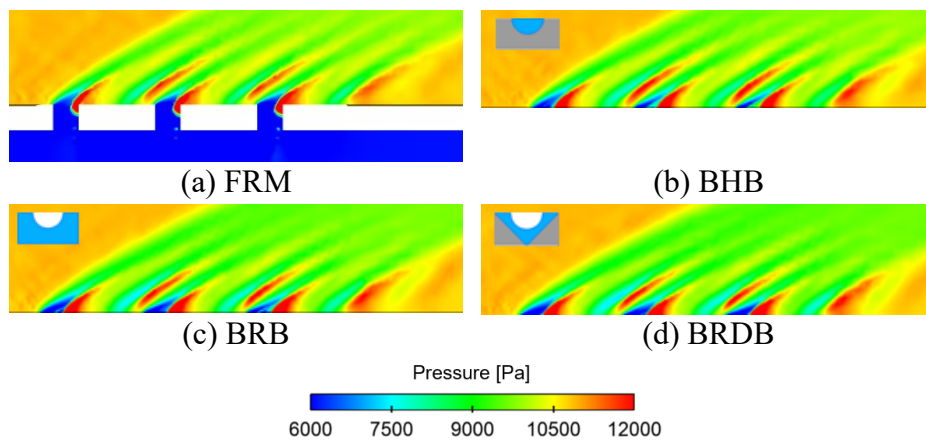
Figure 5.12 Comparison of Pressure Contours at the Symmetry Plane without Shock Interaction for P_{pl}/P_t=0.0348
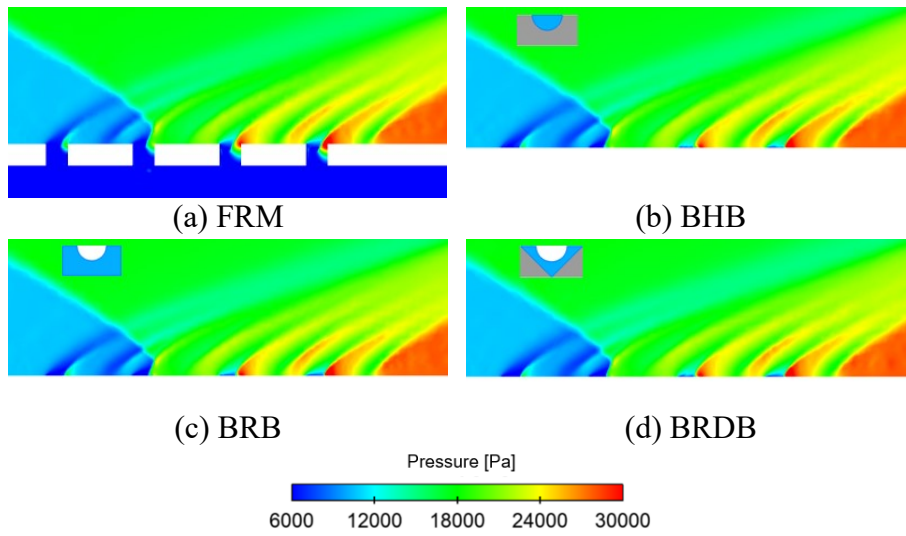
Figure 5.13 Comparison of Pressure Contours at the Symmetry Plane with an Oblique Shock Interaction for P_{pl}/P_t=0.0348

Mach contour distributions at the symmetry plane are also compared with FRM results in Figure 5.14 and Figure 5.15. Analysis results show that the BBC models are very compatible with FRM simulations.
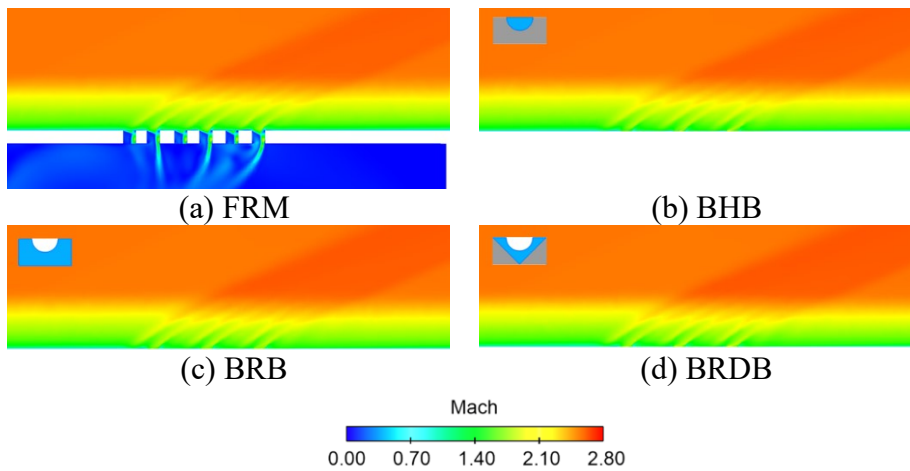
Figure 5.14 Comparison of Mach Contours at the Symmetry Plane without Shock Interaction for P_{pl}/P_t=0.0348

(a) FRM   (b) BHB

(c) BRB   (d) BRDB
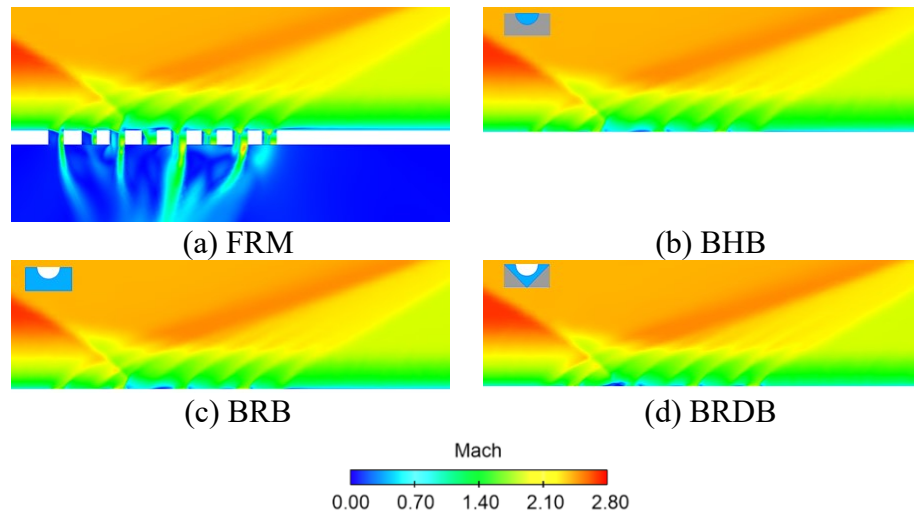
Figure 5.15 Comparison of Mach Contours at the Symmetry Plane with an Oblique Shock Interaction for P_{pl}/P_t=0.0348

5.2. Discussion of Results

In this chapter, three BBC models are evaluated by means of CFD analyses conducted on well known cases. Approaches on solid, grid generation and definition of boundary conditions for simulations are described. CFD analyses are performed using SST k-ω turbulence model for all boundary models with UDF implementation. With the removal of the plenum and cavity details from the model, the grid size is reduced by about half compared to the FRM grids. Moreover, for all boundary models, much stable solution behavior is observed on histories compared to the FRM simulations and the uncertainty values are calculated less than 1% for all cases. In this way, simulation of the cases require much less solution iterations to achieve a converge solution. The maximum number of iteration is reduced to one third with considering both cases, although the case without shock interaction converges in much less number of iteration.

The analysis results for the BBC models are presented along with the test data, the FRM solutions and results of the Slater method which is currently the most common BBC modelling technique. The BRB model is superior on estimating bleed rates for both cases although the BRDB model predicts very close to the BRB model for the

99

case with shock interaction. NRMSD values on estimation of Q_{sonic} data is presented for the bleed flow in Table 5.4.

Table 5.4 NRMSD Values of the BBC Models on Q_{sonic} for Bleed Flow

	NRMSD on Q_{sonic} (without shock interaction)	NRMSD on Q_{sonic} (with an oblique shock)
BHB	0.107	0.100
BRB	0.037	0.053
BRDB	0.073	0.055

Furthermore, prediction of total pressure recovery at the outlet is evaluated even though there is no available PR data in the literature for these cases. Hence the model results are compared with the FRM simulations. As a result of PR comparison, the influence of porous bleed region on efficiency is captured very well with the BBC modelling. The RMSD values on estimation PR are presented in Table 5.5.

Table 5.5 NRMSD Values of the BBC Models on PR for Bleed Flow

	NRMSD on PR (without shock)	NRMSD on PR (with an oblique shock)
BHB	0.0004	0.0015
BRB	0.0017	0.0003
BRDB	0.0033	0.0010

Lastly, for examining the flow structure around the bleed holes, visualizations of flow domain are presented. Although, pressure distribution of the BBC models are different over the bleed openings especially near corners where barrier shocks form, the bleed models capture well pressure distribution around the hole at the bottom surface. Additionally, pressure and Mach contour distributions at the symmetry planes show that the BBC models simulate the flow structure significantly similar as the FRM solutions and the effects barrier shock to main flow is reflected very closely for all models.

CHAPTER 6

CONCLUSION AND FUTURE WORK

In this thesis, modeling of single and porous bleed holes are investigated in computational fluid dynamics on a flat plate with and without an oblique shock interaction. For validation of the engineering approach, three-dimensional CFD simulations are performed for different levels of unstructured grids using Spalart-Allmaras, Realizable k-ε and SST k-ω turbulence models. As a result of the grid convergence studies, the medium grid resolution which has a minimum element size of 0.04D and SST k-ω turbulence model is found optimal for the bleed flow analysis. CFD results of the FRM analyses for different total plenum pressure ratios (P_{pl}/P_t) show good agreement with wind tunnel data. As a result, it is considered that the CFD method is reliable for analysing porous bleed systems where test data is not available

In addition, three new bleed boundary condition models (BBC) are introduced for bleed flow modeling. Although simulation of the blowing phenomena is not aimed in the present study, the data obtained for negative mass flow (blowing) is evaluated for the boundary condition models. The data collapse fairly well along scaled parameters except on the scaled negative $Q_{sonic,b}$ values for the BRB and BRDB models. Moreover, negative mass flow (blowing) rates increases the deviations on bleed modeling for all boundary definitions. Hence, the data of negative mass flow rate are removed from curve fittins. The deviation calculations are done to select best curve fitting model for each BBC model. According to RMSD values, the scaled data used for the BRB model is more compatible over other BBC models.

Moreover, in order to evaluate the validity of the BBC model alternatives, CFD studies are performed with implementation of UDFs for the porous bleed cases with and without shock interaction. CFD analyses are performed using SST k-ω turbulence

model for all boundary models with UDF implementation. The grid size is reduced by about half compared to FRM analyses by means of removing the plenum and cavity details from the model. Also, much stable solution behavior is observed on histories since the uncertainty values are calculated less than 1% for all analyses of the BBC models. The maximum number of iterations are reduced to one third with considering both cases, although the without shock case converge in much less iteration. Obtained results are compared with test data and fully resolved model (FRM) simulations. The analysis results and the percentage of deviations between the FRM results and the BBC model simulations and NRMSD values are presented. Consequently, although each BBC model is considered successful enough to estimate the bleed flow rates, the BRB model based on bleed region flow properties is superior on prediction of bleed rates for both cases. Moreover, all three models achieve a remarkable success on simulation of flow structure and the models reflect well the impacts of bleed region on efficiency in terms of total pressure recovery.

As a result, each boundary model has strengths and drawbacks according to potential applications for bleed systems. Although the BRB model is accomplish superior success on estimation the bleed mass flow rates, the model cannot be applied to bleed region if the porosity is more than 20%. Besides, diamond shape boundary can be applied up to 40% porous region. Among the boundary definitions, BHB is the most effortless model to apply in terms of grid generation and solver implementation processes. Hence the user can prefer one of the models considering the deviations of the models according to the field of application.

For future studies, possible improvement areas on the bleed modeling technique are listed below:

- In this study, no correction is applied to CFD data that is used for bleed boundary condition models. Each bleed boundary model can be adjusted according to sonic flow coefficient obtained from wind tunnel testing. It is

considered that the NRMSD values can be decreased by means of correction of CFD data.

- The BHB model is considered as the most promising method for improvement among all the models. First of all, it is the easiest and most effortless model implemented to the solver. Furthermore, the model has the most potential on estimation blowing compared to other models. Correlation studies show that scaled data for blowing only fit well for data obtained from bleed opening surfaces. Also, the model can be improved on bleeding either by correction of reference data that mentioned previously, or imposing corrected pressure distribution to bleed openings.

- The BRDB model is based on flow properties of diamond area over the bleed region which has 20% porosity. Accuracy of the model is unknown for denser bleed regions, although sonic flow coefficient is changing slightly with porosity as mentioned in Section 1.2.3. Additional CFD studies or wind tunnel tests can be conducted to validate the model on denser regions.

- In presented study, the normal bleed hole configuration that inclined 90° (perpendicular) to surface is examined. Hole configurations at different inclined angles can be studied to increase flexibility of the bleed boundary condition models.

- In order to evaluate the BBC models, determined optimal mesh size and turbulence model for CFD studies on FRM analyses are applied. Mesh convergence studies can be conducted with reassessment of different turbulence models to determine more efficient solution methodology.

- It is discussed that scaled values of negative mass flow (blowing) increases the deviations on bleed modeling for all BBC models. Different analysis approach can be performed to obtain reliable data for this region. Also, any test data on blowing feature is not available in the literature. Wind tunnel tests can be expanded in this region to improve the models on blowing.

REFERENCES

[1]   J. Mahoney, *Inlets for Supersonic Missiles*. AIAA Education Series, Washington, DC, 1990.

[2]   J. D. Mattingly, W. H. Heiser, and D. T. Pratt, *Aircraft Engine Design*. 2nd edition, AIAA, Washington, DC, 2002.

[3]   R. W. Ubbison, E. T. Meleason, and D. F. Johnson, "Effect of Porous Bleed in a High Performance Axisymmetric Mixed Compression Inlet at Mach 2.50," *NASA TM X-1692*, 1968.

[4]   C. Bauer and G. Kurth, "Importance of the Bleed System on the Overall Air Intake Performance," in *47th AIAA/ASME/SAE/ASEE Joint Propulsion Conference & Exhibit*, 2011, no. August, pp. 1–12.

[5]   J. Seddon and E. L. Goldsmith, *Intake Aerodynamics*. 2nd edition, AIAA, Reston, Va, 1999.

[6]   B. Willis, D. Davis, and W. Hingst, "Flow Coefficient Behavior for Boundary-layer Bleed Holes and Slots," in *33rd Aerospace Sciences Meeting and Exhibit*, 1995.

[7]   J. D. Anderson Jr., *Fundamentals of Aerodynamics*. 3th edition, Mc Graw Hill, 2001.

[8]   AGARD, "Air Intakes for High Speed Vehicles," in *Fluid Dynamics Panel Working Group 13*, 1991, no. AR-270, p. 245.

[9]   N. Domel and D. Baruzzini, "A Perspective on Mixed-Compression Inlets and the Use of CFD and Flow Control in the Design Process," in *50th AIAA Aerospace Sciences Meeting including the New Horizons Forum and Aerospace Exposition*, 2012, no. January, pp. 1–14.

[10]   N. Titchener, "An Experimental Investigation of Flow Control for Supersonic Inlets," University of Cambridge, Cambridge, UK, 2013.

[11]   J. M. Oorebeek and H. Babinsky, "Bleed and Vortex Generator Effectiveness for Separation Prevention in a Transonic Diffuser," in *7th AIAA Flow Control Conference*, 2014, no. June, pp. 1–24.

[12]   D. B. Smeltzer and N. E. Sorensen, "Investigation of a Large-Scale Mixed Compression Axisymmetric Inlet System Capable of High Performance at Mach Numbers 0.6 to 3.0," *NASA TM X-1507*, 1968.

[13]   L. J. Koncsek and J. Syberg, "Transonic and Supersonic Test of a Mach 2.65 Mixed-Compression Axisymmetric Intake," *NASA CR-1977*, 1972.

[14] J. F. Wasserbauer and J. Shaw, R, "Minimizing Boundary Layer Bleed For a Mixed Compression Inlet," *NASA TM X-71461*, 1973.

[15] W. E. Anderson and N. D. Wong, "Experimental Investigation of a Large-Scale, Two-Dimensional, Mixed-Compression Inlet System Performance at Design Conditions, M∞ = 3.0," *NASA TM X-2016*, 1970.

[16] J. F. Wasserbauer, E. T. Meleason, and P. L. Burstadt, "Experimental Investigation of the Performance of a Mach-2.7 Two-Dimensional Bifurcated Duct Inlet With 30 Percent Internal Contraction," *NASA TM 106728*, 1996.

[17] G. McLafferty and E. Renard, "Pressure Losses and Flow Coefficients of Slanted Perforations Discharging from Within a Simulated Supersonic Inlet," *United Aircr. Corp. Res. Dep. R–0920–1, East Hartford, CT,* 1958.

[18] J. Bodner, I. Greber, D. Davis, and W. Hingst, "Experimental Investigation of the Effect of a Single Bleed Hole on a Supersonic Turbulent Boundary-layer," in *32nd Joint Propulsion Conference and Exhibit*, 1996, no. July.

[19] D. Davis, M. Vyas, and J. Slater, "Research on Supersonic Inlet Bleed," in *50th AIAA Aerospace Sciences Meeting including the New Horizons Forum and Aerospace Exposition*, 2012, no. August.

[20] M. Eichorn, P. Barnhart, D. Davis, M. Vyas, and J. Slater, "Effect of Boundary-Layer Bleed Hole Inclination Angle and Scaling on Flow Coefficient Behavior," in *51st AIAA Aerospace Sciences Meeting including the New Horizons Forum and Aerospace Exposition*, 2013, no. February.

[21] A. Hamed and Z. Li, "Simulation of Bleed-Hole Rows for Supersonic Turbulent Boundary Layer Control," in *46th AIAA Aerospace Sciences Meeting and Exhibit*, 2008, no. January, pp. 1–9.

[22] A. Hamed, S. Manavasi, D. Shin, A. Morell, and C. Nelson, "Effect of Reynolds Number on Supersonic Flow Bleed," in *48th AIAA Aerospace Sciences Meeting Including the New Horizons Forum and Aerospace Exposition*, 2010, no. January, pp. 1–13.

[23] T. I.-P. Shih, M. J. Rimlinger, and W. J. Chyu, "Three-dimensional Shock-Wave/Boundary-layer Interactions with Bleed," *AIAA J.*, vol. 31, no. 10, pp. 1819–1826, Oct. 1993.

[24] J. Slater, "Improvements in Modeling 90-degree Bleed Holes for Supersonic Inlets," in *47th AIAA Aerospace Sciences Meeting including The New Horizons Forum and Aerospace Exposition*, 2009, vol. 28, no. 4, pp. 773–781.

[25] S. Bunnag, "Bleed Rate Model Based on Prandtl-Meyer Expansion," California State Polytechnic University, 2010.

[26] J. Syberg and T. E. Hickcox, "Design of a Bleed System for a Mach 3.5 Inlet,"

Nasa Cr-2187, no. January, pp. 1–88, 1973.

[27] K. Abrahamson and D. Brower, "An Empirical Boundary Condition for Numerical Simulation of Porous Plate Bleed Flows," in *26th Aerospace Sciences Meeting*, 1988, pp. 0–6.

[28] M. Rimlinger, T. Shih, and W. Chyu, "Three-dimensional Shock-Wave/Boundary-layer Interactions with Bleed through a Circular Hole," in *28th Joint Propulsion Conference and Exhibit*, 1992.

[29] A. Hamed, S. Shih, and J. Yeuan, "An investigation of Shock/Turbulent Boundary-layer Bleed Interactions," in *28th Joint Propulsion Conference and Exhibit*, 1992.

[30] L. Hedges, J. Lewis, C. Carlin, and C. Beck, "Supersonic Inlet Simulation with Closed-loop Control of Moving Control Surfaces," in *34th Aerospace Sciences Meeting and Exhibit*, 1996, no. January.

[31] D. W. Mayer and G. C. Paynter, "Boundary Conditions for Unsteady Supersonic Inlet Analyses," *AIAA J.*, vol. 32, no. 6, pp. 1200–1206, Jun. 1994.

[32] W. J. Chyu, G. W. Howe, and T. I.-P. Shih, "Bleed Boundary Conditions for Numerically Simulated Mixed-Compression Supersonic Inlet Flow," *J. Propuls. Power*, vol. 8, no. 4, pp. 862–868, Jul. 1992.

[33] W. Hingst and F. Tanji, "Experimental Investigation of a Two-dimensional Shock-turbulent Boundary Layer Interaction with Bleed," in *21st Aerospace Sciences Meeting*, 1983.

[34] B. Willis, D. Davis, and W. Hingst, "Flowfield Measurements in a Normal-Hole-Bled Oblique Shock-Wave and Turbulent Boundary-Layer Interaction," in *31st Joint Propulsion Conference and Exhibit*, 1995.

[35] B. Willis and D. Davis, "Boundary Layer Development Downstream of a Bleed Mass Flow Removal Region," in *32nd Joint Propulsion Conference and Exhibit*, 1996, no. July.

[36] A. Hamed, J. Yeuan, and Y. D. Jun, "Flow Characteristics in Boundary-layer Bleed Slots with Plenum," *J. Propuls. Power*, vol. 12, no. 2, pp. 231–236, Mar. 1996.

[37] M. Rimlinger, T. Shih, W. Chyu, B. Willis, and D. Davis, "Computations of Shock-wave/Boundary-layer Interactions with Bleed," in *34th Aerospace Sciences Meeting and Exhibit*, 1996, no. January.

[38] Z. Li, A. Hamed, S. Manavasi, and C. Nelson, "Flow Characteristics through Porous Bleed in Supersonic Turbulent Boundary Layers," in *47th AIAA Aerospace Sciences Meeting including The New Horizons Forum and Aerospace Exposition*, 2009, no. January, pp. 1–14.

[39] G. C. Paynter, D. A. Treiber, and W. D. Kneeling, "Modeling Supersonic Inlet Boundary-layer Beed Roughness," *J. Propuls. Power*, vol. 9, no. 4, pp. 622–627, Jul. 1993.

[40] G. J. Harloff and G. E. Smith, "Supersonic Inlet Boundary Layer Bleed Flow," *AIAA J.*, vol. 34, no. 4, pp. 778–785, Apr. 1996.

[41] S. Dambra, M. Yamamoto, and S. Honami, "Modeling of Boundary Condition for Turbulent Boundary Layer Bleed," in *36th AIAA Aerospace Sciences Meeting and Exhibit*, 1998.

[42] J. Akatsuka, Y. Watanabe, A. Murakami, and S. Honami, "Porous Bleed Model for Boundary Condition of CFD Analysis," in *3rd AIAA Flow Control Conference*, 2006, no. June, pp. 1–14.

[43] D. Benson, T. Shih, D. Davis, and B. Willis, "Boundary Conditions for CFD Simulations of Supersonic Boundary-layer Flow through Discrete Holes," in *38th Aerospace Sciences Meeting and Exhibit*, 2000.

[44] A. T. Morell, "Model for Flow Properties Across the Opening of Normal Bleed Holes in Supersonic Flow," Muskingum University, 2018.

[45] J. Slater and J. Saunders, "Modeling of Fixed-Exit Porous Bleed Systems," in *46th AIAA Aerospace Sciences Meeting and Exhibit*, 2008, no. January, pp. 1–12.

[46] J. W. Slater, D. O. Davis, B. W. Sanders, and L. J. Weir, "Role of CFD in the Aerodynamic Design and Analysis of the Parametric Inlet," *ISABE–2005–1168*, 2005.

[47] R. A. Baurle and A. T. Norris, "A Source-Term Based Boundary Layer Bleed/Effusion Model for Passive Shock Control," *58th JANNAF Propuls. Meet.*, 2011.

[48] N. Wukie, P. Orkwis, M. Turner, and S. Duncan, "Comparison of Simulations and Models for Aspiration in a Supersonic Flow using OVERFLOW," in *50th AIAA Aerospace Sciences Meeting including the New Horizons Forum and Aerospace Exposition*, 2012, no. January, pp. 1–33.

[49] Y. Choe and C. Kim, "Numerical Investigation of Bleed Effects on Supersonic Inlet under Various Bleed and Inlet Conditions," in *34th AIAA Applied Aerodynamics Conference*, 2016, no. June.

[50] *Theory Guide*. ANSYS FLUENT 15.0, 2013.

[51] P. SPALART and S. ALLMARAS, "A one-equation turbulence model for aerodynamic flows," in *30th Aerospace Sciences Meeting and Exhibit*, 1992.

[52] B. E. Launder and D. B. Spalding, *Lectures in Mathematical Models of Turbulence*. Academic Press, London, England, 1972.

[53] T.-H. Shih, W. W. Liou, A. Shabbir, Z. Yang, and J. Zhu, "A new k-ϵ eddy viscosity model for high reynolds number turbulent flows," *Comput. Fluids*, vol. 24, no. 3, pp. 227–238, Mar. 1995.

[54] D. C. Wilcox, *Turbulence Modeling for CFD*. DCW Industries, Inc. La Canada, California. 1998.

[55] F. R. Menter, "Two-equation eddy-viscosity turbulence models for engineering applications," *AIAA J.*, vol. 32, no. 8, pp. 1598–1605, Aug. 1994.

[56] *User Guide*. ANSYS FLUENT 15.0, 2013.

[57] *UDF Manual*. ANSYS FLUENT 15.0, 2013.

APPENDICES

A. UDF for Bleed Boundary Modeling

```
1  /***
2  Bleed Boundary Condition Modeling
3  Compiled UDF
4  Written by GOKHAN AKAR
5  Aerospace Engineering. METU, Ankara, 2019
6  ***/
7
8  #include "udf.h"
9
10 DEFINE_PROFILE(modify_mdot_bleed_hole_1,t_bleed,j)
11 {
12 /* Variables used by serial, host, node versions */
13  int thread_region_id=0;
14
15 /* "Parallelized" Sections */
16
17 #if !RP_HOST  /* Compile this section for computing processes only (serial and node) */
18  /* define variables and initilization*/
19  /* these variables are not available on the host */
20  Domain *domain=Get_Domain(1);
21  Thread* thread_region;
22
23  face_t face;
24  real area[3];
25
26  /* define Plenum Pressure Value */
27  real WSONIC_BLEED_REGION=0.0,QSONIC_SCALED=0.0;
28  real AWA_TEMP=0.0,AWA_PRESSURE=0.0;
29  real AWA_AREA_TOTAL=0.0;
30  real AWA_PRESSURE_TOTAL=0.0;
31  real AWA_TEMP_TOTAL=0.0;
32  real MDOT_BLEED=0.0;
33
34  /* define Plenum Pressure Value */
35   real PRESSURE_PLENUM=6000.0;
36
37 #endif /* !RP_HOST */
38
39  thread_region_id = 52;  /* ID number of the reference boundary in FLUENT */
40
41 #if !RP_HOST  /* SERIAL or NODE */
42  /* thread is only used on compute processes */
43
44  thread_region = Lookup_Thread(domain,thread_region_id);
45
```

```
46   begin_f_loop(face,thread_region)

47

48   /* the total area, addition of all static pressure and temperature values for this node*/
49    if (PRINCIPAL_FACE_P(face,thread_region))
50    {
51     F_AREA(area,face,thread_region);

52

53     AWA_AREA_TOTAL += NV_MAG(area);

54

55     AWA_PRESSURE_TOTAL+=NV_MAG(area)*F_P(face,thread_region);

56

57     AWA_TEMP_TOTAL+=NV_MAG(area)*F_T(face,thread_region);
58    }
59    end_f_loop(face,thread_region)

60

61

62  # if RP_NODE /* Perform node synchronized process */
63    AWA_AREA_TOTAL = PRF_GRSUM1(AWA_AREA_TOTAL);
64    AWA_PRESSURE_TOTAL = PRF_GRSUM1(AWA_PRESSURE_TOTAL);
65    AWA_TEMP_TOTAL= PRF_GRSUM1(AWA_TEMP_TOTAL);
66  #endif /* RP_NODE */

67

68    /* Calculation of Area Weighted Averages*/
69    AWA_PRESSURE=AWA_PRESSURE_TOTAL/AWA_AREA_TOTAL;
70    AWA_TEMP=AWA_TEMP_TOTAL/AWA_AREA_TOTAL;

71

72    /* Calculation of Wsonic,b parameter*/
73    WSONIC_BLEED_REGION=AWA_PRESSURE*1.5818334*pow(10.0,(-
     5.0))*pow(1.4/287.037910474435/AWA_TEMP,(0.5))*pow((1+(1.4-1)/2),(-
     1.0*(1.4+1.0)/(2.0*(1.4-1.0))));

74

75    /* Calculation of Qsonic,b parameter*/
76    QSONIC_SCALED=0.289*pow((PRESSURE_PLENUM/AWA_PRESSURE),3.0)-
     1.192*pow((PRESSURE_PLENUM/AWA_PRESSURE),2.0)+0.299*pow((PRESSURE_PLENUM/
     AWA_PRESSURE),1.0)+0.617;

77

78    /* Calculation of mdot bleed or blow*/
79    MDOT_BLEED=WSONIC_BLEED_REGION*QSONIC_SCALED;

80

81  #endif /* !RP_HOST */

82

83  /* Adjust Mdot value according to sign of calculated MDOT_BLEED */
84  #if !RP_HOST  /* SERIAL or NODE */
85  if(MDOT_BLEED<0.0)
86  {
87  MDOT_BLEED=-1.0*MDOT_BLEED;
88  }
89  begin_f_loop(face,t_bleed)
90  {
91
```

```
92  /* Impose Mdot value */
93  F_PROFILE(face,t_bleed,j)=MDOT_BLEED;
94
95  }
96  end_f_loop(face,t_bleed)
97
98  #endif
99  }
```